AIN SHAMS UNIVERSITY
FACULTY OF ENGINEERING
Electronics and Communications Engineering Department

Modeling and Characterization of VLSI MOSFET for CAD

A Thesis

Submitted in Partial Fulfillment for the Requirements
of the Degree of Master of Science in Electrical Engineering
(Electronics and Communications Engineering)

Submitted By

Alaa El-Din El-Raey Mohamed

B.Sc. of Electrical Engineering
(Electronics and Communications Engineering)
Ain Shams University, 1992

Supervised By

Prof. Dr. Mohamed Kamel El-Said
Dr. Hisham Haddara

Cairo - 1996

جامعة عين شمس – كلية الهندسة

قسم هندسة الإلكترونيات والإتصالات

نمذجة و توصيف الترانزيستور من نوع معدن أكسيد شبة موصل للدوائر المتكاملة واسعة النطاق لبرامج محاكاة الدوائر الالكترونية

رسالة

مقدمة للحصول على درجة الماجستير فى الهندسة الكهربية

(هندسة الإلكترونيات والإتصالات)

مقدمة من

علاء الدين الراعى محمد

بكالوريوس الهندسة الكهربية

(هندسة الإلكترونيات والإتصالات)

جامعة عين شمس – ١٩٩٢

تحت إشراف

الأستاذ الدكتور/ محمد كامل السعيد

الدكتور/ هشام سيد رمضان هداره

القاهرة – ١٩٩٦

STATEMENT

This discertation is submitted to Ain Shams University for the degree of Master of Science in Electrical Engineering (Electronics and Communications Engineering).

The work included in this thesis was carried out by the author at the Electronics and Communications Electrical Engineering Department, Faculty of Engineering, Ain Shams University.

No part of this thesis was submitted for a degree or a qualification at any other university or institution.

Date : / / 1996
Signature :
Name : Alaa El-Din El-Raey Mohamed

جامعة عين شمس

كلية الهندسة

رسالة ماجستير

إسم الباحث : علاء الدين الراعى محمد

عنوان الرسالة : نمذجة و توصيف الترانزيستور من نوع معدن أكسيد شبة موصل للدوائرالمتكاملة واسعة النطاق لبرامج محاكاة الدوائر الالكترونية

إسم الدرجة : ماجستير

القسم : هندسة الإلكترونيات والإتصالات الكهربيه

لجنة الإشراف

١- الإسم: أ.د. محمد كامل السعيد
٢- الوظيفة: أستاذ ورئيس قسم هندسة الإلكترونيات والإتصالات الكهربيه - كلية الهندسة - جامعة عين شمس

٣- الإسم: د. هشام سيد رمضان هداره
٢- الوظيفة: أستاذ مساعد بقسم هندسة الإلكترونيات والإتصالات الكهربيه - كلية الهندسة - جامعة عين شمس

الدراسات العليا

ختم الإجازة **أجيزت الرسالة بتاريخ**

/ / ١٩٩٦

موافقة مجلس الكلية **موافقة مجلس الجامعة**

/ / ١٩٩٦ / / ١٩٩٦

جامعة عين شمس

كلية الهندسة

تعريف بمقدم الرسالة

إسم الباحث : علاء الدين الراعى محمد

تاريخ الميلاد : ١٩٧٠/٤/١٣

محل الميلاد : القاهرة

الدرجة العلميه الأولى : بكالوريوس الهندسة الكهربية – هندسة الإلكترونيات والإتصالات الكهربيه

الجهة المانحه للدرجة العلمية الأولى : كلية الهندسة – جامعة عين شمس

تاريخ المنح : يونية ١٩٩٢

الوظيفة الحاليه : معيد بقسم هندسة الإلكترونيات والإتصالات الكهربيه
كلية الهندسة – جامعة عين شمس

إسم مقدم البحث : علاء الدين الراعى محمد

التوقيع :

التاريخ : / / ١٩٩٦

جامعة عين شمس

كلية الهندسة

شكر

أشكر السادة الأساتذة الذين قاموا بالإشراف وهم

١- أ.د. محمد كامل السعيد

٢- د. هشام سيد رمضان هداره

ثم الأشخاص الذين تعاونوا معى بالبحث وهم

١- مهندس محمد أمين

٢- مهندس تامر أحمد عامر

٣- أعضاء هيئة التدريس وزملائى المعيدين بقسم هندسة الإلكترونيات والإتصالات الكهربيه، كلية الهندسة - جامعة عين شمس

٤-مهندس شريف جلال من شركة ANACAD

جامعة عين شمس
كلية الهندسة

مستخلص

علاء الدين الراعى محمد. نمذجة و توصيف الترانزيستور من نوع معدن أكسيد شبة موصل للدوائرالمتكاملة واسعة النطاق لبرامج محاكاة الدوائر الالكترونية
جامعة عين شمس. كلية الهندسة. ١٩٩٦

تم القيام بتنفيذ نموذج إستاتيكى للترانزستور من نوع معدن – أكسيد – شبـــه موصل بغرض تطبيقه فى برامج محاكاة الدوائر. وقد تم الإهتمام فى هذه الدراسة بنمذجة عمل الترانزستور فى حالة وجود تطعيم غير منتظم للقناة. كما تم الاهتمام بتصميم النموذج ليشمل تطبيقات الدوائر التناظرية و العددية, مما وضع متطـــلبات عالية من الدقة فى النموذج المقترح. وقد تم بناء النموذج على وصف توصيل التيار فى القناة بدلالة جهد السطح عند كل من المنبع والمصـــــب.ومن خصائص النموذج الـــــــذى تم بناؤه أنه قابل للتطبيق على النبائـــــط المصغرة كما إنه متصل من منطقة تحت جهد العتبة حتى منطقة الإنقلاب الشديد. وقد تم البرهنـــــــة على دقة النموذج فى حالات متعددة من جهود الإنحياز وأبعاد النبائـــــط. وجدير بالذكر أن خصائص النمـــــوذج من حيث الدقة والإتصـــــــال والإستقـــــــــرار ترجع الى الأساس الفيزيائـــــــــى لهذا النموذج من حيث توصيف الظواهر والمؤثرات الداخله فى عمل النبطية.

وقد تم تنفيذ هذا النمـــوذج فى برنامج محاكاة الدوائـــــــر ELDO عن طريق لغة HDL-A و بذلك يمكن إستخدام النموذج فى محاكاة الدوائر المكونه من نبائط معدن – أكسيد – شبه موصل.

كما تم أيضا عمل برنامج قياس آلى بأستخدام برنامج LabVIEW للقيام بتوصيف الترانزيستور من نوع MOS . هذا بالاضافة الى برنامج آلى لاستخراج بارمترات النموذج من نتائج القياس العملية.

الكلمات المفتاحية: الدوائر المتكاملة شديدة الاتساع– النمذجة – محاكاة الدوائر الالكترونية

جامعة عين شمس
كلية الهندسة

صفحة العنوان

إسم الباحث : علاء الدين الراعى محمد

إسم الدرجة : ماجستير

القسم التابع له : هندسة الإلكترونيات والإتصالات الكهربيه

إسم الكلية : كلية الهندسة – جامعة عين شمس

سنة التخرج : ١٩٩٢

سنة المنح : ١٩٩٦

بسم الله الرحمن الرحيم

﴿قالوا سبحانك لا علم لنا إلا ما علمتنا إنك أنت العليم الحكيم﴾

(البقرة ٣٢)

ملخـــــــــــص الرسالـــــــــــــــة

إن المتطلبات التي يجب توافرها في النموذج المعد لخدمة برامج محاكاة الدوائـــر الإلكترونية جد متشعبة و متداخلة. فيجب أن يكون النموذج طبيعي المنشـــأ، وأن يمثل بدقة الآلية الإلكترونية الداخلية للنبائط، متضمنا الوصف الهيكلي للنبائط، كما يجب أن يتصل برباط محكم بتكنولوجيا التصنيع ونسق التصميم بالإضافـــة إلـــى الخواص الكهربية. ويجب أن يمثل النموذج بدقة خواص النبائط الكهربية خـــلال مدى التشغيل اللازم و تحت كافة الظروف.

كما أن استحداث النماذج التحليلية الملائمة لبرامج محاكاة الدوائر قد تدفعنـــا إلـــى استخدام معادلات شبة طبيعية تحتوى بدورها على بـــارامترات لا تنتمـــي إلـــى مجموعة قيم وحيدة، لذلك فلتحقيق مأربنا في الحصول على نموذج جيد لـــبرامج محاكاة الدوائر، يجب استحداث برامج قياس آلية بالإضافة إلى خوارزم مناســـب لاستخلاص أفضل قيم لهذه البارامترات حتى يكون النموذج ممثلا دقيقـــا للنتـــائج العملية.

في هذه الرسالة تم استكمال عملية إعداد نموذج للترانزيستورات من نوع معـــدن أكسيد شبة موصل صالح للتطبيقات التماثلية و الرقمية (يتم إعداد هـــذا النمـــوذج بمعمل الدوائر المتكاملة)، عن طريق إدخال الظواهر المصاحبة لعدم انتظام تطعيم القناة. كما تم استحداث برامج آلية علي الحاسب الشخصي للقيام بعمليـــة القيـــاس اللازمة لتوصيف الترانزيستورات، وتم استحداث برنامج لاستخلاص قيـــم دقيقـــة لبارمترات النموذج استنادا على خوارزم ليفنبرج–ماركودت، ويتميز هذا البرنامج بأنه لا يعتمد على النموذج ويمكن استخدامه في أي تطبيق أخر يتطلب اســـتخراج البارمترات بطريقة أقل خطأ في المربعات لمعادلات غير خطية.

وقد تم تقسيم الرسالة إلي أربعة فصول:

الفصل الأول: يعطي ملخص لتوصيف الترانزيستور من نوع معدن أكسيد شبة موصل، كما يناقش مفهوم نمذجة الترانزيستورات لبرامج محاكاة الدوائر والقواعد التي يجب تحقيقها للقيام بعمل النموذج للدوائر التناظرية.

الفصل الثاني: يتناول إظهار النموذج المقترح مع توضيح ظواهر القناة الضيقة والقصيرة وكيفية توصيفها بالنموذج، كما تم شرح كيفية استكمال النموذج ليشمل القنوات الغير منتظمة التطعيم وتم التحقق من دقة هذا الاستكمال بالمقارنة مع النتائج العملية.

الفصل الثالث: تم استعراض طريقة القياس الآلية المستحدثة والنبائط المطلوبة، كما تم توضيح بارمترات النموذج وكيفية استخراجها بطريقة جماعية لتلائم مجموعة من النبائط ذات تكنولوجيا تصنيع واحدة.

الفصل الرابع: تم استعراض المبادئ الرياضية المستخدمة في خوارزميات أقل خطأ للمربعات للدوال الغير خطية، وتم التركيز على الخوارزم المستخدم وهو ليفنبرج–ماركودت. وقد لوحظ التطابق القوي بين النتائج التى تم الحصول عليها من القياسات المعملية ونتائج النموذج المبنية علي قيم البارمترات المستخلصة من البرنامج المستحدث فى هذة الرسالة.

ABSTRACT

Alaa El-Din El-Raey Mohamed. Modeling and Characterization of VLSI MOSFET for CAD. Unpublished Master of Science dissertation, University of Ain Shams, 1996.

The main objective of this dissertation is to develop a *circuit-level* dc current model for the MOS transistor. Special care is taken to the modeling of the transistors of non uniform doping. The model is to be used for *analog* and digital circuit design. This puts heavy demands on the accuracy provided by the model. The model is based on the representation of current transport in a sheet channel in terms of the surface potential conditions at the source and drain boundaries. The model is scaleable and results in continuous device characteristics under all operating conditions, from deep subthreshold to strong inversion. Accuracy of the model is demonstrated over a wide range of device geometries and terminal voltages. The features of scalability, continuity, and accuracy are attributed to the physical representation of all important effects occurring in the MOS transistor. The model is implemented under the circuit simulator *ELDO* using HDL-A language and can be used to simulate dc MOSFET circuits.

Also we develop an automated measurements program works under LabVIEW software to characterize the MOS transistors, as well as an automated program to extract the model parameters from the measured characteristics.

Key Words

VLSI - MOSFET- CAD - Modeling - Simulation

SUMMARY

The requirements to be satisfied by a CAD device model for use in circuit simulation are demanding and essentially in conflict. The model should be physically based, representing faithfully the internal electronic mechanisms and the implications of device structure, and should provide a coherent link between fabrication technology, design layout and electrical performance. It should give accurate and continuous representation of device electrical characteristics over the full range of operating modes and conditions.

The required analytical model to be suitable for CAD applications, may force us to the development of some quasi-physical equations and the required parameters in this case do not normally relate to any single identifiable physical set of parameters, so to achieve our purpose to obtain good model for CAD applications, an automated measurement setup must be provided beside an optimization algorithm to best fit the obtained experimental data.

In this work we continue the development of a MOSFET model for analog and digital applications, which is carried out in the ICL lab, by introducing the non-uniform doping effects. Also automated programs for MOSFET characterization, as well as an optimization program based on the Levenberg-Marqudet algorithm have been developed. The developed optimization program is model independent and can be used for any nonlinear least square parameter extraction problem. The thesis is divided into four chapters:

The first chapter, gives a quick review to the MOSFET characteristics since it is our target for modeling and characterization. The concept of

MOSFET modeling for circuit CAD and the required criteria to be satisfied in the model development has been discussed.

In the second chapter, the proposed model is presented, the short channel effects which are included in the model are outlined with their governing equations. Also the extension to the non-uniform doping are presented and is verified by comparison with experimental results.

The third chapter, presents the suggested measurement procedure and the required devices, also it provides the model parameters and an extraction strategy called the group strategy, which is best fit a group of devices based on the same technology, but may have not strong fit for each device alone.

The mathematical foundation required for non linear least square algorithms are presented in chapter four with focusing on the used algorithm called Levenberg-Marqudet algorithm. A good agreement has been observed between the proposed model results and the experimental results obtained using the suggested measurement procedure.

ACKNOWLEDGMENTS

I would like to take the opportunity to acknowledge the direct and indirect help of many people who made this thesis possible.

First, I would like to express my sincere appreciation to Prof. Dr. Mohamed Kamel El-Said and Dr. Hisham Haddara for their continuous support and valuable guidance. I have enjoyed being their student for the past three years and will always be indebted for their encouragement and constructive criticism.

My deepest gratitude to Prof. Dr. Hani Fikry and Dr. Wael Fikry for their valuable help and profound encouragement.

I would also like to thank the development team at Anacad Egypt, especially Eng. Sherif Galal for their generous support.

Special thanks to Eng. Mohamed Amin and Eng. Tamer Amer for their valuable advice and support in all phases of this thesis.

Alaa El-Raey
November 1996

CONTENTS

List 0f Figures

List of Tables

LIST OF SYMBOLS

AI	Impact ionization pre-exponential constant (1/V)
BI	Impact ionization exponent constant (V/cm)
C_d	Depletion capacitance per unit area (F/cm^2)
C_G	Total gate capacitance per unit area (F/cm^2)
C_{it}	Interface trap charge capacitance per unit area (F/cm^2)
C_{ox}	Gate oxide capacitance per unit area (F/cm^2)
C_s	Total surface capacitance per unit area (F/cm^2)
d_{inv}	Thickness of the inversion layer (50 - 100 A°)
D_{it}	Total interface trapped charge density per unit area, and per unit energy (cm^{-2}.eV^{-1})
D_{ita}	Acceptor like interface trapped charge density per unit area, and per unit energy (cm^{-2}.eV^{-1})
D_{itd}	Donor like interface trapped charge density per unit area, and per unit energy (cm^{-2}.eV^{-1})
E_c	The lowest energy level of the conduction band (eV)
E_f	Fermi level (eV)
E_{fn}	Electrons quasi-Fermi level (eV)
E_{fp}	Holes quasi-Fermi level (eV)
E_g	Energy band gap (eV)
E_i	Intrinsic level (eV)
E_t	Interface trap level (eV)
E_v	The upper energy level of the valence band (eV)
F_{max}	The critical electric field in the channel at which carriers move with their limiting velocity v_{max} (V/cm)
F_x	The electric field component parallel to the Si-SiO_2 interface (V/cm)
F_y	The electric field component perpendicular to the Si-SiO_2 interface (V/cm)

F_{yb}	The electric field component perpendicular to the Si-SiO_2 interface just below the inversion layer (V/cm)
F_{ys}	The electric field component perpendicular to the Si-SiO_2 interface at the surface (V/cm)
$f(E)$	Fermi-Dirac distribution function
g_m	Transconductance (A/V)
g_{mb}	Bulk transconductance (A/V)
g_d	Drain conductance (A/V)
I_D	Drain current (A)
I_{D1}	Drift current component (A)
I_{D2}	Diffusion current component (A).
I_{Dsat}	Drain current at saturation (A)
I_{st}	Substrate current due to impact ionization (A)
k	Boltzmann constant (=1.380662E-23) (J/K)
L	Mask Channel length (cm)
L_{eff}	Effective channel length (cm)
L_s	The width of the source depletion region (cm)
L_d	The width of the drain depletion region (cm)
ΔL	Channel shortening in the saturation region (cm)
l_d	Drain induced barrier lowering characteristic length (cm)
N_A	Acceptor impurity density per unit volume (cm^{-3})
N_D	Donor impurity density per unit volume (cm^{-3})
N_{sub}	Substrate impurity doping density per unit volume (cm^{-3})
n	Electron density per unit volume (cm^{-3})
n_i	Intrinsic carrier density per unit volume (cm^{-3})
p	Hole density per unit volume (cm^{-3})
Q_B	Depletion (bulk impurity) charge density per unit area (C/cm^2)
Q_{ox}	Effective oxide charge per unit area at the Si-SiO_2 interface (C/cm^2)
Q_i	Inversion charge density per unit area (C/cm^2)
Q_{it}	Interface trapped charge density per unit area (C/cm^2)
Q_{it}'	$= Q_{it}(\psi_s,\phi_c)-Q_{it}(0,0)$ (C/cm^2)

Q_{ita}	Acceptor like interface trap charge density per unit area (C/cm^2)
Q_{itd}	Donor like interface trapped charge density per unit area (C/cm^2)
Q_{sc}	Semiconductor charge density per unit area (C/cm^2)
q	Magnitude of the electronic charge (=1.60219E-19) (C)
R_d	Drain parasitic series resistance (Ω)
R_s	Source parasitic series resistance (Ω)
R_t	Total parasitic series resistance (Ω)
SF	The smoothing function
T	Temperature (°K)
T_{ox}	Gate oxide thickness (cm)
V_{bi}	Built-in voltage of the drain and source junctions (V)
V_D	Drain voltage referenced to the bulk potential (V)
V_{DS}	Drain to Source voltage (V)
V_{DS1}	Drain to Source voltage taking into account velocity saturation effects (V)
V_{DSsat}	Drain to Source voltage at the saturation point (V)
V_{FB}	Real flat band voltage (V)
V_{FBD}	Effective Flat band voltage including the effect of the interface trap charge (V)
V_{FB}'	Effective Flat band voltage (V)
V_G	Gate voltage referenced to the bulk potential (V)
V_{GS}	Gate to Source voltage (V)
V_{GF}	$=V_G-V_{FB}$ (V)
V_{GT}	$=V_G-V_T$ (V)
V_S	Source voltage referenced to the bulk potential(V)
V_T	Gate to bulk voltage at threshold (V)
V_{th}	Gate to source voltage at threshold (V)
v_{max}	Maximum velocity of the carriers in the channel (cm/s.)
W	Channel width (cm)
w	Depletion region width (cm)
X_{dep}	Depletion region width at threshold (cm)

y_j	Source/drain junctions depth (cm)
β	$1/\phi_t$ (V^{-1})
β_{eff}	Transconductance parameter using μ_{eff} (A/V^2)
β_{eff}'	Transconductance parameter using μ_{eff}' (A/V^2)
β_g	Transconductance parameter using μ_g (A/V^2)
β_o	Transconductance parameter using μ_o A/V^2)
γ	Body factor ($V^{½}$)
ε_{ox}	Permittivity of SiO_2 (F/cm)
ε_s	Permittivity of Si (F/cm)
θ	Normal mobility coeffeicient (1/V)
μ_{eff}	Effective electron mobility in the channel, taking into consideration the effect of both normal, and lateral field scattering ($cm^2/V.s$)
μ_{eff}'	Effective electron mobility in the channel, taking into consideration the effect of both normal, and lateral field scattering, in addition to the parasitic series resistance R_t ($cm^2/V.s$)
μ_g	Effective electron mobility in the channel, taking into consideration the effect of the normal field scattering only ($cm^2/V.s$)
μ_n	Electron surface mobility in the channel ($cm^2/V.s$)
ρ	Space charge density in the semiconductor (C/cm^3)
ϕ_c	The Quasi-Fermi potential (the difference between E_{fn} at the surface of the semiconductor and E_{fp} in the bulk of the semiconductor) (V)
ϕ_f	The difference between E_i and E_f in the bulk of the semiconductor (V)
ϕ_m	Metal work function (eV)
ϕ_{ms}	Metal-semiconductor work function difference (eV)
ϕ_s	Semiconductor work function (eV)
ϕ_{si}	Surface potential referenced to the source at threshold (V)
ϕ_t	Thermal voltage (V)

ϕ_v	Channel potential induced by the drain-source bias (V)
ψ_s	Surface potential referenced to the bulk potential (V)
ψ_{sw}	Estimated surface potential ψ_s in the weak inversion regime (V)
ψ_{ss}	Estimated surface potential ψ_s in the strong inversion regime (V)
ψ_{s0}	Surface potential at the source end of the channel referenced to the bulk (V)
ψ_{sL}	Surface potential at the drain end of the channel referenced to the bulk (V)
ψ_{s0}'	Surface potential at the source end of the channel referenced to the bulk , used in the calculation of the drift current component (V)
ψ_{sL}'	Surface potential at the drain end of the channel referenced to the bulk , used in the calculation of the drift current component (V)

Abbreviations

CAD	Computer Aided Design
CPU	Central Processing unit
CMOS	Complementary Metal Oxide Semiconductor
CLM	Channel Length Modulation
DIBL	Drain Induced Barrier Lowering
GCA	Gradual Channel Approximation
MOSFET	Metal Oxide Semiconductor Field Effect Transistor
VLSI	Very Large Scale Integration
HDL-A	Hardware Description Language - Analog part
LabVIEW	Laboratory Virtual Instrument Engineering Workbench
HP VEE	Hewlett Packard Visual Engineering Environment

CHAPTER 1

MOSFET Modeling for CAD

1.1 Introduction

The requirements to be satisfied by a CAD device model for use in circuit simulation are demanding and essentially in conflict. The model should be physically based, representing faithfully the internal electronic mechanisms and the implications of device structure, and should provide a coherent link between fabrication technology, design layout and electrical performance. It should give accurate and continuous representation of device electrical characteristics over the full range of operating modes and conditions.

In the following chapter we shall deal with the MOSFET structure and its basic governing equations, and also we shall discuss the basic requirements implied by CAD applications in order to develop a good model of the MOSFET suitable for analog CAD applications.

1.2 Basic MOSFET electrostatics

In the following section we shall review the basic MOSFET characteristics, and governing equations which will be used to get a suitable model for circuit CAD applications. The MOSFET structure is shown in Fig. 1.1

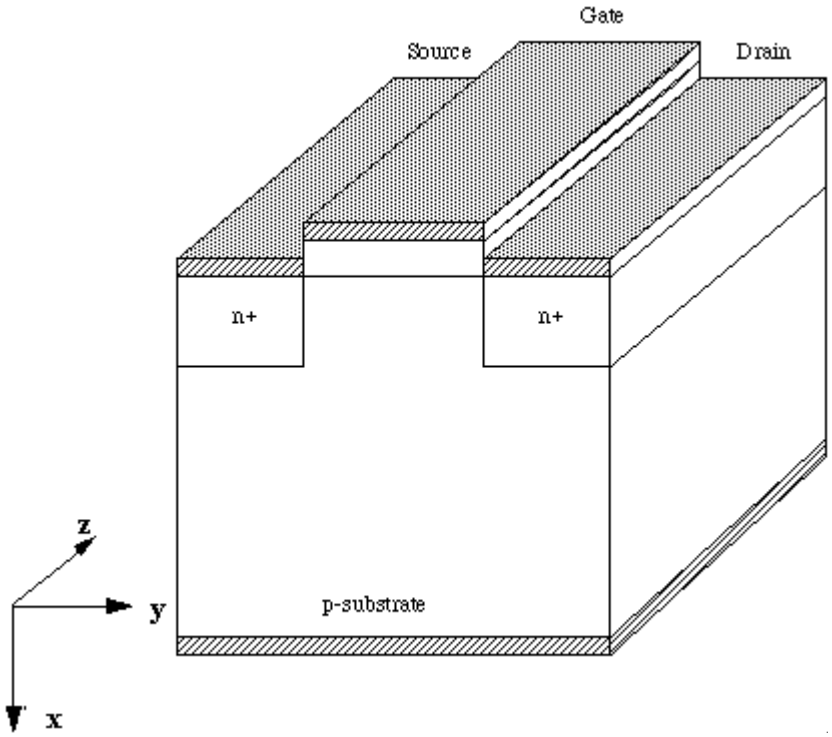

Figure 1.1 *MOSFET structure*

1.2.1 Surface and Fermi Potentials

Fig. 1.2*a* shows the energy band diagram at the middle of the channel. This case corresponds to a device in equilibrium (V_S=V_D=0) and an applied gate voltage V_G that makes the device in inversion i.e. ψ_s>2ϕ_f.

Fig. 1.2*b* shows the same device in the non-equilibrium case (V_D>0), such that we use the quasi-Fermi levels E_{fn} and E_{fp} [1], instead of the Fermi level E_f. A split in the quasi-Fermi level equal to ϕ_c is noticed due to the applied drain bias. This shift is equal to V_D at the drain side of the channel. This is equivalent to assuming that the electron quasi-Fermi levels remains essentially constant over the transition region (between the channel and the drain)[1]. ϕ_c is then the Fermi potential induced by the drain-source bias. In the general case where V_S≠V_D≠0, we have V_S<ϕ_c<V_D.

[1] A corresponding assumption is often made in *pn* junction theory [2]

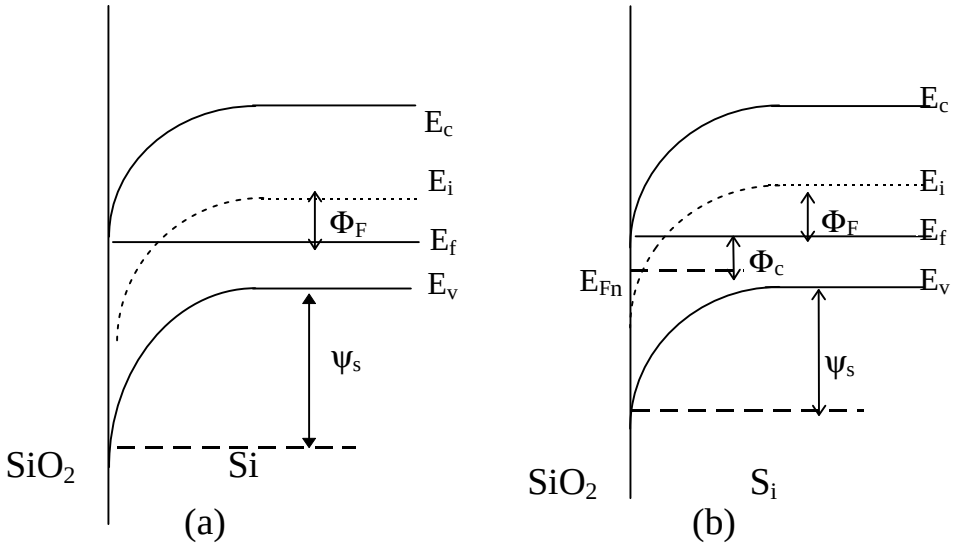

Figure 1.2 *Comparison of the energy band diagram of an inverted n-channel MOS for: (a) the equilibrium case and (b) the nonequilibrium case (applied drain bias).*

A potential convention is always used; ψ_s, ϕ_f, and ϕ_c are positive downward (in the normal operation of the *n*-channel MOS), and negative upwards (in the normal operation of the *p*-channel MOS).

1.2.2 MOS Charges

Fig. 1.3 shows different charges associated with the MOS structure, together with the associated electric field and potential in the *y*-direction. In this section we try to calculate those charges as a function of the surface potential ψ_s.

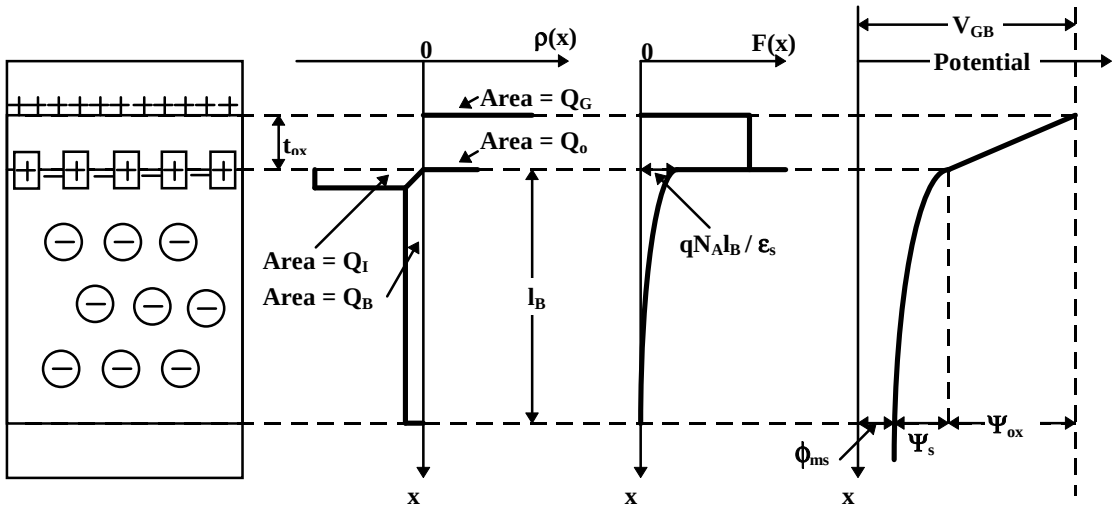

Figure 1.3 *The MOS charges and associated electric field and potential.*

1.2.2.1 The Semiconductor Charge

The semiconductor charge is a major parameter to get a good quantitative description to MOSFET operation, it may be found from the integration of the one dimensional Possions's equation in the x direction. The semiconductor charge is divided into two components the inversion charge Q_i and the bulk charge Q_B, they may be found in all operating regimes of the device, from accumulation to strong inversion, as follows.

In the semiconductor the electrons and holes density can be expressed as [2]:

$$n(x) = (n_i^2 / N_A) e^{\beta(\psi(x)-\phi_c(x))} \qquad (1.2.1)$$

$$p(x) = N_A e^{-\beta\psi(x)} \qquad (1.2.2)$$

where n_i is the intrinsic carrier density per unit volume, N_A is the acceptor impurity density per unit volume, β is the inverse of the thermal voltage ($=1/\phi_t$), ψ_s is the surface potential referenced to the bulk potential, and ϕ_c is the quasi Fermi potential (the difference between E_{fn} at the surface of the semiconductor and E_{fp} in the bulk of the semiconductor).

Substituting equations (1.2.1) and (1.2.2) into the one dimensional Possion's equation, we get

$$\frac{d^2\psi}{dx^2} = -\frac{q N_A}{\varepsilon_s}[e^{-\beta\psi(x)} - 1 - e^{\beta(\psi(x)-\phi_c(x)-2\phi_f)}] \qquad (1.2.3)$$

with ϕ_f defined as the difference between E_i and E_f in the bulk of the semiconductor,

$$\phi_f = \phi_t \ln(\frac{N_A}{n_i}) \qquad (1.2.4)$$

Equation (1.2.3) may be solved to yield :

$$Q_{sc}(\psi_s,\phi_c) = -\frac{\gamma C_{ox}}{\sqrt{\beta}}\sqrt{(\beta\psi_s + e^{-\beta\psi_s} - 1) + e^{-\beta(\phi_c+2\phi_f)}(e^{\beta\psi_s} - 1)} \qquad (1.2.5)$$

where

$$\gamma = \frac{\sqrt{2\varepsilon_s q N_A}}{C_{ox}} \qquad (1.2.6)$$

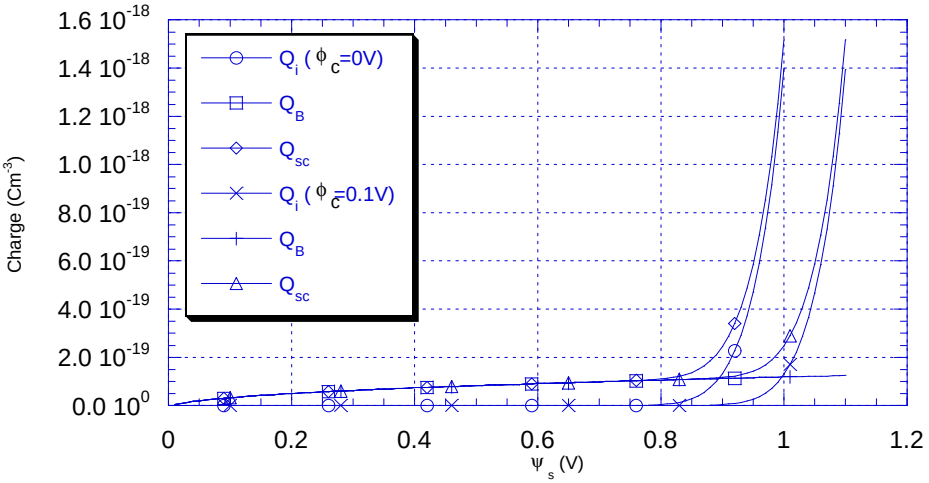

Figure 1.4 *Semiconductor charges versus ψ_s for two values of the quasi Fermi potential ϕ_c.*

and

$$Q_B(\psi_s) = -\frac{\gamma C_{ox}}{\sqrt{\beta}}\sqrt{\beta\psi_s + e^{-\beta\psi_s} - 1} \qquad (1.2.7)$$

Finally, the *inversion* charge can then be computed using

$$Q_i(\psi_s,\phi_c) = Q_{sc}(\psi_s,\phi_c) - Q_B(\psi_s) \quad (1.2.8)$$

Fig. 1.4 shows the above semiconductor charges (Q_{SC}, Q_B & Q_i) versus the surface potential ψ_s, for two values of the quasi Fermi potential. The higher the quasi Fermi potential, ϕ_c the lower is the *inversion* charge.

1.2.2.2 Oxide Charges

Generally speaking, the gate oxide of the MOSFET is not perfect. Oxide charges [2] include the oxide fixed charge, the oxide trapped charge, and the mobile ionic charge. They are represented in device analysis by an effective net oxide charge per unit area Q_{ox} at the Si-SiO_2 interface. Q_{ox} can be regarded as a fixed charge sheet located at the interface, and it is generally a positive charge, refer to Fig. 1.3.

1.2.2.3 Interface Trap Charge

An interface trap is an allowed electronic state, spatially located at a surface (or at an interface), due to the interruption of the periodic lattice structure [3]. It possesses the following properties:

i. It can exchange charge with the silicon. Specifically, they can interact with the silicon conduction band by capturing or emitting electrons and with the valence band by capturing or emitting holes.
ii. Its energy level is located in the forbidden gap or in either band (valence or conduction). However only the energy levels located within the forbidden gap or slightly above or below the band edges, will have the possibility to charge or discharge with bias.

iii. It can be of either type: *donor* or *acceptor*

- A monovalent *donor* trap possesses two states of charge: +1 and 0. Its charge is positive (in thermal equilibrium) when the trap level E_t is above the

Fermi level E_f. Its charge is zero when E_t is below E_f.

- A monovalent *acceptor* trap possesses two states of charge: 0 and -1. Its charge is zero when E_t is above E_f. Its charge is negative when E_t is below E_f.

The interface trap level distribution in the bandgap is typically a rather smooth function of energy. Such a distribution is often called a *continuum* of interface trap levels. The interface trap charge is usually identified by the density of interface trap levels per unit area per electron volt D_{it}, that is the number of interface trap levels per unit area which is present between E_t and E_t+dE_t with energy in electron volts, i.e. $D_{it}=(1/q)(dQ_{it}/\ dE)$.

Changes in occupancy can be produced by changes in gate bias as illustrated in Fig. 1.5 for a *p*-type substrate.

For an acceptor trap, the interface trapped charge can be calculated using Fig. 1.5 as

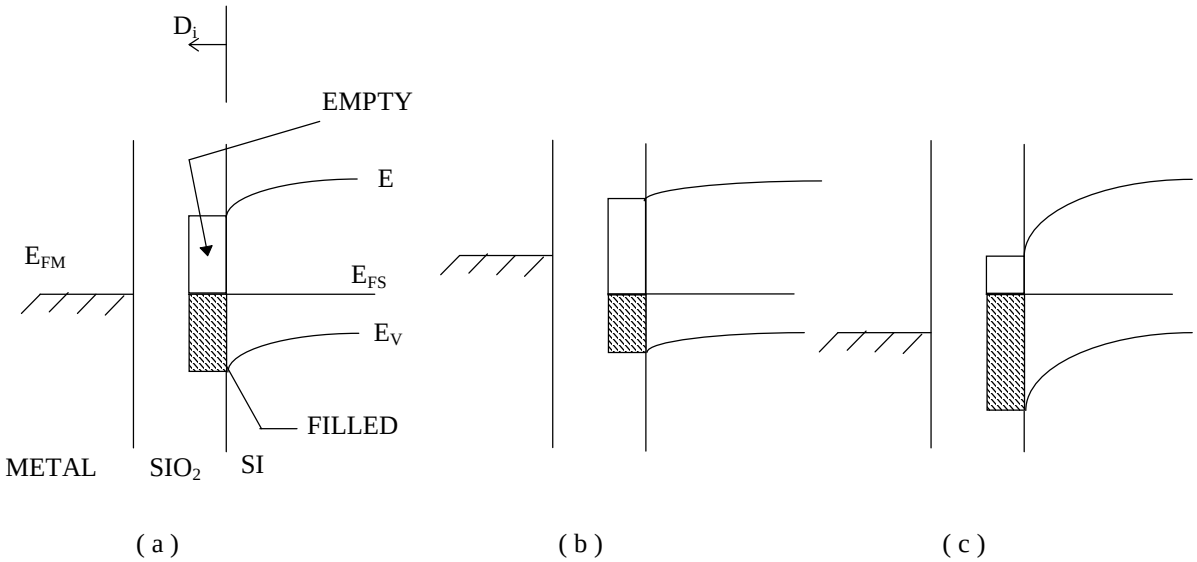

Figure 1.5 *Band-bending diagram showing how interface traps change occupancy with gate bias. The sample is p-type. (a) No gate bias; (b) negative gate bias; (c) positive gate bias.*[4]

$$Q_{ita} = -q\int_{E_v}^{E_c} D_{ita}(E_t)f(E_t)dE_t \tag{1.2.9}$$

where $f(E_t)$ is the Fermi-Dirac distribution function given by

$$f(E_t) = \frac{1}{1+e^{\beta(E_t-E_{fn})}} \tag{1.2.10}$$

Similarly the donor interface trapped charge can be calculated as follows

$$Q_{itd} = q\int_{E_v}^{E_c} D_{itd}(E_t)(1-f(E_t))dE_t \tag{1.2.11}$$

The net interface trapped charge per unit area Q_{it} is given by

$$Q_{it} = Q_{itd} + Q_{ita} \tag{1.2.12}$$

using eqs. (1.2.9), and (1.2.11)

$$Q_{it} = q[\int_{E_v}^{E_c} D_{itd}(E_t)dE_t - \int_{E_v}^{E_c} D_{it}(E_t)f(E_t)dE_t] \tag{1.2.13}$$

where we have defined a total interface trapped density $D_{it}=D_{itd}+D_{ita}$.

Experimentally, it has been shown [4] that interface traps in the upper half of the silicon bandgap are donor like in device grade oxide. There are no reliable measurements to determine whether interface traps in the lower half of the silicon bandgap are donor or acceptor like. However there exist different reliable ways of measuring the total interface trap density D_{it} such as charge pumping technique [5,6]. As will be shown later, it is this total density that affects the device characteristics.

The following assumptions have been introduced to simplify the analytical determination of the interface trap charge Q_{it} [7]:

1. The interface trap density D_{it} is taken to be constant in the whole energy range of interest, referring to Fig. 1.5, that is the average density in the region of interest.

2. In nonequilibrium i.e. an applied drain-source bias, the occupancy of the interface traps is determined by the position of the quasi-Fermi level of the minority carriers.

Using the above two assumptions the trapped charge Q_{it} can be calculated using eq. (1.2.13) in the form

$$Q_{it}(\psi_s,\phi_c) = q\{D_{itd}\,E_g - \frac{D_{it}}{\beta}[\beta(\frac{E_g}{2} - \phi_f + \psi_s - \phi_c) + \ln(1 + e^{-\beta(\frac{E_g}{2}-\phi_f+\psi_s-\phi_c)})]\} \quad (1.2.14)$$

Practically, Q_{it} is expressed in terms of its constant term at flat band plus a variable term

$$Q_{it}(\psi_s,\phi_c) = Q_{it}(0,0) + Q_{it}'(\psi_s,\phi_c) \quad (1.2.15)$$

where

$$Q_{it}(0,0) \approx q[\,D_{itd}\,E_g - D_{it}(\frac{E_g}{2} - \phi_f)] \quad (1.2.16)$$

and

$$Q_{it}'(\psi_s,\phi_c) \approx -q\frac{D_{it}}{\beta}[\,\beta(\psi_s - \phi_c) + \ln(1 + e^{-\beta(\frac{E_g}{2}-\phi_f+\psi_s-\phi_c)})\,] \quad (1.2.17)$$

As shown from the above equations, the nature of the interface traps (*acceptor*- or *donor*-like traps) affects only the constant part of the interface trapped charge $Q_{it}(0,0)$. This constant part can't be practically distinguished from the oxide fixed charge at flat band, and is determined through flat-band voltage measurements (sec. 1.2.3). On the other hand, the variable part of the interface trapped charge $Q_{it}'(\psi_s,\phi_c)$, depends only on the total interface trapped charge density D_{it}. The interface trapped charge is comparable to the total semiconductor charge in subthreshold, and affects the device characteristics in that region, while it is negligible compared to this charge in strong inversion.

Note that for a heavily doped bulk in strong inversion where $\psi_s > 2\phi_f + 6\phi_t$ [1], the quasi Fermi level E_{fn} approaches the conduction band, Fig. 1.5 (c). The upper limit for Q_{it} is then $q(D_{itd}-D_{it})E_g$.

Fig. 1.6 shows the above calculated interface trapped charge, which is assumed to be composed only of acceptor-like traps (i.e. $D_{it}=D_{ita}$ and $D_{itd}=0$),

versus the surface potential for two different values of the quasi Fermi potential ϕ_c, in an *n*-channel MOS transistor. As ϕ_c increases, more levels *emit* their electrons, and Q_{it} decreases. When ϕ_c approaches the valence band edge E_v, Q_{it} tends to zero. On the other hand as ψ_s increases, more levels *trap* electrons, and Q_{it} increases. The interface trapped charge is shown to vary only while ψ_s changes within the range of E_g.

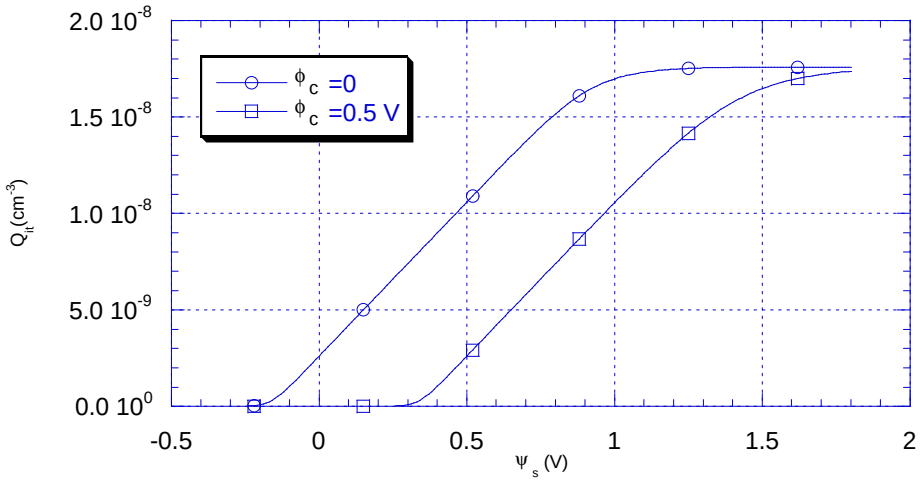

Figure 1.6 *Interface trap charge versus the surface potential.*

1.2.3 The Flat Band Voltage

The flat band voltage, may be defined as the gate-bulk voltage necessary to obtain a zero surface potential ψ_s [3], it expressed as

$$V_{FB} = \phi_{ms} - \frac{1}{C_{ox}}[Q_{ox} + Q_{it}(0,0)] \qquad (1.2.18)$$

In the above equation, ϕ_{ms} is the gate-semiconductor work function difference. This value depends on the gate material (metal, *N*-Poly, or *P*-Poly).

This voltage is usually measured practically, and it is difficult to distinguish its components from such measurements. Any variation in the flat band voltage appears directly as an equal variation in the threshold voltage value.

1.3 The MOSFET Mobility

The mobility of electrons in the inversion layer (called *surface mobility*) is smaller than the bulk mobility, due to *scattering mechanisms*. The effective mobility used in the long channel model must include the effect of the normal field due to the gate. The effect of the longitudinal field on the mobility is important only in short channel devices.

For a given temperature, the value of the surface mobility is found to be only a function of the average normal electric field F_{xav} in the inversion layer, defined by

$$F_{xav} = \frac{F_{xs} + F_{xb}}{2} \tag{1.3.1}$$

where F_{xs} is the value of the normal field at the surface and F_{xb} is its value just below the inversion layer. The experimental data appear to conform to the following relation:

$$\mu = \frac{\mu_o}{1 + \alpha F_{xav}} \tag{1.3.2}$$

where μ_o is the low field mobility, and α is a fitting parameter.

The effective normal electric field at the surface is related to the total charge per unit area below the surface by gauss law:

$$F_{xs} = -\frac{Q_{sc}}{\varepsilon_s} \tag{1.3.3}$$

where Q_{sc} is given by (1.2.5)

Similarly the field just below the inversion layer can be determined by assuming a very thin inversion layer, so that the total charge per unit area below the inversion layer is practically all of Q_B, given by eq. (1.2.7):

$$F_{xb} = -\frac{Q_B}{\varepsilon_s} \tag{1.3.4}$$

Using the above equations, we obtain

$$\mu = \frac{\mu_o}{1 - \frac{\alpha}{2\varepsilon_s}(Q_{sc} + Q_B)} \tag{1.3.5}$$

The effective mobility [8] may be obtained by substituting with eq. (1.3.5) in the drain current equation and integrate from 0 to L on the assumption that ψ_s is linear with y (i.e $d\psi_s/dy \cong (\psi_{sL} - \psi_{s0})/L$), to simplify the integration , thus we obtain

$$\mu_{eff} = \frac{\mu_o}{1 + \theta f_\mu} \tag{1.3.6}$$

where

$$f_\mu = (V_G - V_{FBD}) - 0.5(\psi_{sL} + \psi_{s0}) + \frac{2}{3}\gamma \frac{((\psi_{sL} - \frac{1}{\beta})^{3/2} - (\psi_{s0} - \frac{1}{\beta})^{3/2})}{(\psi_{sL} - \psi_{s0})} \tag{1.3.7}$$

and

$$\theta = \frac{C_{ox}\alpha}{2\varepsilon_s} \tag{1.3.8}$$

1.4 MOSFET Modeling

The reason for MOSFET modeling as any other device modeling is two fold. First, the device designer needs to understand how a device operates and hence is primarily interested in the internal device mechanisms. Second, the circuit designer looks for a quantitative description of the terminal behavior only, which should be as accurate as necessary and as simple as possible. In his part of the overall design process, the circuit designer wants to predict circuit performance by numerically simulating a proposed circuit topology. Generally, he relies on an established process for device fabrication and hence is able to improve model accuracy by introducing fitting parameters into the analytical formulas of his model. Extending this approach may lead to the point where the measured parameters constitute a table and the model acts only as an interpolation routine between neighboring table values. During this process, the

connection to device physics is gradually lost gaining computational efficiency which is the uppermost concern in simulating large circuits. However, this introduces a serious drawback for such models, that they are likely to fail in predicting ahead of time what will happen if some fabrication process parameters are changed. Developing a model is an art involving constant tradeoffs between accuracy and computational time efficiency.

On the other hand, the device designer is also somewhat interested in circuit performance at least of small-scale building blocks, since the devices he is designing are to operate in a circuit environment. He seeks to preserve the connection to device physics in order to be guided by circuit performance criteria in his design process. Ideally, the desired device performance should arise from those criteria and the device design process should result in specifications for a wafer process to be developed. In practice, however, process and device development are carried out simultaneously and device modeling should aid the iterative process of device specification and wafer processing by saving part of the otherwise necessary cycles of the iteration loop.

1.4.1 Numerical MOSFET Modeling

A device simulator calculates the electrical characteristics of devices when structure shape, and impurity profile are given.

The behavior of electronic devices is governed by a set of basic semiconductor equations, these equations are summarized as follows [9]:

1- Poisson's equation

$$\nabla^2 \psi = -\frac{q}{\varepsilon}(p - n + N_D^+ - N_A^-) \qquad (1.4.1)$$

2- The continuity equations

$$\frac{\partial p}{\partial t} = -\frac{1}{q}\nabla . J_p - R + G$$
$$\frac{\partial n}{\partial t} = \frac{1}{q}\nabla . J_n - R + G \qquad (1.4.2)$$

3- The current equations

$$J_p = -q\,\mu_p\, p\nabla\psi - q\,D_p\nabla p - \mu_p kp\nabla T_p$$
$$J_n = -q\,\mu_n n\nabla\psi + q\,D_n\nabla n + \mu_n kn\nabla T_n \qquad (1.4.3)$$

4- The energy balance equations [10]

$$\nabla . S_P - F . J_P + U\omega_p + p\frac{\omega_p - \omega_p^*}{\tau_p} = 0$$
$$\nabla . S_n - F . J_n + U\omega_n + n\frac{\omega_n - \omega_n^*}{\tau_n} = 0 \qquad (1.4.4)$$

where R represents the recombination rate, G the generation rate , S_p and S_n represent the energy flux of holes and electrons respectively, F is the electric field, ω_p and ω_n are the carrier energies, and τ_p and τ_n are the energy relaxation times.

The semiconductor equations contain quantities, such as the recombination (R)/generation (G) rates and the mobilities (μ_n and μ_p), which themselves are the result of complicated physical mechanisms. Therefore, these quantities are not constant but depend on the local values of carrier densities and electric field.

The complete set of nonlinear differential device equations together with the given boundary conditions are then solved numerically using different methods yielding the device's physical characteristics.

The device simulator aims to derive from the input set of physical and technological parameters, the electrostatic potential ψ and quasi-Fermi levels for electrons E_{fn} and holes E_{fp} in space and time. These three quantities yield, in turn, the vector fields of the electric field strength and electric current density. Finally, integration of the first vector along a contour between

respective contacts and the second over respective contact areas results in the terminal characteristics of a device.

1.4.2 Analytical MOSFET Modeling

In order to be used in a circuit simulator where thousands of MOSFETs are present, numerical modeling turns to be ineffective, as it turns to be very time consuming. Analytical models must then be used. An analytical model is simply a system of algebric equations describing the terminal *I-V* performance of the device.

All analytical MOSFET models use the *Gradual Channel Approximation (*GCA) [11] (which will be discussed in the next chapter), which decomposes and simplifies the two-dimensional problem into two analytical one-dimensional problems. One deals with the solution of the oxide field due to the voltage applied between the gate and the Si bulk. The other deals with the current in the channel due to voltage applied between the drain and source terminals. More Details about analytical modeling are given in chapter 2.

The circuit simulator aims only to calculate the voltage and current at every circuit node by a numerical procedure that depends on the terminal *I-V* characteristics of each circuit element. This requires that every circuit element (including the MOSFET) must provide an analytical (closed-form) relation between the terminal voltages and output currents.

1.5 MOSFET Modeling for Analog Circuit CAD

The modeling of MOS transistors for computer-aided design has been driven by the needs of digital circuit designers for many years, but unfortunately these models give poor results when used in analog simulation [8].

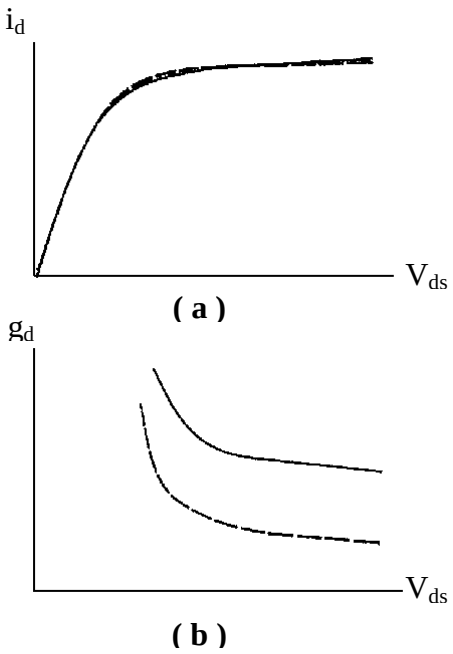

Figure 1.7 *(a) I_D-V_{DS} characteristics as resulting from measurement (solid line) and simulation (dashed line). (b) The output conductance resulting from taking the slopes in (a).*[8]

As an example [8], consider Fig. 1.7(a). It would seem that the model (dashed line) is an adequate representation of the experiment (solid line). Yet, consider the drain-source small-signal conductance g_d, given by the slope of the I_D-V_{DS} characteristics: for the case of Fig. 1.7(a) that slope is given in Fig. 1.7(b), and a very large discrepancy between the model and experiment becomes obvious. To argue about the seriousness of this problem, one needs only to recall that the amplifier voltage gain can be inversely proportional to sum of g_d quantities.

Recently, many laboratories have put a considerable effort into the development of new analog MOS models to comply with the new technological trend towards mixed analog-digital chips, not only for direct interfacing to the physical world, but also for aiding digital systems to increase their performance. It is predicted that in a few years, most chips will contain at least some analog circuits.

1.5.1 The Special Nature of Analog Modeling Needs

From the last discussed example, it becomes obvious that, if somebody claims a model to give a good drain current fit to measurements, all we can conclude is that, maybe, the model can predict satisfactorily the bias point of an analog circuit. Since the design of such a circuit involves much more than just bias point evaluation, many more requirements need to be met by the model before we could call it adequate for analog work.

A MOSFET model for analog circuit design should ideally satisfy the following criteria [12]:

1. The model should, of course, meet common requirements for digital work, such as reasonable *I-V* characteristic accuracy, shift register speed prediction, charge conservation, etc.
2. It should give accurate values for all small-signal quantities as g_m, g_{mb}, g_d, and capacitances. In particular, all of these parameters should be *continuous* with respect to *any* terminal voltage.
3. It should meet the above requirements over large bias ranges, including $V_{SB}\neq 0$, and encompassing the weak, moderate, and strong inversion regions.
4. It should do all of the above over the temperature range of interest.
5. It should do all of the above for any combination of channel width and length values, from the minimum specified upwards. The user should only have to specify the geometrical dimensions for each device, and *one* set of model parameters valid for *all* devices of the same type and independent of dimensions.
6. The model should provide a flag at any attempt to use it outside its limits of validity. For example, if the model is quasi-static and one attempts to use it, say, around the unity gain frequency of the device, a warning should be given to the user that the result may be inaccurate.
7. The model should have as few parameters as possible (but just enough), and those parameters should be linked as strongly as possible to ones

related to the device structure and fabrication processing (e.g. oxide thickness, substrate doping, junction depth). This would allow meaningful worst-case simulations and predictions. Empirical parameters without physical meaning should be avoided as much as possible. This requirement strongly points to the direction of a *physically-based model*.

8. The model should be linked to an efficient parameter extraction method; one could even go so far as to say that parameter extraction should be constantly kept in mind during model development from the beginning. The number of required test devices and tests for parameter extraction should be as small as possible.
9. The model should ideally provide links to device simulators (refer to table 1.1).
10. For application in a circuit simulator, the model also needs to be relatively simple in its formulation to achieve low computer CPU time per model call.

1.6 CAD requirements

In order to develop a *working* model, one should understand the working nature of the circuit simulator which incorporates the model.

The circuit simulator starts an analysis by writing a set of *nodal* equations which describe the elements in the circuit. This set of nodal equations is often a system of transcendental equations, and a nonlinear solution technique known as Newton-Raphson algorithm is applied to the system matrix. The Newton-Raphson algorithm, a method of successive approximations, is an iterative approach to solving a set of nonlinear equations. The circuit simulator starts with an initial guess for every node voltage in the circuit and begins iterating. With each successive iteration, a new set of node voltages is predicted. The solution routine monitors the node voltage of the present iteration and the previous iteration value.

Ideally, at the exact solution, the node voltage between successive iterations should be identical, or the difference between iterative voltage

values should be zero. But because of the way digital computers represent numbers, saying when two numbers are exactly equal can be difficult (because of round-off errors). Because of this difficulty, the circuit simulator monitors the difference between iterative node voltage values and compares the difference with a predefined error tolerance. When the difference between iterative voltage values is less than the error tolerance for every node of the circuit, the circuit simulator terminates the iterative process for that solution point.

1.6.1 Nonconvergence

In addition to the error tolerance limits, the simulator limits the total number of iterations each analysis type is allowed to process. If the iterative node voltages have not satisfied the error tolerance requirements before the simulator exceeds the iteration limit, the simulator *aborts* the simulation and proclaims the infamous *nonconvergence* error message.

One of the main problems that causes nonconvergence in the calculation of the bias point is *model discontinuities*. As an example we consider Level 3 MOSFET SPICE model. Classical MOSFET theories split the transistor curves into the linear region and the saturated region of operation. The device equations in SPICE follow the same regions of operation. But, unlike the real device, SPICE uses separate equations for each region of operation. Because of the mathematical difficulty in writing an equation which describes the entire family of curves, two different sets of equations were written, one for the linear region and one for the saturation region, and joined together. Unfortunately, because of the way the equations were joined, there is a discontinuity in the conductance characteristics (the slope of the I-V curve) of the device.

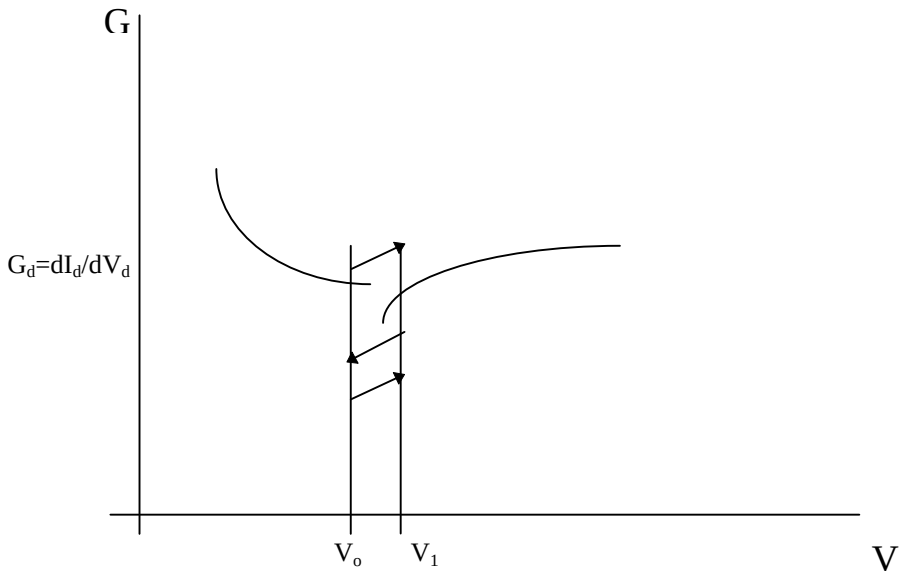

Figure 1.8 *Iterations around a model discontinuity.* [13]

A discontinuity in conductance may lead to problems for the Newton-Raphson algorithm. Fig. 1.8 illustrates the conductance vs. voltage characteristics around one of the model discontinuities. On the first Newton iteration close to the discontinuity, the conductance value leads to a new iterative voltage on the other side of the discontinuity. The next Newton iteration falls on a conductance value which predicts a solution back on the original side of the discontinuity. The third Newton iteration again predicts a solution on the far side of the discontinuity. When SPICE steps close to or on top of a model discontinuity, the Newton-Raphson iterations may begin to oscillate around the discontinuity. These oscillations use up iterations without progressing towards a solution. A solution to this problem is by using mathematical smoothing functions between different operating regions.

1.6.2 The smoothing function

While moving from one region of operation of the MOSFET to the other some variables (voltage, charge, current, ...) may have an upper limit to which they tend. The model thus may have an output characteristic composing of segments of different slopes i.e. discontinuity in the output conductance, that may lead to *nonconvergence* problems in the circuit simulator (refer to Section 1.4.1). Besides, this discontinuity may lead to non-practical solutions if the bias is close to it.

In order to prevent such discontinuities, a smoothing function will be used, this function has the form

$$SF(x, x_o, m) = \frac{x}{\left(1 + \left(\frac{x}{x_o}\right)^m\right)^{(1/m)}} \qquad (1.6.1)$$

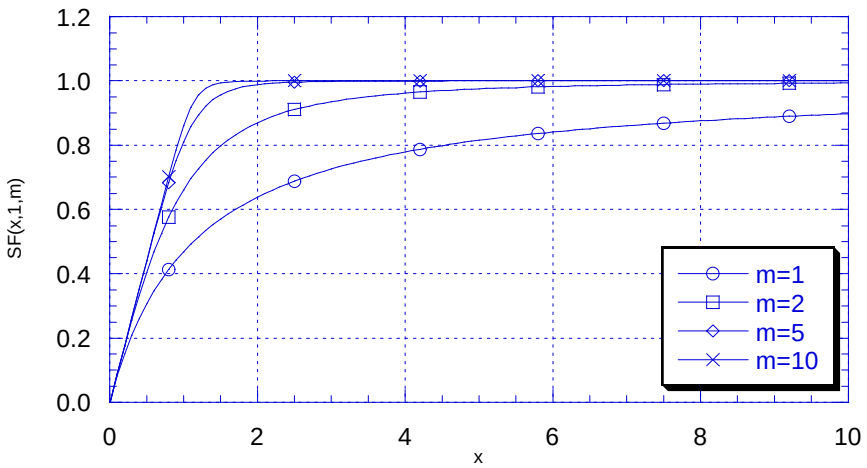

Figure 1.9 *The smoothing function*

and is plotted in Fig. 1.9 for different values of m, and for x_o =1. As shown in Figure, for small values of $x \ll x_o$, the function SF tends to x, as x increases, SF tends to x_o. The parameter m determines the width of the transition (knee) region.

1.7 Overview of various simulators.

Simulator level	Input data	Objective	Example
Process simulator	Heating process Chemical procedure Ion implant condition Chemical environment	Impurity profile estimation Ion implantation optimization Cross-sectional shape	SUPREM
Device simulator	Electrode structure Oxide layer shape Materials Impurity distribution	Threshold and punch-through d.c. characteristics of MOSFETs Wire capacitance and resistance Latchup and soft errors analysis	MINI-MOS [31] PRISM [10]
Circuit simulator	MOSFET parameters Capacitance parameters Resistance parameters Circuit connectivity	Circuit voltage and current Component parameter optimization Mask pattern verification Worst-case prediction	SPICE ELDO
Logic simulator	Gate logic function Rise and fall time Gate connectivity Gate delay scattering	System function check Logic net optimization Logic connectivity check	HILO QuickSim
Behavior simulator	Block functions Block connectivity	System behavior prediction Block level optimization Block connectivity check	SIMU-LINK [MATLAB]

Table 1.1 *Overview of various simulators*

CHAPTER 2

Model Description

2.1 Introduction

The modeling procedure is introduced in this chapter, taking into consideration the requirements for a *good* MOSFET analog model, discussed in the previous chapter.

We note here two main aspects of our modeling approach;

a. The model must describe *accurately* all the operating regions in order to be integrated in a circuit simulator.
b. The current, conductance, and transconductance must be continuous in all regions of operation.

Our main goal in this chapter is to determine the drain current for any combination of terminal voltages. The chapter is divided into two main parts. Throughout the first part, it is assumed that the channel is sufficiently *long* and *wide*, so that edge effects are confined to a negligible part of it. While in the second part we incorporate the short and narrow channel effects to the model. We also assume that the substrate is *uniformly* doped. The doping concentration will be assumed to be *p*-type and the modification to non uniform doping will be discussed later in this chapter.

2.2 Gradual Channel approximation (GCA)

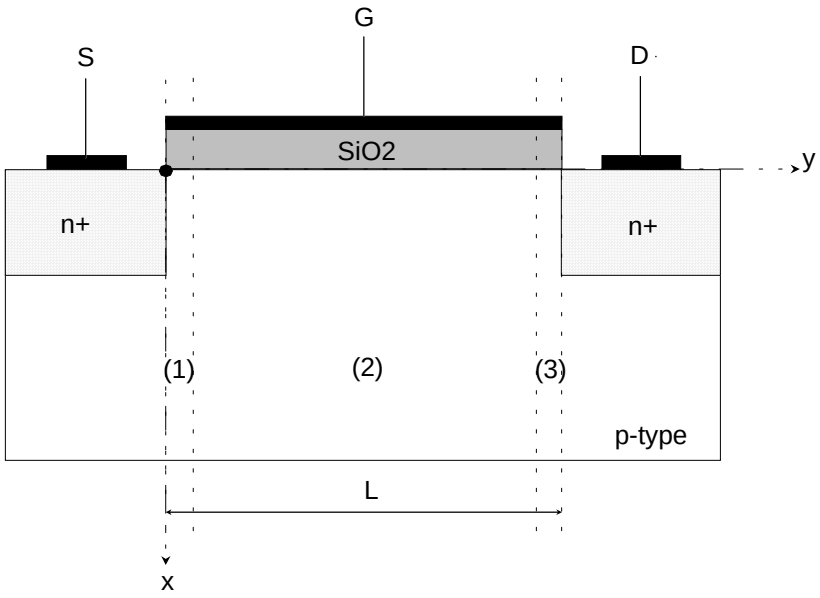

Figure 2.1 *The MOSFET structure.*

Analytical or semi-analytical modeling of MOSFET characteristics is usually based on the so-called *Gradual Channel Approximation* (GCA) [11]. In this approximation, we assume that the gradient of the electric field in the y direction, ∂F/∂y is much smaller than the gradient of the electric field in the x direction ,∂F/∂x. Which enable us to determine the inversion and depletion charge densities under the gate in terms of a one-dimensional electrostatic problem for the direction perpendicular to the channel. By applying of the two dimensional Poisson's equation for the semiconductor, refer to Fig. 2.1 region (2),

$$\frac{\partial F_x}{\partial x} + \frac{\partial F_y}{\partial y} = \frac{\rho}{\varepsilon_s} \qquad (2.2.1)$$

if we assume that the GCA is valid equation 2.2.1 may be approximated to the following one dimensional differential equation

$$\frac{\partial F_x}{\partial x} \approx \frac{\rho}{\varepsilon_s} \qquad (2.2.2)$$

As we approach the source and drain junctions, the GCA becomes invalid (Fig. 2.1 regions (1) and (3)) because of the increasing longitudinal field due to the pn junctions which make $\partial F/\partial y$ comparable or even larger than $\partial F/\partial x$. However, for the long channel MOSFET's these transition regions can be neglected with respect to the total length of the device. In order to account for the effect of these regions, it is necessary to use two-dimensional analysis requiring a numerical solution of 2.2.1.

Validity of the GCA

The validity of GCA can be checked by making rough estimates of the variation in the longitudinal and vertical field components. We will establish expressions that allow the GCA to be checked under strong inversion[1] [11].

$$\frac{\partial F_x/\partial x}{\partial F_y/\partial y} = \left(\frac{\varepsilon_{ox} L}{\varepsilon_{si}}\right)^2 \frac{q(V_{GS} - V_T)^2}{kT.t_{ox}^2.V_{DS}} >> 1 \qquad (2.2.3)$$

For a MOSFET at 300K with L = 1.0μm, t_{ox} = 30 nm, V_{GS}-V_T = 0.5, and V_{DS} = 0.5 V, the left hand side of inequality 2.2.3 is ~ 2300, indicating that the the GCA is a very good approximation for such a MOSFET. This also implies that the GCA can be valid even in submicron MOSFETs, provided that V_{GS}-V_T is not too small.

2.3 The long channel current model

The derivation of the dc drain current relationship recognizes that, in general, the current in the channel of a MOSFET can be caused by both drift and diffusion current. In an NMOSFET we may assume the following resonable approximation :

i- The drain current is mainly carried by electrons .

ii- The current flows almost in the y direction.

iii- No sources or sinks in the channel.

[1] Note that in weak inversion the surface potential along the channel in long channel MOSFETs is almost constant. Thus $\partial F_y/\partial y$ is very small, implying that $\partial F_y/\partial y << \partial F_x/\partial x$. Thus in long channel MOSFET the GCA is valid both in strong and weak inversion regions [11].

Which enable us to reach to the following general relationship of drain current.

1- General Drift-Diffusion current equation in MOSFET:

This is the drift-diffusion drain current of the form [8]

$$I_D(y) = \mu_n W(-Q_i)\frac{d\phi_c}{dy} = \mu_n W(-Q_i(y))\frac{d\psi_s(y)}{dy} + \mu_n W \phi_t \frac{dQ_i(y)}{dy} \qquad (2.3.1)$$

where μ_n is the electron surface mobility in the channel, W is the channel width, Q_i is the inversion charge density per unit area, ϕ_c is the quasi Fermi potential (the difference between E_{fn} at the surface of the semiconductor and E_{fp} in the bulk of the semiconductor), ψ_s is the surface potential referenced to the bulk potential, and ϕ_t is the thermal voltage ($=kT/q$).

The first term is the *drift current component*, while the second term is the *diffusion current component*. In both components, μ_n is the electrons' surface mobility being less than the mobility in the bulk due to surface scattering.

2- Voltage-Charge equation from the Transverse electric field:

In order to eliminate the electron charge density Q_i term in the current-charge equation, a second relationship is required that relates the electron charge density to the applied potentials.
Using the relationship between voltage and charge appearing across the MOS capacitor we have [8]

$$C_{ox}(V_G - \phi_{ms} - \psi_s) = -(Q_i + Q_B + Q_{ox} + Q_{it}) \qquad (2.3.2)$$

where V_G is the gate voltage referenced to the bulk potential, ϕ_{ms} is the metal-semiconductor work function difference, Q_B is the depletion (bulk impurity) charge density per unit area, Q_{ox} is the sum of the effective net oxide charge per unit area at the Si-SiO_2 interface, and Q_{it} is the interface trapped charge density per unit area.

Different approximations have been introduced in order to express the different MOS charges (Q_B, Q_{ox}, Q_{it}) in terms of the applied voltages, then using eq. (2.3.2) to compute the inversion charge density Q_i. The resulting charge is then used in eq. (2.3.1) to determine the drain current; Four main approaches then follow, after them we shall discuss the proposed approach recently developed in ICL[1] and modified by this work.

2.3.1 The classical long-channel Pao and Sah model

The Pao-Sah model [11,14], published in 1966, was the first advanced long channel MOSFET model to be developed. While it retained the GCA, it didn't invoke the depletion approximation and permitted carrier transport in the channel by both drift and diffusion current. The formulation of the drain current equation is therfore general, but as a result requires numerical integration in two dimensions, which limits its application in CAD tools.

Approximations:

i. Gradual Channel Approximation is used.
ii. Constant mobility is assumed.
iii. Uniform substrate doping is considered.

Advantages:

i. It is physically based.
ii. It gives a continuous representation of the device characteristics from weak to strong inversion even to the saturation mode of operation.

Disadvantages:

i. It requires excessive computational requriments since it requires numerical integration in two dimension, rendering it unsuitable to be used for circuit CAD.

[1] Integrated Circuit Laboratory - Ain Shams University - Faculty of Engineering

2.3.2 The charge-sheet based models

The limited practical utility of the Pao-Sah model motivated a search for an approximate advanced analytical model, that is still accurate over a wide range of operating conditions. The charge sheet model, introduced separately by Bacarani and Brews in 1978, has become the most widely adopted long channel MOSFET model that is accurate over the entire range of inversion.

In this model the inversion layer is supposed to be a charge sheet of infinitesimal thickness [11,15,16] (*charge sheet approximation*). The inversion charge density Q_i can then be calculated in terms of the surface potential ψ_s.

The drain current (2.3.1) is then expressed in terms of the surface potential at the source and drain boundaries of the channel.

Approximations:

i. Gradual Channel Approximation is used.
ii. The mobility is assumed to be proportional to the electric field and is constant with position along the channel.
iii. Uniform substrate doping is considered.

Advantages:

i. It is physically based.
ii. It gives a continuous representation of the device characteristics from weak to strong inversion even to the saturation mode of operation.
ii. The charge sheet approximation introduces negligibly small error, and it is more computationally efficient than the classical model.

Disadvantages:

i. The boundary surface potentials cannot be expressed explicitly in terms of the bias voltages applied to the device, but must be found by a numerical process.
ii. The model is not valid in depletion or accumulation.

Different approaches have been introduced to circumvent this disadvantage. In [17-19] it is shown that accurate numerical solutions for these surface potentials can be obtained with negligible computation time penalty. In [20] the surface potentials are computed using cubic splines functions. In [21] and [22], the implicit equation including the surface potential is replaced by an approximate function. Although all of these approaches have given good results, they have neglected the effect of the *interface trap* charge which is important in determining the subthreshold characteristics of the device, namely the subthreshold swing (the gate voltage swing needed to reduce the current by one decade).

2.3.3 Bulk Charge Model

The Bulk Charge model [11], also known as variable depletion charge model, was developed in 1964, describes the MOSFET drain current only in strong inversion but of course has less computational requirements.

Approximations :

i. Drift current component only is considered
ii. Constant surface potential is assumed
iii. I_d considered zero below threshold

Advantages :

i. Less computational time than the charge sheet model

Disadvantages :

i. The subthreshold region not defined

2.3.4 Square law model

This model [1,11] has great popularity, when a first estimate to device operation, or simulating a circuit with a large number of devices is required. This model is obtained from the bulk charge model, on the assumption that $V_{DS} << 2\phi_f+V_{BS}$ [11].

Approximations :

i. Drift current component only is considered
ii. Constant surface potential is assumed
iii. I_d considered zero below threshold
iv. $V_{DS} << 2\phi_f+V_{BS}$

Advantages :

i. Very small computational time than any other model
ii. Suitable for hand calculations

Disadvantages :

i. The subthreshold region is not defined
ii. Overestimates the drain current in saturation region

2.3.5 Approximate models

There exists a large number of introduced approximate models [8,23-29]. All of these models originate from Brews' charge sheet model, where approximations to the surface potentials in various operating regions of the device have been used. This leads to different current equations each valid only in a specific region. The resulting equations are then empirically joined using different mathematical conditions of continuity.

Advantages:

i. They have good accuracy in the desired region of operation.
ii. They are very efficient from the point of view of computational time.

Disadvantages:

i. The error increases in the transition regions between different modes of operations.
ii. They include many non-physical fitting parameters.

2.3.6 Modified charge sheet model

The last discussed MOSFET models, have a common illness, no interface charges are included which play a great role in subthreshold region. So a modified model to the charge sheet model, which include the effect of interface charges is carried out in ICL, and will be presented now [30].

The derivation begins by rewriting equation (2.3.1) in the following form :

$$I_D = I_{D1} + I_{D2} \tag{2.3.6.1}$$

where I_{D1} is due to the presence of drift:

$$I_{D1} = \frac{W}{L}\int_{\psi_{s0}}^{\psi_{sL}} \mu_n(-Q_i)d\psi_s \tag{2.3.6.2}$$

and I_{D2} is due to the presence of diffusion:

$$I_{D2} = \frac{W}{L}\phi_t \int_{Q_{i0}}^{Q_{iL}} \mu_n dQ_i \tag{2.3.6.3}$$

after mathematical manipulation and following the same approximations as charge sheet model we reach the following drain current equations:

$$\begin{aligned} I_{D1} = \frac{W}{L}\mu_{eff} C_{ox}[(V_G - V_{FBD})(\psi_{sL} - \psi_{so}) - \frac{1}{2}(\psi_{sL}^{\,2} - \psi_{so}^{\,2}) \\ - \frac{2}{3}\frac{\gamma}{\beta^{3/2}}((\beta\psi_{sL} - 1)^{3/2} - (\beta\psi_{so} - 1)^{3/2})] \end{aligned} \tag{2.3.6.4}$$

$$\begin{aligned} I_{D2} = \frac{W}{L}\frac{\mu_{eff} C_{ox}}{\beta}[(\psi_{sL} - \psi_{s0}) + \frac{\gamma}{\sqrt{\beta}}(\sqrt{\beta\psi_{sL} - 1} - \sqrt{\beta\psi_{s0} - 1}) \\ - \frac{1}{C_{ox}}(Q_{it}'(\psi_{sL}, V_D) - Q_{it}'(\psi_{s0}, V_S))] \end{aligned} \tag{2.3.6.5}$$

where ψ_{s0} is the surface potential at the source end of the channel, ψ_{sL} is the surface potential at the drain end of the channel, both are referred to the bulk. And their values are computed from the following two implicit equations.

$$\begin{aligned} C_{ox}(V_G - V_{FB} - \psi_{s0}) = \frac{\gamma C_{ox}}{\sqrt{\beta}}\sqrt{(\beta\psi_{s0} - 1) + e^{\beta(\psi_{s0} - V_s - 2\phi_f)}} \\ + \frac{q D_{it}}{\beta}[\beta(\psi_{s0} - V_s) + \ln(1 + e^{-\beta(E_g/2 - \phi_f + \psi_{s0} - V_s)})] \end{aligned} \tag{2.3.6.6}$$

$$C_{ox}(V_G - V_{FB} - \psi_{sL}) = \frac{\gamma C_{ox}}{\sqrt{\beta}}\sqrt{(\beta\psi_{sL} - 1) + e^{\beta(\psi_{sL} - V_D - 2\phi_f)}} + \frac{q D_{it}}{\beta}[\beta(\psi_s - V_D) + \ln(1 + e^{-\beta(E_g/2 - \phi_f + \psi_{sL} - V_D)})] \quad (2.3.6.7)$$

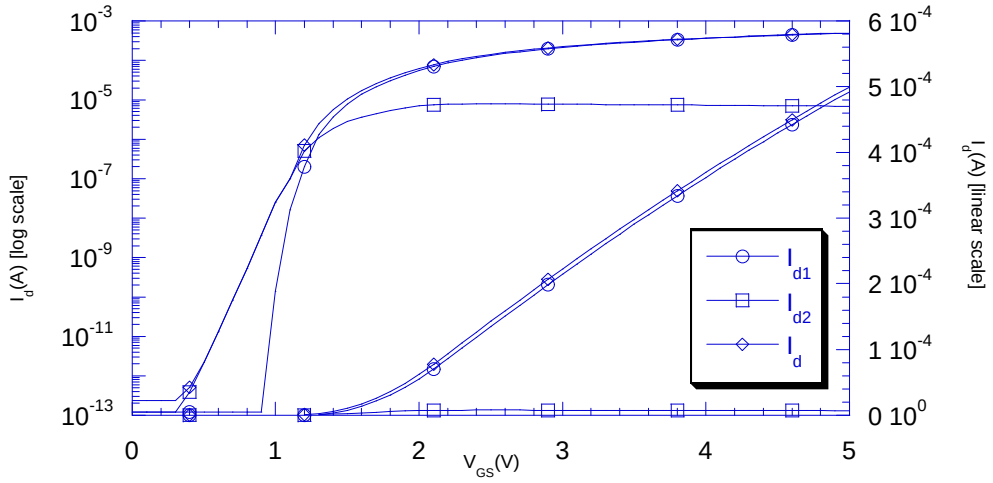

Figure 2.2 *Drain current components: The drift current, I_{d1}, and the diffusion current, I_{d2}. The device has W/L=50μ/6μ, Nsub=5E16 cm-3, and Tox=40 nm.*[30]

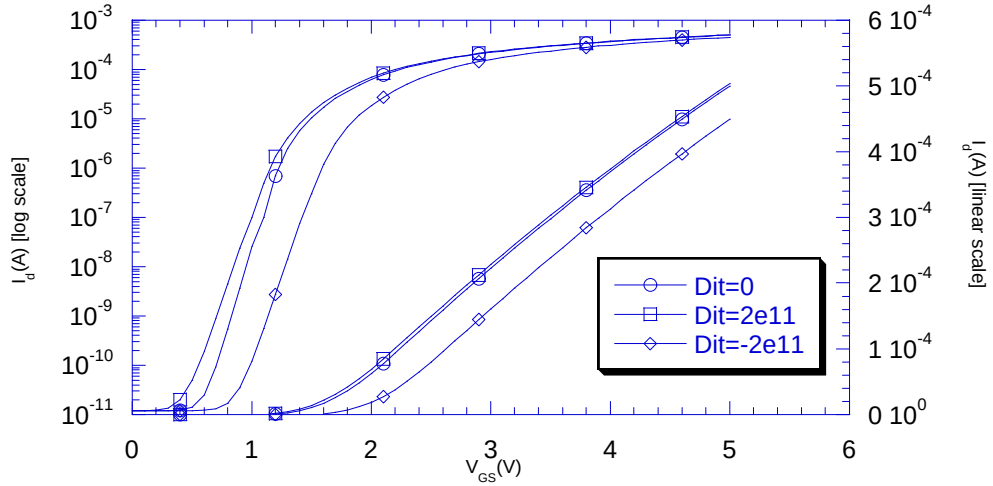

Figure 2.3 *Drain current for different interface trapped charge densities. Positive Dit are donor like traps, while negative Dit are acceptor like. The device has W/L=50μ/6μ, Nsub=5E16 cm-3, and Tox=40 nm* [30].

Fig. 2.2 shows the current components: the drift current component, I_{D1}, and the diffusion current component, I_{D2}. The logarithmic scale is used to show the exponential subthreshold current. The plot is computed by the model using equations (2.3.6.4) and (2.3.6.5). Fig. 2.3, on the other hand, shows the effect of the interface trapped charge density D_{it} on the total drain current. The curve for $D_{it}=2E11$ 1/(cm^{2}e.V.), only donor-like traps are considered to be present, i.e. the interface trapped charge is a positive one. As shown in Fig. 2.3, as V_{GS} increases the surface potential ψ_s increases, more trap levels capture new electrons, empty levels thus decreases and so is the interface trapped charge, thus the curve approaches that for $D_{it}=0$. The curve for $D_{it}=-2E11$ 1/(cm^{2}e.V.), only acceptor-like traps are considered to be present, i.e. the interface trapped charge is a negative one. As shown from Fig. 2.3, as V_{GS} increases the surface potential ψ_s increases, more trap levels capture new electrons, filled levels thus increases and so is the interface trapped charge, thus the curve deviates more from that for $D_{it}=0$. As shown the interface trapped charge affects both the slope of the subthreshold characteristics (shown on the logarithmic scale), as well as the threshold voltage value. It is to be noted that the slope of the subthreshold characteristics is equal for equal densities of interface trapped charge D_{it}, irrelevant of the type of this traps.

2.4 The Short Channel Model

The two major goals of MOSFET scaling are to increase the density and speed of the digital ICs in which such scaled down devices are used. Increasing density of course means using smaller channel lengths and widths, also increasing speed means to increase saturation drain current I_{Dsat} (to allow faster charging and discharging of parasitic capacitance).

Long-Channel MOSFET Behavior	Short-Channel MOSFET Behavior
The threshold voltage V_T is independent of channel length L and channel width W	V_T is decreased as L is decreased, and may be also affected by changes in W
V_T is independent of drain voltage	V_T decreases with increasing V_{DS}
V_T depends on V_{BS} according to equation (2.6.15)	V_T increases less rapidly with V_{BS} than predicted by equation (2.6.15)
The subthreshold current I_{Dst} increases linearly as L decreases	I_{Dst} increases more rapidly than linearly as L decreases
I_{Dst} is independent of drain bias	I_{Dst} increase with increasing V_{DS}
The subthreshold swing S_t is independent of gate length	S_t increases with decreasing L
The drain saturation current I_{Dsat} is independent of V_{DS}	I_{Dsat} increases as V_{DS} increases
I_{Dsat} is proportional to $(V_{GS}-V_T)^2$	I_{Dsat} is proportional to $(V_{GS}-V_T)$
I_{Dsat} is proportional to 1/L	As $L \rightarrow 0$, I_{Dsat} becomes indep. of L

Table 2.1 *Comparison of Long-Channel and Short-Channel MOSFETs C/Cs*

From long-channel current equation discussed in the previous section it is apparent that this may be achieved by either reducing channel length (L), oxide thickness t_{ox}, or both. The long channel equation predicts an indefinite increase in I_{Dsat} by this decrease in L and t_{ox}, seeming to imply that only the limitations of process technology (and not device effects) prevent the manufacture of even smaller, higher-performing MOSFETs.

However, as process technology improved to the point where channel lengths smaller than ~ 1 μm were fabricated, it turned out that MOSFETs began to exhibit phenomena not predicted by the long channel MOSFET models. Such phenomena were thus termed *short channel effects.*

Table 2.1 show us a brief comparison between long and short channel MOSFETs model which will be discussed in the following sections.

Two- and three-dimensional analyses can be carried out numerically with the help of a computer [31]. However, such analyses, although accurate, do not provide a simple model for efficient calculation. Thus, much has been done on the way to simplification by using empirical approximations and semi-empirical approaches. In these approaches, usually the complex two- or three-dimensional phenomena are broken down into simple, separate phenomena *examined one at a time*. A number of simplifying assumptions are then made, and relatively simple relations are derived. Often such techniques are characterized by an attempt to maintain the general form of the *I-V* relations for the long- and wide-channel devices, and to *stretch* these relations by modifying them somewhat so that they can be used in the case of short and/or narrow channels.

2.4.1 Channel Length Modulation

The GCA is assumed to be valid in the whole channel, except in the regions near the source and the drain. The net effect can then be taken into account by replacing the channel length L in the current equations by an equivalent channel length L_{eff}, in which the GCA is still valid. It is now required to calculate this effective channel length.

A) Subthreshold Operation

Since the channel is nearly depleted of carriers, we can use the abrupt *p-n* junction approximation to compute the length of the depletion regions

near the source and drain [32,33], i.e. applying the depletion approximation for these two regions and solving Poisson's equation in the *x*-direction, we get

$$L_s = \sqrt{\frac{2\varepsilon_s}{q N_A}(V_{bi} + V_s - \psi_{s0})} \qquad (2.4.1)$$

$$L_d = \sqrt{\frac{2\varepsilon_s}{q N_A}(V_{bi} + V_D - \psi_{sL})} \qquad (2.4.2)$$

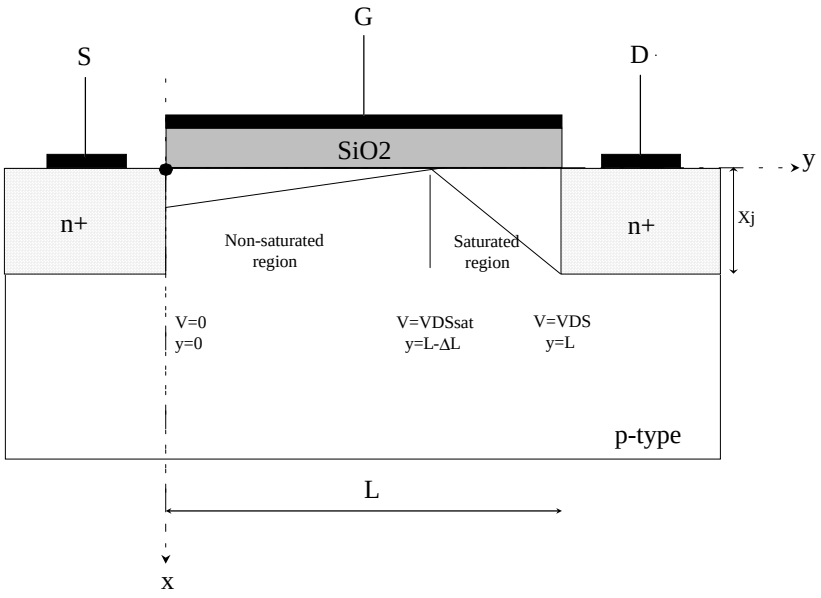

Figure 2.4 *Schematic representation of a MOSFET in saturation, where the channel is divided into a non-saturated region and a saturated region.*

where L_s and L_d are the lengths of the source and drain depletion regions respectively, V_{bi} is the built in potential of the source and drain regions, $V_{bi}=\phi_t ln((N_A N_{sd})/n_i^2)$, ψ_{s0} and ψ_{sL} are the surface potentials at the source and drain ends of the channel respectively referenced to the bulk.

The channel length L in the diffusion current component (which represent subthreshold conduction) is replaced by the effective channel length equal to $(L-L_s-L_d)$.

B) Strong Inversion Operation

When a MOSFET is biased in saturation, the GCA fails in a small region near the drain. This so-called saturated part of the channel is characterized by a two-dimensional electric field pattern. Hence it is natural to describe the channel in terms of a two region model, as indicated in Fig. 2.4.

The long channel model discussed in the previous chapter takes into consideration the strong inversion saturation operation by allowing the inversion charge near the drain to drop to very small values (pinch-off condition) and the current is continuous from the linear to the saturation region.

Fig. 2.4 shows a transistor in saturation with V_{DS} greater than V_{DSsat}. The channel cannot support more voltage than V_{DSsat}, since it becomes pinched off when the voltage across it reaches that value. The *excess* voltage V_{DS}-V_{DSsat} must then be dropped between the drain and the tip of the channel. Such a nonzero voltage can only exist over a region of nonzero length ΔL, as shown. If V_{DS} is raised still further, more excess voltage must be dropped across this region. To support this voltage, the region must widen, and the inversion layer will shrink somewhat in length. This channel length shortening ΔL is found to be of the form [34]:

$$\Delta L = L\frac{\sqrt{V_{sl}^2 + 2A(1+BI_{Dsat})(V_D - V_{Dsat})} - V_{sl}}{A(1+BI_{Dsat})} \qquad (2.4.3)$$

where

$$\begin{aligned} V_{sl} &= F_{\max} L \\ A &= qN_A L^2 / 2\varepsilon_s \\ B &= [\ln(x_j / d_{inv}) - 1] / (qN_A W v_{\max} x_j) \end{aligned} \qquad (2.4.4)$$

2.4.2 Velocity Saturation

As indicated in the previous section, the long channel model takes into consideration the strong inversion saturation operation by allowing the inversion charge near the drain to drop to very small values, i.e. pinch off, thus the carrier velocity is assumed to approach infinity. This description works reasonably well for long-channel devices, but the notion of an infinite carrier velocity is, of course, unphysical. Instead, current saturation is better described in terms of a saturation of the carrier velocity when the electric field near the drain becomes sufficiently high.

An approximation often used for the carrier mobility to represent this effect is [21]

$$\mu_{eff} = \frac{\mu_g}{\left[1+\left(\frac{\mu_g F_x}{v_{\max}}\right)^m\right]^{1/m}} \qquad (2.4.5)$$

where μ_g is the mobility including the gate scattering effects (equal to the effective mobility taking only the gate field scattering effect into consideration, calculated in Section 1.4), F_x is the lateral electric field approximated by the average value $F_x=(\psi_{sL}-\psi_{s0})/L$, and $m=2$ for electrons, and $m<2$ for holes. Note that the functional form of the effective mobility is the same as the smoothing function (Section 1.6), with $x=\mu_g$, and $x_o=F_x/v_{max}$ which is plotted in Fig. 1.9 for different values of m.

The long channel current model discussed above does not include the effects of velocity saturation in the channel at high drain-source bias. An extension of this model, incorporating velocity saturation, is to consider the effect of velocity saturation on the saturation voltage V_{DSsat}.

In order to calculate V_{DSsat}, taking the effect of velocity saturation, an analysis is carried to get the following results :

$$I_{Dsat} = \beta_g V_L^2 \left[\sqrt{1+\left(\frac{V_{GT}}{V_L}\right)^2} - 1\right] \qquad (2.4.6)$$

where

$$\beta_g = C_{ox}\mu_g \frac{W}{L} \qquad (2.4.7)$$

is the transconductance parameter, and $V_{GT} = V_G - V_T$.

$$\begin{aligned} V_L &= F_{\max} L \\ F_{\max} &= F_x(L) \end{aligned} \qquad (2.4.8)$$

$$V_{DSsat} = V_{GT} - \frac{I_{Dsat}}{\beta_g V_L} = V_{GT} + V_L - \sqrt{V_{GT}^2 + V_L^2} \qquad (2.4.9)$$

We use here a modification to eq. (2.4.9), in order to improve the accuracy of V_{DSsat} calculation, by substituting V_{GT} with $V_{GT}/(1+FB)$, where FB is given by $FB = 1/(2(1+2\phi_f+V_S)^{½})$. The physical origin of this $(1+FB)$ factor is to try to compensate for the variation of the bulk charge with potential neglected while calculating the current to get equation (2.4.6).

This last equation for V_{DSsat} is of course meaningful only above threshold where $V_G > V_T$.

In order to incorporate this velocity saturation effect in our model, we have to limit the drain-source voltage V_{DSsat}. To avoid model discontinuities, we perform this limiting using the smoothing function (refer to Section 1.6). Thus in model equations we use a modified drain-source voltage, namely $V_{DS1} = SF\ (V_{DS}, V_{DS\,sat}, 10)$, which approaches V_{DS} in the linear region when $V_{DS} < V_{DSsat}$, and tends to V_{DSsat} in saturation when $V_{DS} > V_{DSsat}$.

As mentioned above, the drain-source saturation voltage V_{DSsat} tends to zero below threshold, and so does the modified drain-source voltage V_{DS1}. Since the drift current component also tends to zero below threshold, this does not affect the accuracy of the model. But for the diffusion current component we can't use this modified drain-source voltage during its calculation. Another drain-source voltage V_{DS2} is used that tends to V_{DS} below threshold, and to V_{DS1} above threshold. The modified drain-source voltages used in the calculation of the drift and diffusion current components are thus given by

$$V_{DS1} = \frac{V_{DS}}{[1 + (\frac{V_{DS}}{V_{DSsat}})^{10}]^{1/10}} \qquad (2.4.10)$$

$$V_{DS2} = V_{DS}(1 - X1) + V_{DS1} X1 \qquad (2.4.11)$$

where

$$X1 = \frac{(V_G / V_T)^{15}}{1 + (V_G / V_T)^{15}} \tag{2.4.12}$$

and

$$V_T = 2\phi_f + 6\phi_t + V_S + \gamma\sqrt{2\phi_f + 6\phi_t + V_S} \tag{2.4.13}$$

2.4.3 Drain induced barrier lowering

It has been observed experimentally that the threshold voltage does not remain the same if the length *L* is reduced. As the channel length continues to decrease, the depletion layer of the drain starts to interact with the source-channel junction to lower the source junction potential barrier. This is known as *drain induced barrier lowering* (DIBL).

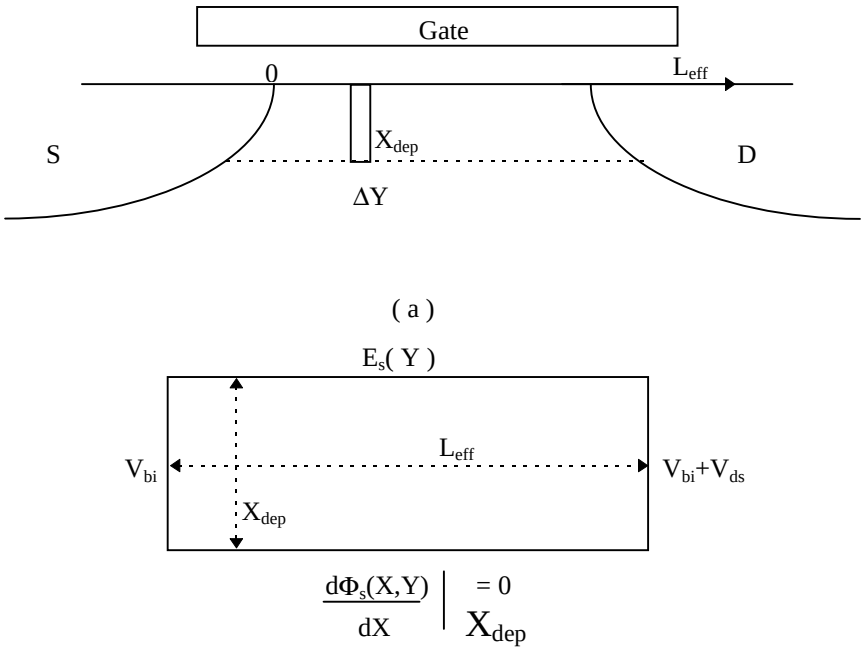

Figure 2.5 *Diagram showing (a) the Gaussian box used in the quasi-two-dimensional analysis, (b) the boundary conditions for solving eq. (2.4.14).* [35]

The lowering of the source barrier allows electrons to be injected into the channel regardless of the gate voltage. As a result, the gate voltage loses control of the drain current in the subthreshold regime.

To describe this effect analytically, we have two approaches:

i. The charge sharing approach [32,33].

i . Solving Poisson's equation in the depletion region, between the source and drain region [35-37].

We use here the second approach as it yields a better representation of the DIBL as shown in [36].

Solving Poisson's equation in the depletion region was done by many authors [33,34,36], each introducing his own simplifications. In our model, we use the method introduced recently by Liu [35], as it gives satisfactory results in representing the threshold voltage shift produced by the DIBL. The derivation is demonstrated as shown below:

Here, we proceed to develop a model for the distribution of the surface potential, ψ_s. From such a model, it is possible to calculate the interface potential near its minimum, which defines the barrier for charge injection into the channel. In principle, this involves the solution of a two-dimensional Poisson's equation for the whole device, using proper boundary conditions.

By applying Gauss' law to a rectangular box of height X_{dep} and length Δy in the channel depletion region Fig. 2.5 and neglecting mobile carrier charge, the following equation can be derived:

$$\varepsilon_s \frac{X_{dep}}{\eta} \frac{\partial F_y(y)}{\partial y} + \varepsilon_o \frac{V_G - V_{FB} - \phi_s(y) - V_S}{T_{ox}} = q\, N_A\, X_{dep} \qquad (2.4.14)$$

where $F_x(y)$ is the lateral surface electric field. ϕ_s is the surface potential referenced to the interior bulk potential at $V_S = 0$, V_G and V_S are the gate and source potentials referenced to the bulk potential respectively. The depletion layer thickness, X_{dep}, is equal to

$$X_{dep} = \sqrt{\frac{2\varepsilon_s(\phi_{si} + V_S)}{q N_A}} \qquad (2.4.15)$$

where $\phi_{si}=2\phi_f$ is the surface potential at the threshold of surface inversion, and η is a fitting parameter.

The first term on the left hand side of eq. (2.4.14) is equal to the net electric flux entering the Gaussian box along the *y* direction. The second term represents the electric flux entering the top surface of the Gaussian box. There is no electric flux passing through the bottom of the Gaussian box.

The solution to eq. (2.4.14) under the boundary conditions of $\phi_s(0)=V_{bi}$ and $\phi_s(L)=V_{DS}+V_{bi}$ is

$$\phi_s(y) = V_{sL} + (V_{bi} + V_{DS} - V_{sL})\frac{\sinh(y / l)}{\sinh(L / l)} + (V_{bi} - V_{sL})\frac{\sinh[(L - y) / l]}{\sinh(L / l)} \qquad (2.4.16)$$

In eq. (2.4.16), $V_{sL} = V_{GS} - V_{tho} + \phi_{si}$ represents the long-channel surface potential, and $V_{tho} = V_{FB} + qN_aX_{dep}T_{ox}/\varepsilon_o + \phi_{si}$ represents the long channel threshold voltage. V_{bi} is the built-in potential between the source-substrate and drain-substrate junctions, and *l* is the characteristic length defined as

$$l = \sqrt{\frac{\varepsilon_s T_{ox} X_{dep}}{\varepsilon_o \eta}} \qquad (2.4.17)$$

Note that X_{dep} is assumed to be a constant when solving eq. (2.4.14). In reality, X_{dep} is a function of the drain voltage and the channel length [35]. One may treat the term X_{dep}/η in eq. (2.4.17) as an average of the depletion layer thickness along the channel.

At a given V_G, V_B, V_D, the channel potential distribution calculated using eq. (2.4.17) is plotted in Fig. 2.6 for devices of different channel lengths.

The model [35] predicts a large variation in potential along the channel for devices with short-channel length even when the drain voltage is low. The

channel potential has a minimum at y_o which can be found by solving the equation $d\phi_s(y)/dy = 0$. The minimum value of channel potential increase, i.e. the potential barrier for electron flow from source to drain will decrease, with decreasing channel length and increasing the drain voltage. Location y_o and minimum potential ϕ_s can be obtained by solving

$$\phi_{smin} = \phi_s(y_o)$$
$$\frac{\partial \phi_s}{\partial y}\Big|_{y=y_o} = 0 \qquad (2.4.18)$$

For $L>>l$ and small y, eq. (2.4.16) can be approximated as

$$\phi_s(y) = V_{sL} + (V_{bi} + V_{DS} - V_{sL})e^{(y-L)/l} + (V_{bi} - V_{sL})e^{-y/l} - (V_{bi} + V_{DS} - V_{sL})e^{-L/l} \qquad (2.4.19)$$

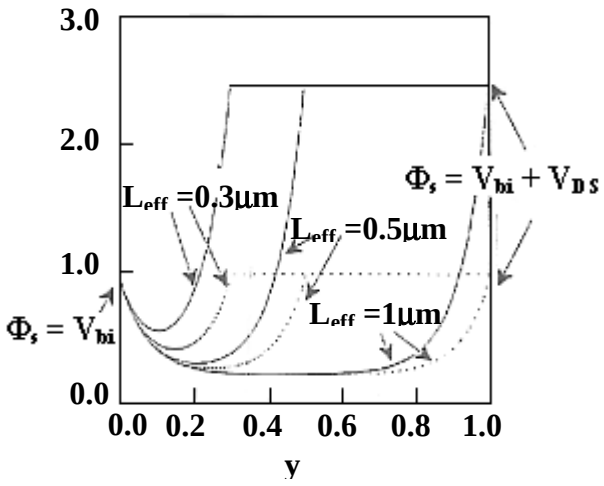

Figure 2.6 *Calculated surface potential along the channel for different channel lengths. The dashed lines show the data for V_{DS}=0.05V and the solid lines show the data for V_{DS}=1.5V.* [35]

Using eqs (2.4.18) and (2.4.19), y_o can be found to be

$$y_o = \frac{L}{2} - \frac{l}{2}\ln\left(\frac{V_{bi} - V_{sL} + V_{DS}}{V_{bi} - V_{sL}}\right) \qquad (2.4.20)$$

Then using eq. (2.4.16), ϕ_{smin} can be found using eq. (2.4.14)

$$\phi_{smin} = V_{sL} - (V_{bi} + V_{DS} - V_{sL})e^{-L/l} + 2\sqrt{(V_{bi} - V_{sL} + V_{DS})(V_{bi} - V_{sL})e^{-L/l}} \qquad (2.4.21)$$

Thus, defining the threshold voltage as the gate voltage which causes ϕ_{smin} to be equal to $2\phi_f$, V_{th} can be solved as [35]

$$V_{th}(L) = V_{tho} - \Delta V_{th} \qquad (2.4.22)$$

where

$$\Delta V_{th} = \frac{2V_1 + V_2(1 - e^{-L/l}) + 2\sqrt{V_1^2 + V_1 V_2(e^{L/l} - 1)}}{4\sinh^2(L/2l)} \qquad (2.4.23)$$

and

$$\begin{aligned} V_1 &= V_{bi} - \phi_{si} \\ V_2 &= V_1 + V_{DS} \end{aligned} \qquad (2.4.24)$$

Figures 2.7 and 2.8 show this threshold shift given by eq. (2.4.23), versus the channel length L and the drain-source voltage V_{DS} respectively, compared to numerical simulations, obtained from [35].

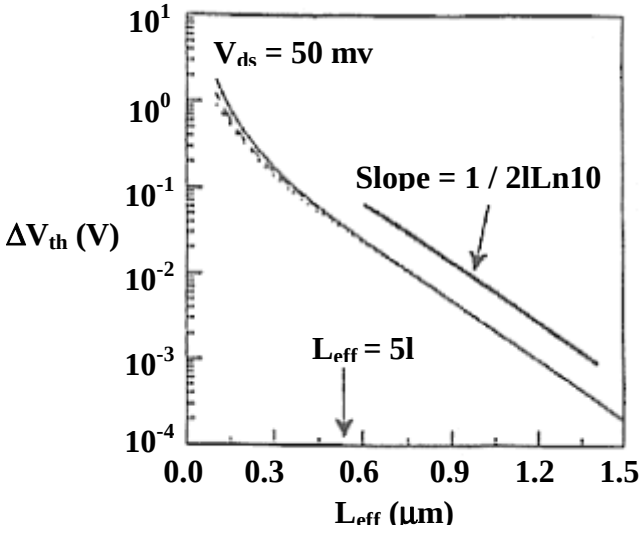

Figure 2.7 *Calculated V_{th} shifts versus channel length at V_{DS} = 0.05 V. The continuous line denotes numerical calculations, while the dashed one is obtained by eq. 2.4.23* [35].

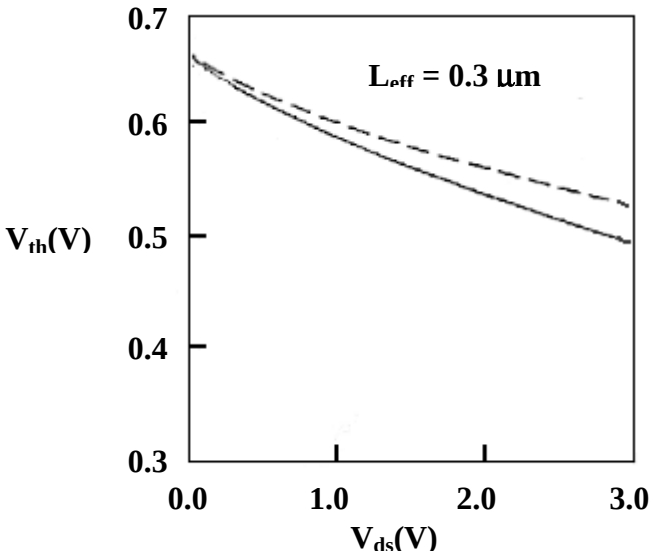

Figure 2.8 *Calculated V_{th} shifts versus the drain voltage V_{DS} at a channel length of 0.3µm. The continuous line denotes numerical calculations, while the dashed one is obtained by eq. 2.4.23.*[35]

Although the calculated l from eq. (2.4.17) has the correct order of magnitude and function form, exact values of l need to be extracted from actual devices because of the unknown parameter η. The extraction of l can be done by fitting the experimental data of $\log(\Delta V_{th})$ versus L_{eff} in the region of $L_{eff} > 5l$. Based on Fig. 2.7, the slope of the fitted straight lines is equal to $1/(2l \ ln \ 10)$. According to, experimentally extracted l's versus the depletion layer thickness X_{dep} for several technologies suggest that l is proportional to $X_{dep}^{2/3}$, i.e. not proportional to $X_{dep}^{½}$ as suggested by 2.4.16. This can be interpreted as saying η is also a function of X_{dep}. An empirical relation for l has been established from experimental data , this emprical relation is [35]:

$$l = 0.1(y_j T_{ox} X_{dep}^2)^{1/DSB} \qquad (2.4.25)$$

where $DSB=3.0$ that's to say that l is proportional to $(\phi_{si}+V_S)^{1/DSB}$, refer to eq. (2.4.15). In our model this proportionality exponent (DSB in the last eq.) is taken as a model parameter which determines the variation of threshold voltage with the substrate bias.

Referring to Section 1.3.3, we recall that any variation in the flat band voltage appears directly as an equal variation in the threshold voltage value.

This fact is used in our model to account for the threshold shift caused by the DIBL by defining an *effective* flat band voltage given by

$$V_{FB}' = V_{FB} + \Delta V_{th} \tag{2.4.26}$$

where ΔV_{th} is that threshold shift caused by DIBL.

In this section, the drain induced threshold voltage shift was analyzed in terms of the lowering of the injection barrier between the source and the channel in the subthreshold regime. In strong inversion, however, the injection barrier is reduced owing to the effect of the gate-source bias, and will eventually disappear well above threshold. Hence, the importance of DIBL will decrease with increasing gate-source voltage and should gradually be phased out [21]. To represent this effect in our model, the shift in the threshold voltage ΔV_{th} is well reduced to zero above threshold by the following relations

$$V_T = 2.5(2\phi_f + \phi_t + V_S + \gamma\sqrt{2\phi_f + 6\phi_t + V_S}) \tag{2.4.27}$$

$$X2 = \frac{(V_G / V_T)^5}{1 + (V_G / V_T)^5} \tag{2.4.28}$$

$$V_{F'B}' = V_{FB} + \Delta V_T(1 - X2) \tag{2.4.29}$$

2.4.4 Series Resistance

The parasitic source/drain resistance due to carrier crowding in the source-to-channel and channel-to-drain regions, is an important device parameter which can affect the MOSFET performance significantly. While scaling down MOSFET channel length, parasitic resistance will not be proportionally scaled, and will become more and more of a problem. The straightforward and accurate way of modeling parasitic resistance effect leads to a complicated drain current expression. In order to make calculations

efficient, we model the parasitic resistance using simple expressions. Fig. 2.9 shows a MOSFET with parasitic resistance R_s and R_d. Assume $R_s=R_d=R_t/2$.

The effect of this parasitic resistance is apparent only in strong inversion where the drop across it is not negligible, thus we take into account its effect by considering strong inversion operation as follows:

The intrinsic MOSFET model described in the last sections can be converted to an extrinsic model by expressing the intrinsic bias voltages (upper case subscripts) in terms of their extrinsic counterparts (lower case subscripts), i.e.

$$V_{DS} = V_{ds} - I_D R_t \tag{2.4.29}$$

$$V_{GS} = V_{gs} - I_D R_s \tag{2.4.30}$$

Thus the drain drift current reduces to [8]

$$I_D = \frac{W}{L_{eff}} C_{ox} \frac{\mu_{eff}}{(1 + \frac{W}{L_{eff}} \mu_{eff} C_{ox} R_t V_{GT})} (V_{GT}) V_{ds} \tag{2.4.31}$$

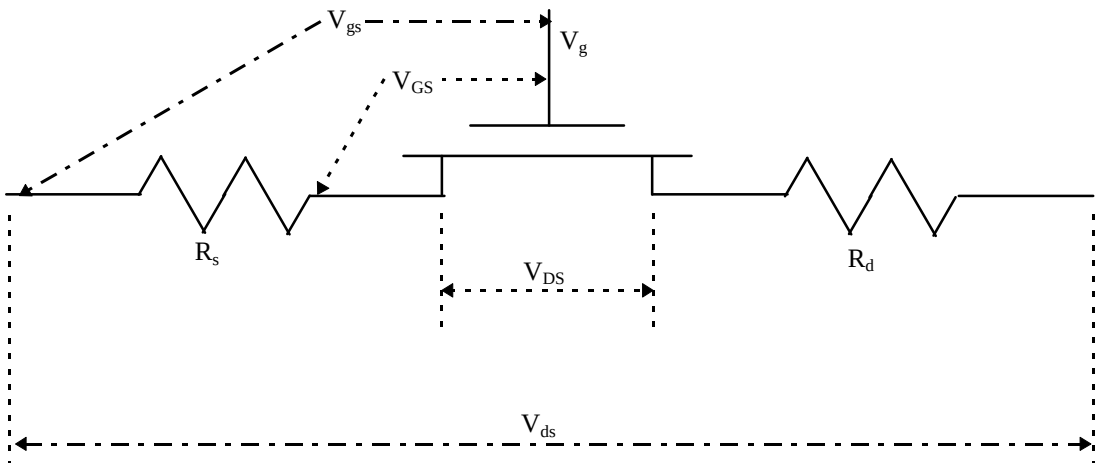

Figure 2.9 *MOSFET with parasitic source and drain resistance.*

We thus represent the effect of the parasitic series resistance by a reduction in the mobility as shown in the previous equation by defining an effective mobility taking into account the series resistance effect , μ_{eff}', as follows:

$$\mu_{eff}' = \frac{\mu_{eff}}{(1+\frac{W}{L_{eff}}\mu_{eff} C_{ox} R_t V_{GT})} \tag{2.4.32}$$

Also, due to the parasitic resistance, the saturation voltage V_{DSsat} will be larger than what is predicted by eq. (2.4.9). A calculation of the modified I_{DSsat} yield [34]:

$$I_{DSsat} = \beta_g V_L{}^2 \frac{\sqrt{1+2\beta_g V_{gt} R_s + (V_{gt}/V_L)^2} - (1+\beta_g V_{gt} R_s)}{(1-(\beta_g V_L R_s)^2)} \tag{2.4.33}$$

where V_L is given by eq. (2.4.8). The extrinsic saturation voltage, V_{dssat}, can be obtained in the form:

$$\begin{aligned} V_{dssat} &= V_{DSsat} + R_t I_{DSat} \\ V_{dssat} &= V_{gt} + \left(R_d - \frac{1}{\beta_g V_{ss}} \right) I_{DSsat} \end{aligned} \tag{2.4.34}$$

2.5.5 Impact Ionization and the Substrate Current

As characteristic device sizes are scaled down, the electric field in the MOSFET channel increases and, in the saturation regime, the high field region near the drain occupies a large fraction of the device channel. This leads to the so-called hot carrier effects which manifest themselves as a superlinear increase of the drain current in the saturation regime and in the degradation of device parameters with time.

The physics of impact ionization can be described as follows: The high electric field near the drain leads to electron heating. Some electrons acquire so much energy from the electric field that they can cause generation of electron-hole pairs. The generated holes lead to a substrate current whereas the generated electrons increase the drain current. The process of

electron-hole pair generation can be described by a generation rate per unit length $\alpha(F_x)$ defined by [2,34]

$$\alpha(F_x) = A\exp(-B/F_x) \tag{2.4.35}$$

where F_x is the tangential electric field, A and B are impact ionization constants.

The substrate current, I_{st} due to impact ionization can thus be calculated by the following formula [38]:

$$I_{st} = I_D \int_{L_{eff}-\Delta L}^{L_{eff}} \alpha(F_x)dx \tag{2.4.36}$$

The tangential field is computed by its average value

$$F_{xav} = \frac{V_{DS} - V_{DSsat}}{\Delta L} \tag{2.4.37}$$

ΔL is the length of the *impact ionization region* given by

$$\Delta L = l\ln\left(\frac{2(V_{DS} - V_{DSsat})}{lE_{\max}}\right) \tag{2.4.38}$$

where l is a parameter which characterizes the electric field distribution in the impact ionization region. l depends on T_{ox} and the junction depth y_j and is given by

$$l = \sqrt{\frac{\varepsilon_s}{\varepsilon_{ox}} T_{ox} y_j} \tag{2.4.39}$$

Equation (2.4.38) has been obtained by applying Poisson's equation to the saturated part of the channel (refer to Fig. 2.4) [39].

Substituting with equations (2.4.35), (2.4.37), and (2.4.38) into eq. (2.4.36) we get

$$I_{st} = A I_D (V_{DS} - V_{DSsat})\exp(-\frac{Bl}{V_{DS} - V_{DSsat}}) \tag{2.4.40}$$

2.5 Narrow Channel Effect

The reduction of channel width causes an increase of the threshold voltage [2]. This shift is related to the depletion region spreading laterally in the substrate along the width (see Fig. 2.10). Assuming that the lateral extension of the depletion region is approximately cylindrical, the total charge in the depletion region, Q_B, is thus

$$Q_B = q\,N_A\,LW\,X_B(1+\frac{\pi}{2}\frac{X_B}{W}) \qquad (2.5.1)$$

This last equation shows that the bulk charge has increased by a factor of $(1+\pi X_B/2W)$. Therefore, the threshold voltage is increased by

$$\Delta V_{th} = \frac{\pi q\,N_A\,X_B^2}{2\,C_{ox}\,W} = \pi\frac{\varepsilon_s\,T_{ox}}{\varepsilon_{ox}\,W}(\phi_{si}+V_S) \qquad (2.5.2)$$

where ϕ_{si} is the surface potential referenced to the source potential at threshold ($=2\phi_f$).

Similar to the effect of the DIBL, this shift is added to the effective flat-band voltage as in eq. (2.5.25).

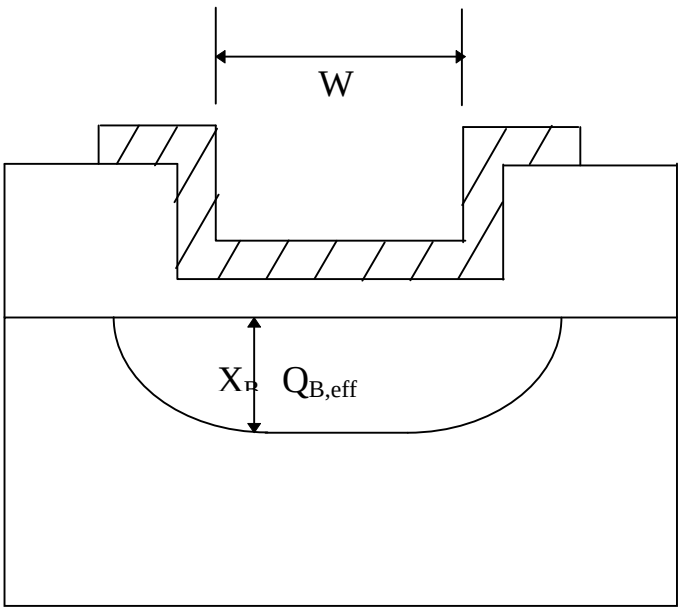

Figure 2.10 *Depletion charge along the width of the transistor.*

2.6 Non uniform doping [40]

In the model discussed above, a uniform substrate doping has been assumed. For practical MOSFETs this assumption is not valid, since ions are normally implanted in the region between the source and the drain, to control threshold voltage and punchthrough of the drain region to the source. Implantation has two aspects, first, new ions are introduced into the depletion layer. Second, these newly introduced ions modify the depletion width. Both effects modify MOSFET behavior, in both strong or weak inversion regions.

2.6.1 Non uniform doping profile

In dealing with the enhancement mode MOSFET having an ion-implanted channel, the impurity profile chosen plays a main role in the prediction of the device behavior and also in the simulation time taken by CAD tools especially for large numbers of devices. The most simple model achieved using the so called box profile (step profile) is suitable for CAD tools and is now implemented in BSIM3 model, but this profile proves to give an error as large as a few tenths of a volt in terms of the threshold voltage at a substrate bias of the order of a few volts. This discrepancy is quite large considering a usually designed threshold voltage in the order of 1 V. But also the use of Gaussian profile which is of course in agreement with the implantation process give rise to complicated calculations required by the simulator due to the presence of the error function as a direct result of using the Gaussian profile in Poisson`s equation. The chosen profile is a power profile which for some order range gives a good agreement with the Gaussian profile, it takes the following form :

$$N(y)=N_B+(N_o-N_B)(1-(x/D)^n) \qquad (2.6.1)$$

where N_B represents the bulk impurity concentration, N_o represents the impurity concentration at the channel surface, D represents the total depth

of the implanted layer at the final step of fabrication, x is the in-depth distance from the channel surface and n is a positive real number determining the shape of the impurity profile.

Using Fig. 2.11 we may calculate the value of N_o from the assumption of constant implanted dose; i.e.

$$Dose = \int_0^D (N(y) - N_B)dx \qquad (2.6.2)$$

which yields N_o in the form :

$$N_o = (1+1/n)(Dose/D)+N_B \qquad (2.6.3)$$

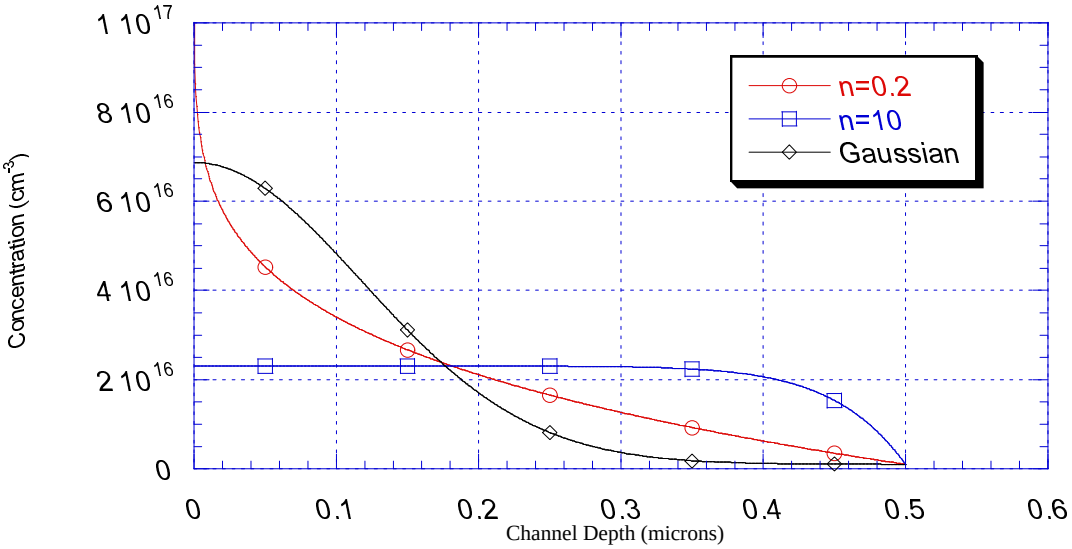

Figure 2.11 *Comparison between Gaussian profile and suggested profile using equation (2.6.1) for n=0.2 and n=10*

From Fig. 2.11 it is clear that the value of n=0.2 will give a behavior close to the Gaussian one, while n=10 will give a behavior close to the box profile discussed earlier. So we shall take the value of n=0.2 in our model. Now if we substitute by the impurity profile into the one dimensional Poisson`s equation we may solve it to get the depletion width as follow :

i) For W ≤ D

$$\frac{2}{n+2}(\frac{N_o}{N_B}-1)(\frac{W}{D})^{n+2}-\frac{N_o}{N_B}(\frac{W}{D})^2+\frac{V}{V^*}=0 \qquad (2.6.4)$$

ii) For W ≥ D

$$W=D\sqrt{1+\frac{V}{V^*}-\frac{1}{n+2}(n\frac{N_o}{N_B}+2)} \qquad (2.6.5)$$

where $V=2\phi_f - V_B$, $V^*=qN_BD^2/(2\varepsilon_s)$ with V_B being the substrate bias, ϕ_f is the Fermi potential, and ε_s is the dielectric constant of the substrate material. The depletion width will play a main role in our model as will be shown in the next section. The critical value of V at which W=D is determined by direct substitution in (2.6.4) or (2.6.5), if we denote this value by V_{thro} we obtain :

$$V_{thro}=\frac{1}{n+2}(n\frac{N_o}{N_B}+2)V^* \qquad (2.6.6)$$

2.6.2 Model implementation

In our model we assume that the effect of the implanted layer is the modification of MOSFET parameters which is doping dependent such as Fermi voltage ϕ_f, and body factor γ. Of course this variation is from high bulk doping when the depletion layer width is much smaller than D to light bulk doping when it is much greater than D, also this variation must be simple and continuous to fulfill the simulator requirements. So we use the smoothing function discussed in Section 1.6 of the form $SF(1,1/W_n,m)$

The parameters are suggested to vary according to the following simple equation :

$$\theta=\theta_l+SF(W_n).(\theta_h-\theta_l) \qquad (2.6.7)$$

where θ represents the parameter of interest, which is doping dependent, suffix *l* stands for lightly doped bulk (N_B), and suffix *h* stands for highly doped bulk N_o.

The dependent parameters which are chosen in our model are Fermi voltage (ϕ_f), body factor (γ), and fixed oxide charge (N_{ox}).

The high and low doping values will be shown below :

$$\phi_{fl} = \phi_T . \ln(\frac{N_B}{n_i}) \quad (2.6.8)$$

$$\phi_{fh} = \phi_T . \ln(\frac{N_o}{n_i}) \quad (2.6.9)$$

$$\gamma_l = \frac{\sqrt{2.q.\varepsilon_s . N_B}}{C_{ox}} \quad (2.6.10)$$

$$\gamma_h = \frac{\sqrt{2.q.\varepsilon_s . N_o}}{C_{ox}} \quad (2.6.11)$$

$$N_{oxl} = N_{ox} + Dose \quad (2.6.12)$$

$$N_{oxh} = N_{ox} \quad (2.6.13)$$

where n_i is the intrinsic concentration of the semiconductor material, ϕ_T is the thermal voltage and C_{ox} is the oxide capacitance.

2.6.3 Effect on threshold voltage

Now we shall use the proposed model to calculate the threshold voltage dependence on the substrate bias and compare the results with the experimental data.

The used formula is the usual formula for large channel MOSFET which is :

$$V_T = V_{FB} + 2\phi_f + \gamma\sqrt{2\phi_f - V_{bs}} \quad (2.6.15)$$

where V_{FB} is the flat band voltage which depends on $N_{ox.}$

We shall refer to the sample devices by MOS1, MOS2 and MOS3 where their parameters are as shown in Table 2.2. The obtained results are shown in Fig. 2.12, and the percentage error in V_T is plotted in Fig.2.13.

From Fig. 2.12 it is clear that, the results obtained using the proposed model are in good agreement with the experimental results.

Sample	MOS1	MOS2	MOS3
t_{ox} (Angstroms)	500	710	300
N_B (atom/cm^3)	7x10^{14}	1.8x10^{15}	2.5x10^{16}
Dose (atom/cm^2)	1x10^{12}	2.2x10^{11}	5.5x10^{11}
D (microns)	0.3187	0.3586	0.3928

Table 2.2 *Sample devices parameters*

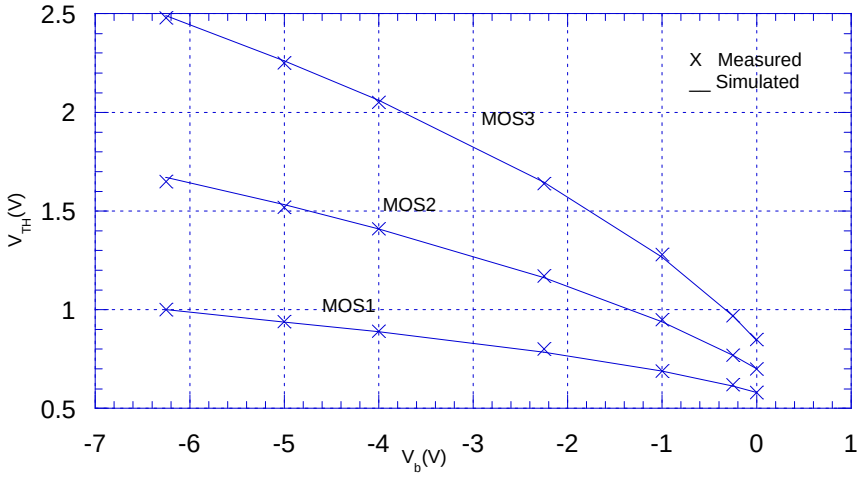

Figure 2.12 *Obtained results for sample devices in Table 2.2*

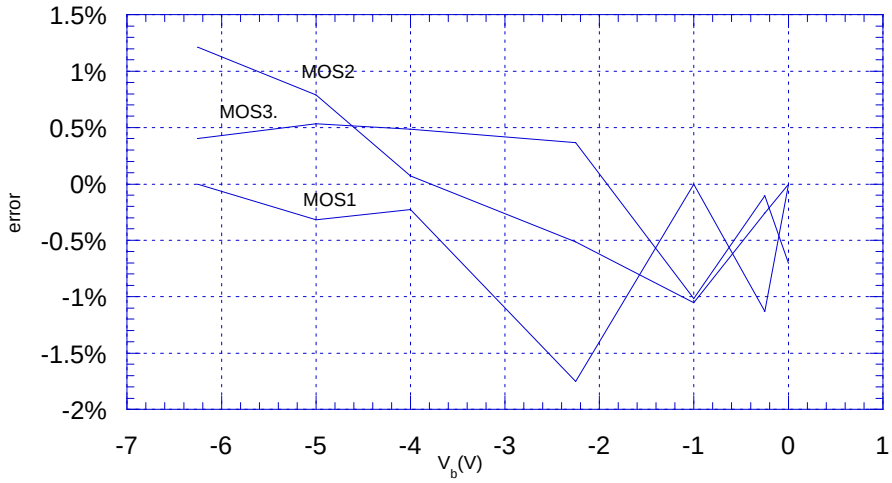

Figure 2.13 *Percentage error in the threshold voltage calculations for sample devices in Table 2.2.*

Since the slope of the drain current in subthreshold region depends mainly on the body factor, it is clear that this model will predict the behavior in this region. Fig. 2.14 shows the drain current versus gate voltage for the sample device MOS3, and Fig. 2.15 shows the body factor variation for the same sample.

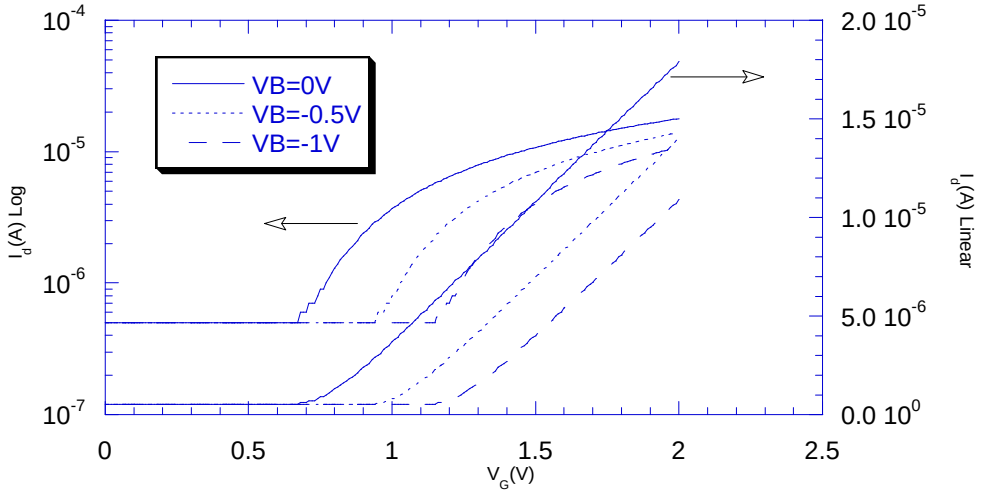

Figure 2.14 *Drain current dependence on the substrate bias at subthrethold region .*

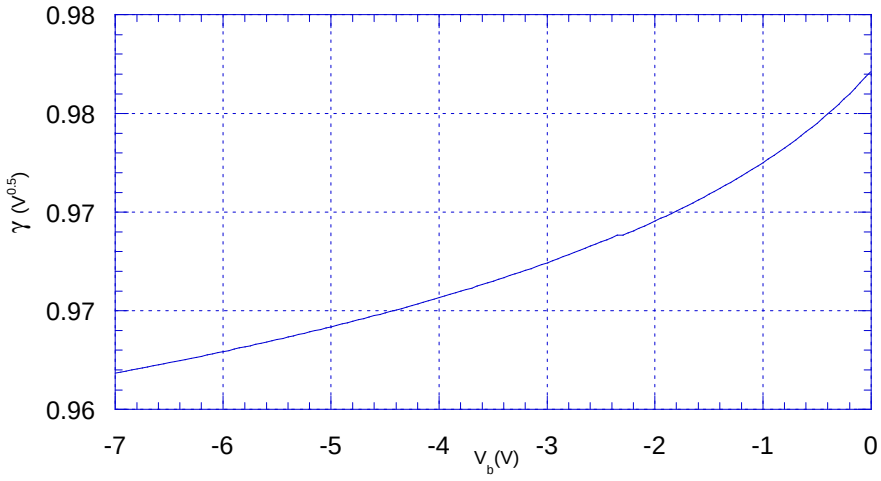

Figure 2.15 *Variation of the body factor (γ) parameter for sample device MOS3*

2.7 Temperature effects

MOS transistor characteristics are strongly temperature-dependent [2,8,39]. The threshold voltage is found to exhibit an almost linear decrease with temperature, thus as temperature increases, the drain current also increases due to the decrease in threshold voltage. The current is also affected by temperature through the carrier mobilities, since also the effective mobility is decreased with temperature.

Temperature effects are included in the model through the following parameters: The parameter n_i, the concentration of intrinsic carriers, E_g, the energy gap and μ_o, the low field mobility, where all depend on temperature through the following semi-empirical relations [2,39,41]:

$$n_i = 1.45x10^{10}\left(\frac{T}{300}\right)^{1.5} e^{\left[\frac{qE_g}{2K}\left(\frac{1}{300}-\frac{1}{T}\right)\right]} \quad (2.7.1)$$

$$E_g = 1.16 - 7.02x10^{-4}\frac{T^2}{T+1108} \quad (2.7.2)$$

and

$$\mu_o(T) = \mu_o\left(\frac{300}{T}\right)^{1.5} \quad (2.7.3)$$

CHAPTER 3

Measurements and Parameter Extraction

3.1 Introduction

In the previous chapter the proposed model was presented, and the model equations have several parameters. Some of these parameters are process and technology dependent, others are fitting parameters, but all of them play a major role in the determination of the device characteristics. Our purpose in this chapter is the determination of these parameter values, to best fit our devices. The first step to achieve this purpose is the development of an automated measurement procedure, the second step is to present an extraction algorithm.

Finally we develop an optimization algorithm to best fit the obtained data. This optimization algorithm and its implementation will be discussed in the next chapter.

3.2 Model Parameters

The model parameters, defined by the equations of the preceding chapter, are listed in Table 3.1:

Table 3.1 *Model parameters.*

Name	Description	Default	Units
L	Channel length	20.0	μm
W	Channel width	20.0	μm
DEL	Lateral diffusion into channel from drain and source diffusion	0	μm
DEW	Total channel width reduction	0	μm
rj	Source-Drain junction depth	0.5	μm
Tox	Oxide thickness	20.0	nm
Dose	Ion implantation dose	0.0	cm^{-2}
D	Implanted layer depth at final step of fabrication	0.5	μm
nimp	Parameter to control the implanted layer shape	0.2	-
mimp	Non uniform doping dependent parameters knee factor	5	-
VTO(1)	Threshold voltage at V_S=0, for a large channel length L	0	V
Gamma(2)	Body factor	0	$V^{1/2}$
PHI(3)	Surface potential at threshold	0	V
VFB	Flat-band voltage	0	V
Nsub	Effective substrate doping	1.0E+16	$1/cm^3$
Nsd	Effective source-drain doping	1.0E+19	$1/cm^3$
Pms(4)	Work function difference (if Pms is not given, it is computed intern al ly using the parameter TPG)	0	V
TPG(4)	Gate material type (metal: TPG=0 , P-poly: TPG=1, N-poly: TPG=-1)	-	-

Table 3.1: (continued).

Name	Description	Default	Units
Nox(4)	Effective number of the oxide charge density per unit area	1.0E+10	$1/cm^2$
Dit	Interface trapped charge density (+ve: donor like, and -ve: acceptor like).	0	$1/cm^2$-.eV
Muo	Low field mobility	650.0	$cm^2/V.$-sec
THETA	Normal field mobility coefficient	0.05	1/V
vmax	Maximum drift velocity of carriers	1.0E+7	cm/sec
beta	Mobility lateral field knee factor	2.0	-
xsat	Saturation voltage knee factor	10.0	-
Ileak	Leakage current of the source-drain junctions	1.0E-12	A
AI	Impact ionization pre-exponential constant	1.0	1/V
BI	Impact ionization exponent constant	1.0E+6	V/cm
Rt	Series resistance of the source and drain terminals	10	Ohm
Ld(5)	DIBL characteristic length (if Ld is not given it is calculated internally)	0	μm
DSB	Bulk effect on the threshold voltage	3	-

(1) This parameter is optional. If it is not given, it is calculated internally using $V_{tho} = V_{FB} + \phi_{si} + \gamma(\phi_{si})^{0.5}$.

(2) This parameter is optional. If it is not given, it is calculated internally using $\gamma = \frac{\sqrt{2.q.\varepsilon_s.N_{sub}}}{C_{ox}}$.

(3) This parameter is optional. If it is not given, it is calculated using $\phi_f = \phi_T . \ln(\frac{N_{sub}}{n_i})$.

(4) This parameter is discarded if either *VTO* or *VFB* is given.

(5) If this parameter is not given, it is calculated internally using $ld = \sqrt{\frac{\varepsilon_s T_{ox} X_{dep}}{\varepsilon_o \eta}}$.

3.3 Measurement Procedure

In the next section we shall discuss the measurement requirements which is the first stage to get good parameter extraction scheme.

3.3.1 Required equipment and samples

In order to carry the required automated measurements, the following equipment is required as shown in Fig. 3.1.

- IBM-PC with labVIEW[1] [42] (or HP VEE[2]) software
- A device analyzer (e.g. HP4142 Modular DC Source/Monitor)
- Probe Station (or suitable casing for device connections)
- Printer (optional)

note that: we may replace the HP4142 by the system in Fig. 3.2

[1] Laboratory Virtual Instrument Engineering Workbench. © National Instruments Corporation.

[2] Hewlett Packard Visual Engineering Environment. © Hewlett Packard Corporation.

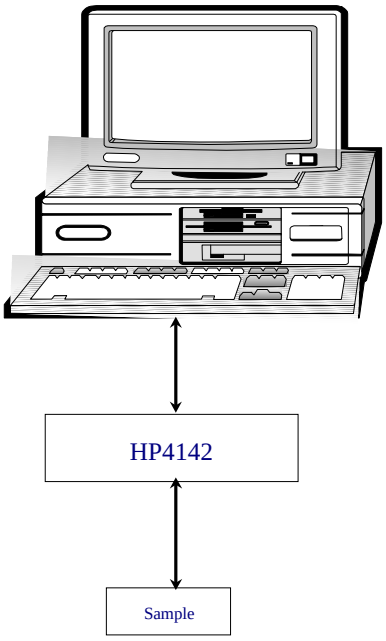

Figure 3.1 *Automated measurement using HP4142*

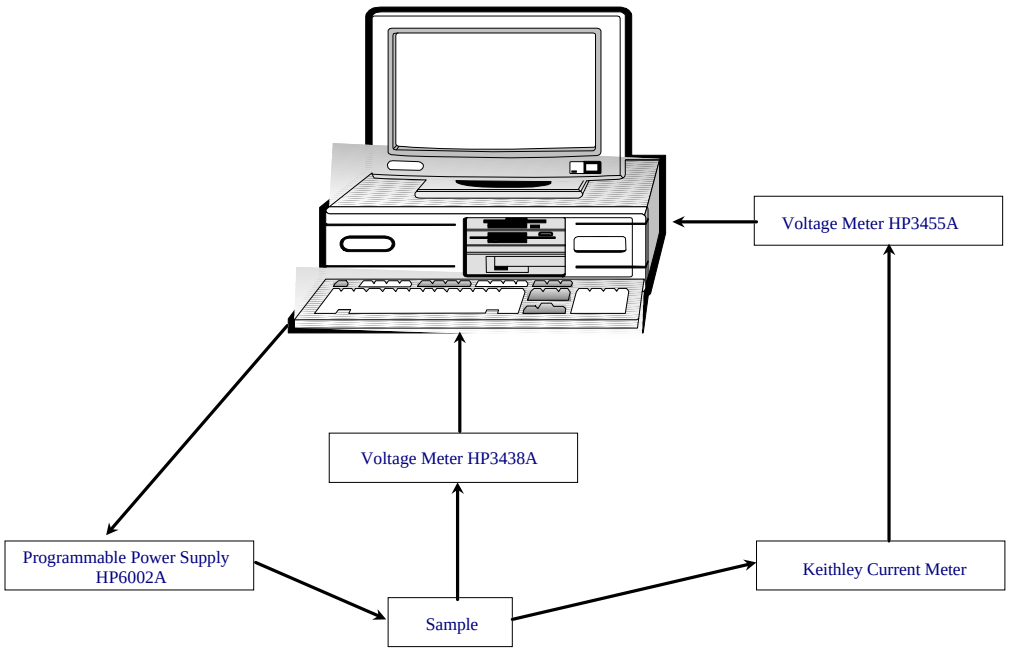

Figure 3.2 *Automated measurement connections*

Devices needed for measurements

One large size device and two sets of smaller size devices are needed, as shown in Fig. 3.3.

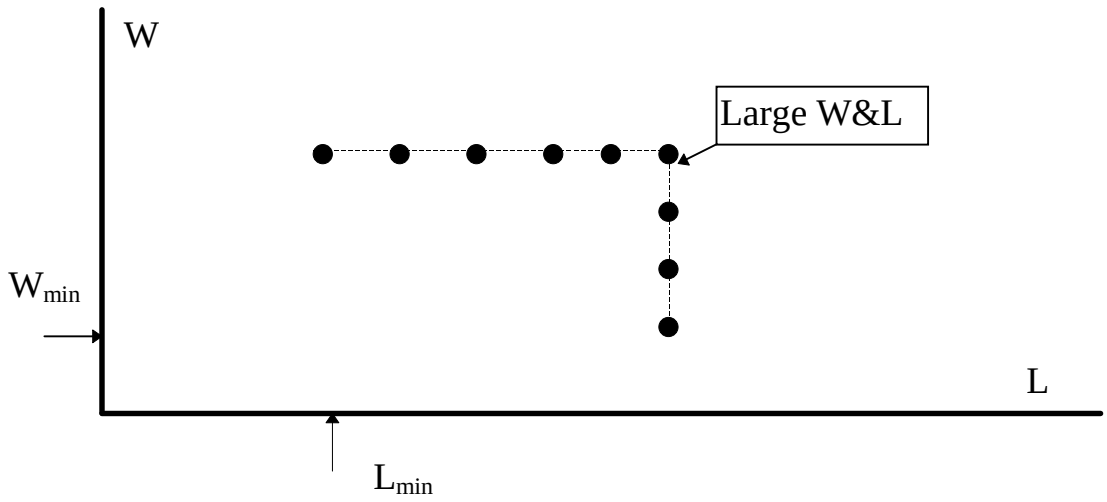

Figure 3.3 *Distribution of device's sizes used for parameter extraction*

The large size device (W&L ≥ 10μm) is used to extract the parameters which are independent of short/narrow channel effects such as V_{To} . One set of devices with fixed large channel width, but different channel lengths is used to extract parameters which are related to the short channel effects such as DIBL characteristic length (Ld) and maximum drift velocity of carrie rs (v_{max}). The other set of devices have a fixed, long channel length, but different channel widths. This set of devices is used to extract parameters which are related to narrow width effects.

3.3.2 Measurement procedure

The measurement is done by an automated program written with the G language implemented in the LabView program [42]. The program has a simple user interface as shown in Fig. 3.4

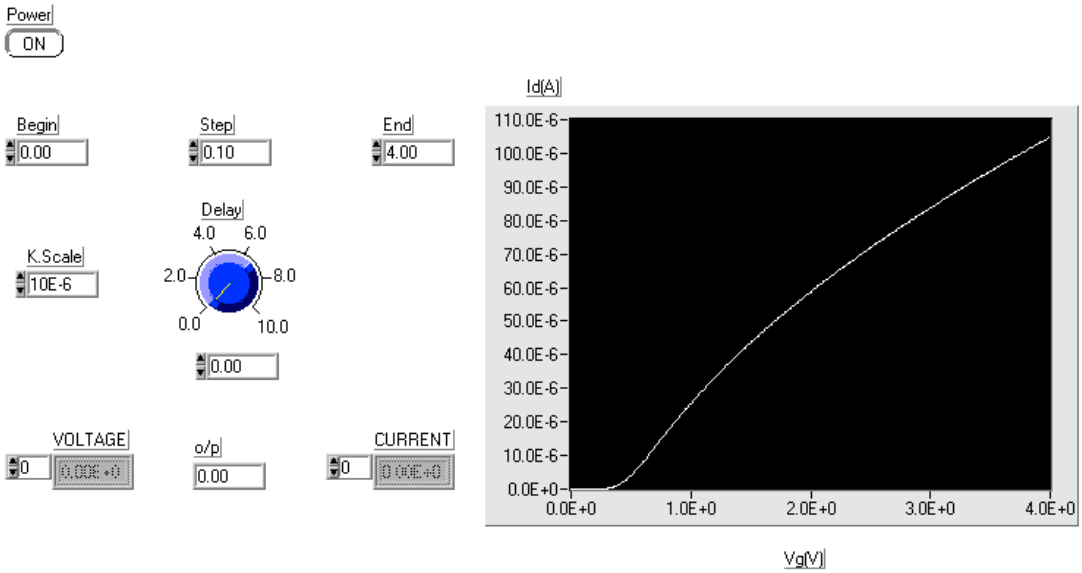

Figure 3.4 *User interface for the measurement program*

3.3.3 Results

Now we represent the obtained results using the last procedure, and we shall apply the optimization algorithm for them, in the next chapter.

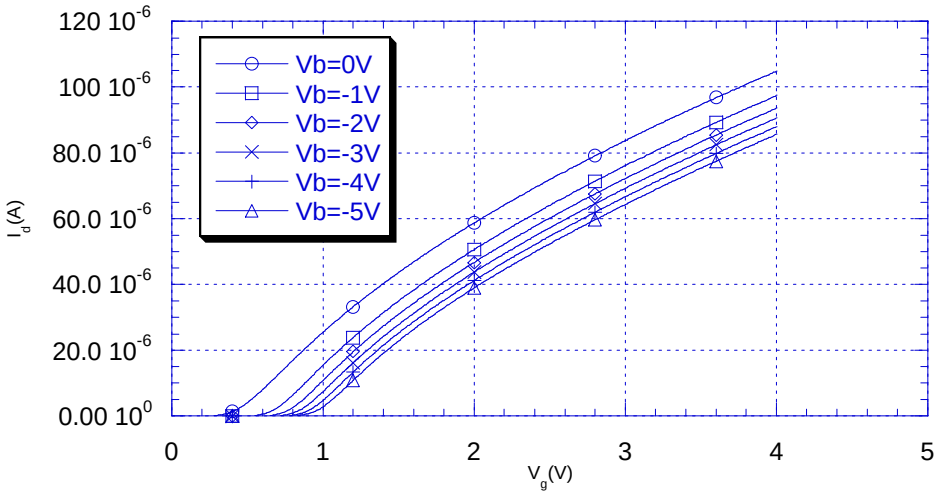

Figure 3.5 *Drain Current versus Gate voltage for low drain voltage (10mV) [W/L=50μ/1.2μ]*

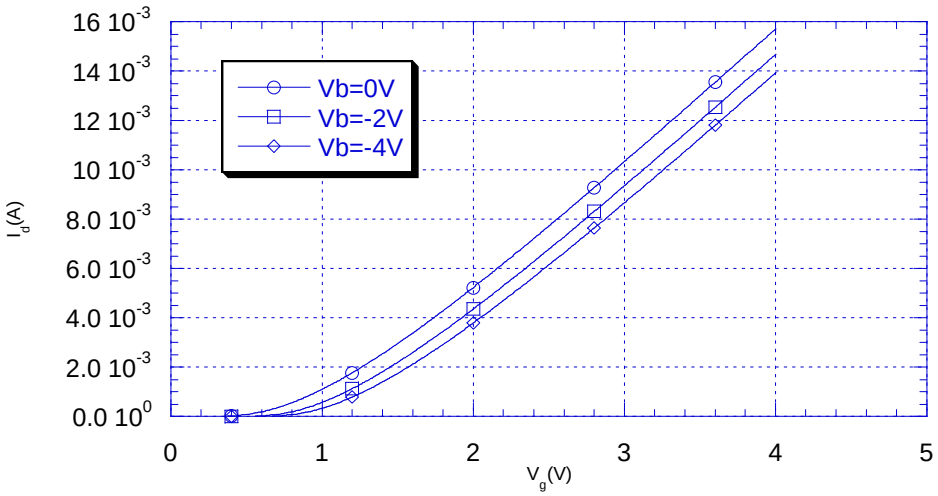

Figure 3.6 *Drain Current versus Gate voltage for high drain voltage (5V) [W/L=50µ/1.2µ]*

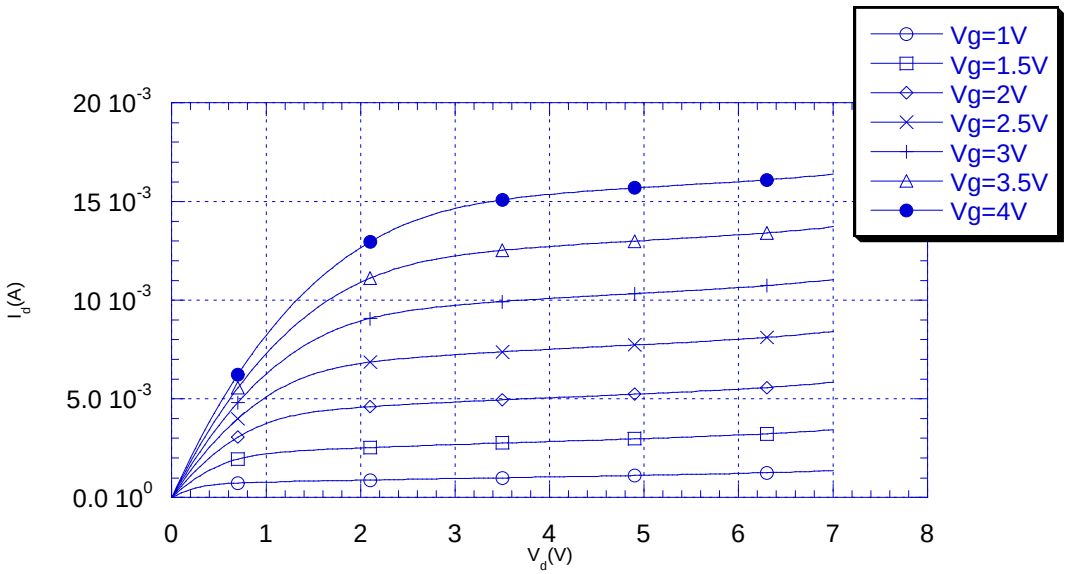

Figure 3.7 *Drain Current versus Drain voltage for V_{bs}=0 [W/L=50µ/1.2µ]*

3.4 Parameter extraction

By parameter extraction we mean: to find the model parameters described in Section 3.2 which best fit a given set of *I-V* data. Parameter extraction is an important part of model development. Because without a good parameter extraction algorithm, even a perfect device model is useless.

3.4.1 Extraction Strategy

There are two different strategies for extracting parameters: the single device extraction strategy and group device extraction strategy [39].

Single device extraction strategy

In the single device extraction strategy, one uses the obtained data from a single device to extract the complete set of model parameters.

Advantages:

i- It may be used even if one transistor only is available

ii- This strategy can fit one device very well.

Disadvantages:

i- It may not fit other devices with different geometry.

ii- The single device extraction strategy can not guarantee that extracted parameters are physical. The only concern is to fit the given device.

In the next chapter we will consider this procedure (optimization).

The Group device extraction strategy

In the group device extraction strategy, we extract parameters using obtained data from different devices with different channel lengths, and fabricated by the same technology. This data is taken in the same operating region for each device.

Advantages:

i- It can fit many devices with different geometries.

ii- The obtained parameters are near to the physical ones.

iii- The complete set of model parameters is effectively a characterization statement for a given IC processing technology. The electrical performance of all device structures fabricated by this technology should be accurately represented by this set of model parameters.

Disadvantages:

i- It may not fit each device perfectly as in the Single device extraction strategy.

ii- It can't work if only one transistor is available.

3.4.2 Parameters extraction procedure

In this section we shall use the second strategy, namely the group device extraction strategy. But since required sample dimensions are not available, we shall use MINIMOS [31] simulations instead of actual measurements. The device parameters were: the gate type was chosen to be *N*-poly, the oxide thickness is 20 nm, the bulk concentration is 5E16 cm^{-3}, a fixed oxide charge of 1E10 cm^{-2} is present, the junction depth computed by MINIMOS is approximately 0.5 μm, the gate width is large W=50 μm and the gate lengths are 20μm, 6μm, 2μ, 1.5μm, 1.2μm and 1μm.

3.4.2.1 Theory

Most parameters are obtained from the strong inversion region of operation, thus we use the simplified current expression in this region given by eq. (2.4.31). After the substitution with μ_{eff} , also if we operate at a very low V_{DS} (V_{DS}=*0.05* V), we may neglect the velocity saturation effects to get

$$I_D = \frac{W}{L_{eff}} C_{ox} \frac{\mu_o}{[(1+\theta Q)+(\theta + \frac{W}{L_{eff}} \mu_o C_{ox} R_t)V]} (V) V_{ds} \qquad (3.4.1)$$

where $Q=2\gamma(\phi_{si}+V_s)^{1/2}$ and $V=V_{gs}-V_{th}-V_{ds}/2$.

The transconductance, g_m, is obtained by differentiating eq. (3.4.1) w.r.t. V_{gs} (or V), such that

$$g_m = \frac{W}{L_{eff}}\mu_o C_{ox}\frac{1+\theta Q}{[(1+\theta Q)+(\theta+\frac{W}{L_{eff}}\mu_o C_{ox}R_t)V\ ]^2}V_{ds} \qquad (3.4.2)$$

From equations (3.4.1) and (3.4.2), the ratio $I_D/(g_m)^{1/2}$ takes the form

$$\frac{I_D}{\sqrt{g_m}} = \sqrt{\frac{W\mu_o C_{ox}V_{ds}}{L_{eff}(1+\theta Q)}}\ \ V \qquad (3.4.3)$$

It is seen that the ratio $I_D/(g_m)^{1/2}$ does not depend on R_t and is directly proportional to V.

A) Determination of threshold voltage (V_{To})

From equation 3.4.3 it is clear that, when $I_D/(g_m)^{1/2}$ is plotted against V_{gs}, we get a straight line with slope, $m_1=(W\mu_o C_{ox}V_{ds}/(L_{eff}(1+\theta Q)))^{1/2}$ and the intercept on the V_{gs} axis equal $(V_{th}+V_{DS}/2)$ so if we use large device length we obtain the threshold voltage for long channel device, V_{To}. (See Fig. 3.8).

B) Determination of ΔL

Consider the quantity:

$$\frac{1}{m_1^2} = \frac{(L-\Delta L)(1+\theta Q)}{W\mu_o C_{ox}V_{ds}} \qquad (3.4.4)$$

if it is plotted against the mask channel length L, the slope, m_2, of this straight line is equal to

$$m_2 = \frac{(1+\theta Q)}{W\mu_o C_{ox}V_{ds}} \qquad (3.4.5)$$

and the intercept on the *L*-axis is ΔL, allowing ΔL to be determined. (See Fig. 3.9).

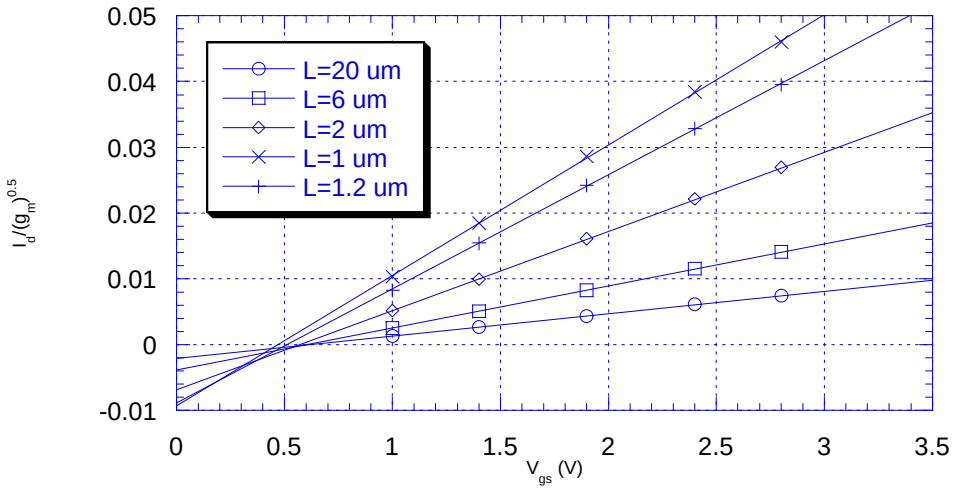

Figure 3.8 *The variation of $I_D/g_m^{1/2}$ as a function of gate voltage for different channel lengths.*

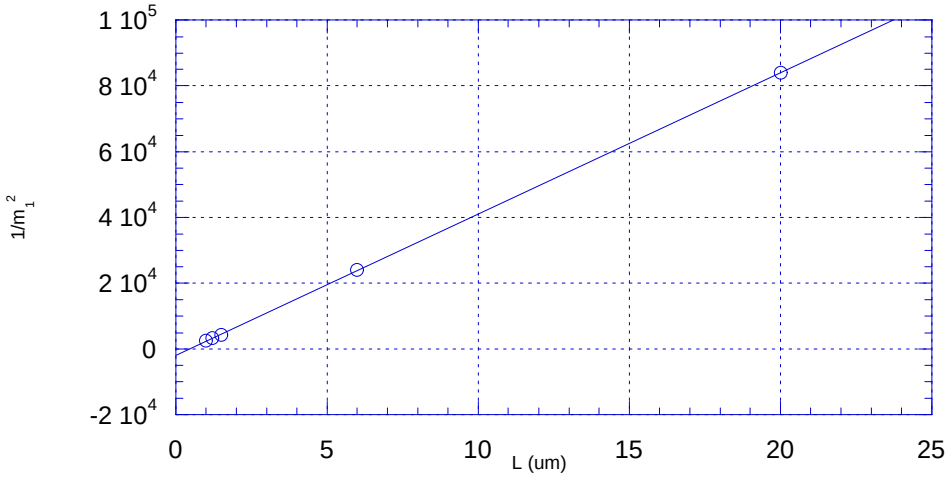

Figure 3.9 *The variation of $1/m_1^2$ as a function of channel length.*

C) Determination of the parasitic resistance (R_t)

From eq. (3.4.1) the output resistance, R_o, defined by V_{ds}/I_D is equal to

$$R_o = R_t + (L - \Delta L)\frac{1 + \theta(V + Q)}{W \mu_o C_{ox} V} \qquad (3.4.6)$$

When R_o is plotted against the mask channel length L, for a given value of V, we get a straight line, the slope of such straight line is

$$m_3 = \frac{1 + \theta(V + Q)}{W \mu_o C_{ox} V} \qquad (3.4.7)$$

and from the intercept we can determine the parasitic series resistance R_t as :

$$R_t = Intercept + \Delta L * m3 \qquad (3.4.8)$$

(See Fig. 3.10).

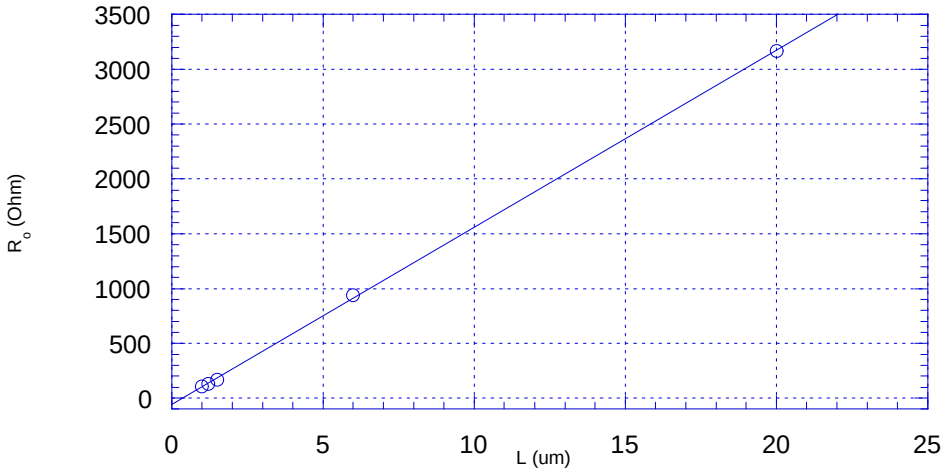

Figure 3.10 *The variation of R_o as a function of the mask channel length L*

D) Determination of low field mobility parameters (μ_o and θ)

Dividing equations (3.4.5) and (3.4.7), we get the parameter θ as

$$\theta = \frac{\frac{m_2 V_{ds}}{m_3 V} - 1}{Q - \frac{m_2 V_{ds}}{m_3 V}(V + Q)} \qquad (3.4.9)$$

then using eq. (3.4.5) we can determine μ_o as

$$\mu_o = \frac{1+\theta Q}{W C_{ox} V_{ds} m_2} \tag{3.4.10}$$

E) Determination of high field mobility parameters (v_{max})

The effective mobility μ_{eff}' given by eq. (2.4.32) can be written as

$$\mu_{eff}' = \frac{(\frac{\mu_g}{D})}{1+\frac{W}{L_{eff}}(\frac{\mu_g}{D})C_{ox} R_t V} \tag{3.4.11}$$

where

$$D = [1+(\frac{\mu_g V_{DS}}{L_{eff} v_{\max}})^m]^{1/m} \tag{3.4.12}$$

$$\mu_g = \frac{\mu_o}{1+\theta(Q+V)} \tag{3.4.13}$$

The factor (D) represents the velocity saturation effect (refer to Section 2.4.2). Thus if the effective mobility is found in strong inversion at a given value of V, using the strong inversion approximated current equation at high V_{DS} (but still in the linear region),μ_h, and knowing μ_o and θ i.e. knowing μ_g at the specified V, and R_t, we can find v_{max} using

$$D = \frac{\mu_g(1-\mu_h \frac{W}{L_{eff}} C_{ox} R_t V)}{\mu_h} \tag{3.4.14}$$

and eq. (3.4.12).

F) Determination of the characteristic length of barrier lowering (Ld)

Referring to Section 2.4.3, we can find the parameter Ld by measuring the slope of ΔV_{th} versus L_{eff}, where ΔV_{th} is drawn on logarithmic scale. (See Fig. 2.7 and Fig. 3.11).

G) Determination of the Impact ionization parameters (AI and BI)

We may find these parameters, by referring to eq. 2.4.40, this curve is bell shape, so if we find the point at which maximum bulk current occur (V_{gsm},I_{bm}) we find BI from the relation

$$BI = \left(\frac{g_{mm}(V_{ds} - V_{gsm} + V_{th})}{I_{dm}} - 1\right)(V_{ds} - V_{gsm} + V_{th}) \qquad (3.4.15)$$

$$AI = \frac{I_{bm}}{I_{dm}(V_{ds} - V_{gsm} + V_{th})\exp\left(-\frac{Bl}{V_{ds} - V_{gsm} + V_{th}}\right)} \qquad (3.4.16)$$

where g_{mm} and I_{dm} are the transconductance and drain current at this maximum point respectively. (See Fig. 3.12).

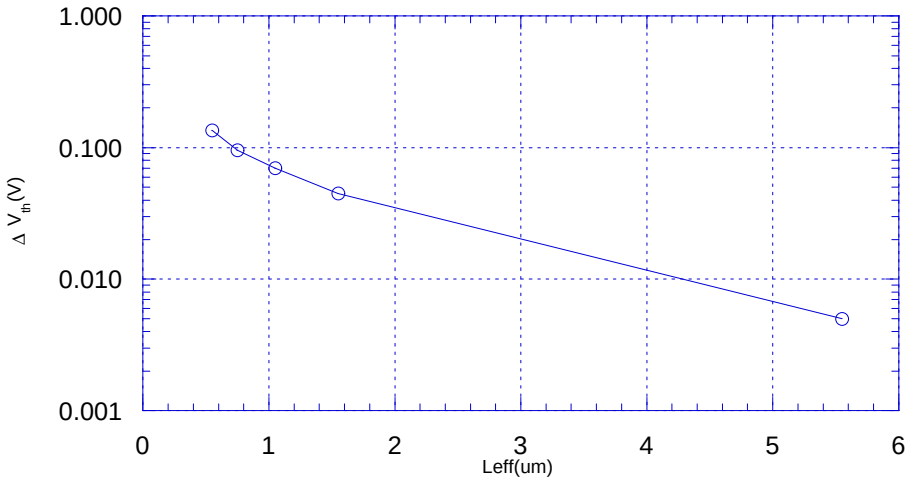

Figure 3.11 *ΔV_{th} as a function of the effective channel length.*

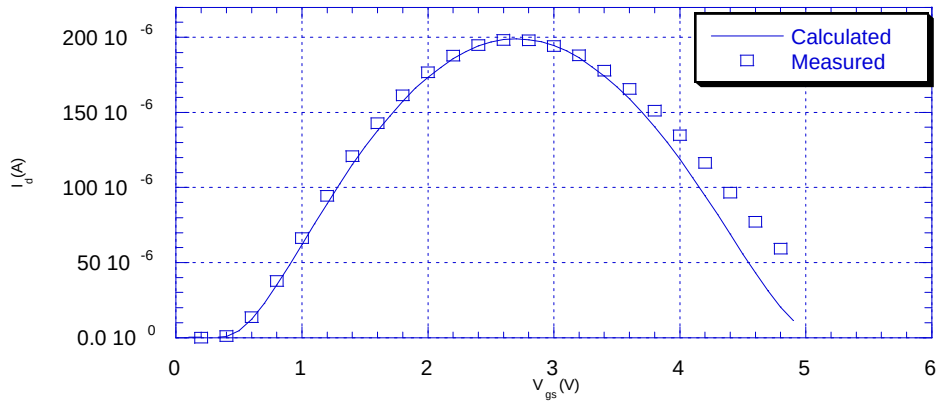

Figure 3.12 *Determination of Impact ionization parameters*

3.4.2.2 Extraction Results

From the above, we get the parameters' values shown in Table 3.2. Also we have made small manual optimization to the mobility parameters to get best fit to the measured data.

Table 3.2 *Obtained parameters*

Parameter	Value	After Optimization	Unit
VTo	0.58	0.58	V
DEL	0.45	0.45	µm
Rt	10	10	Ohm
Muo	610	670	$cm^2/V.s$ ec
THETA	0.097	0.091	1/V
vmax	7e6	1.2e7	cm/sec
Ld	0.155	0.155	µm
AI	1.148e-6	1.148e-6	1/V
BI	4.185e4	4.185e4	V/cm

Now to validate the used extraction method, we use the extracted parameters for two different channel lengths 6 µm (long channel), and 1 µm (short channel), and we compare the obtained results with the MINIMOS results. See Figures from 3.13 to 3.18 for comparison, from these figures we note the good agreement between the simulated results and the experimental results, for both short and long channel transistors.

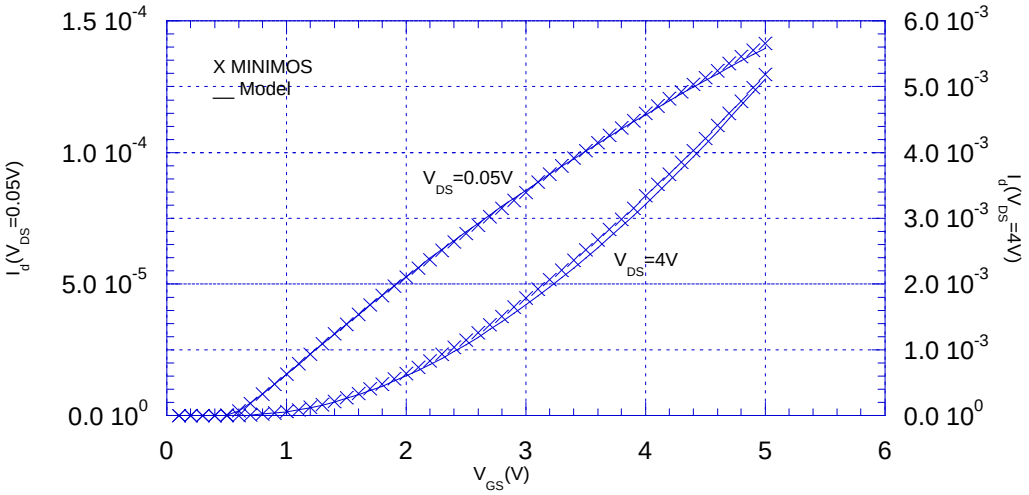

Figure 3.13 *Drain current versus gate voltage for long device (6µm)*

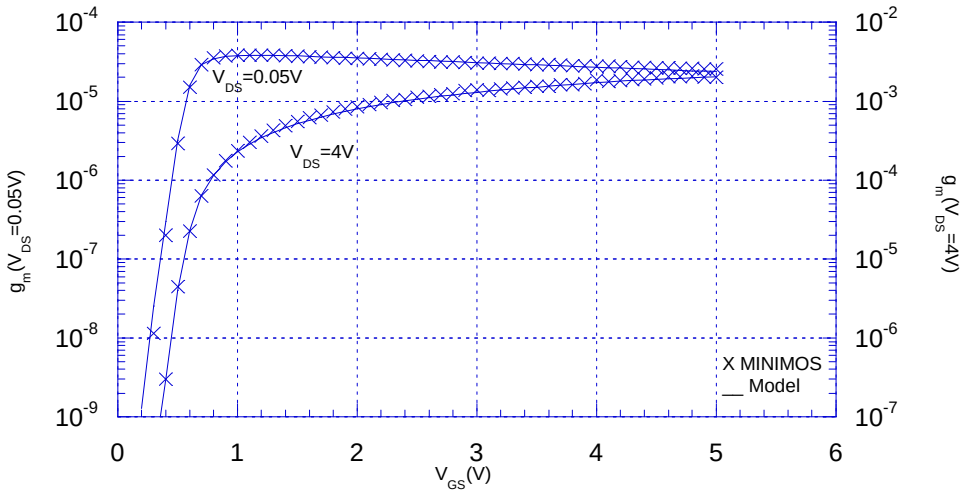

Figure 3.14 *Transconductance versus gate voltage for long device (6µm)*

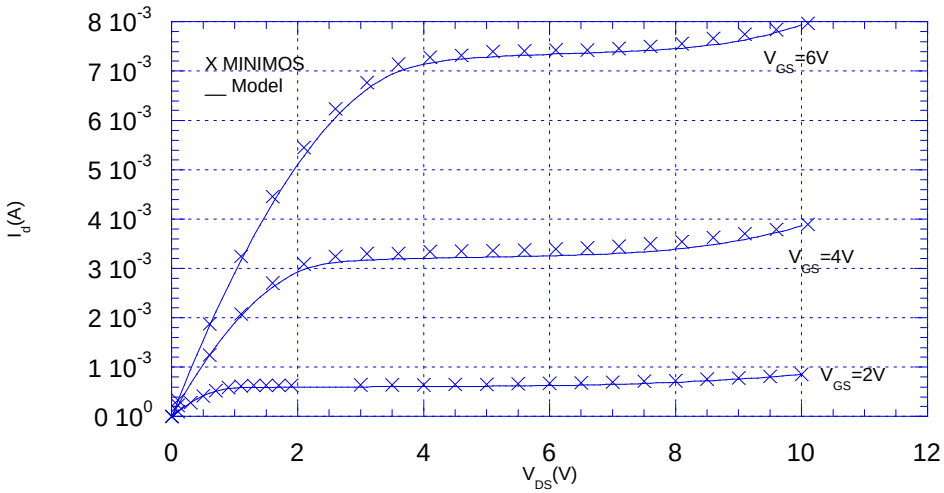

Figure 3.15 *Drain current versus drain voltage for long device (6µm)*

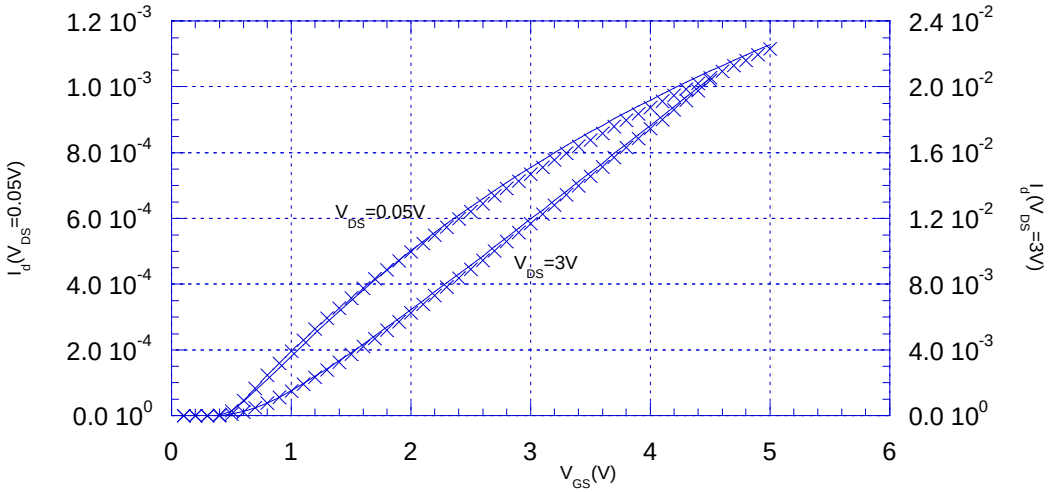

Figure 3.16 *Drain current versus gate voltage for short device (1µm)*

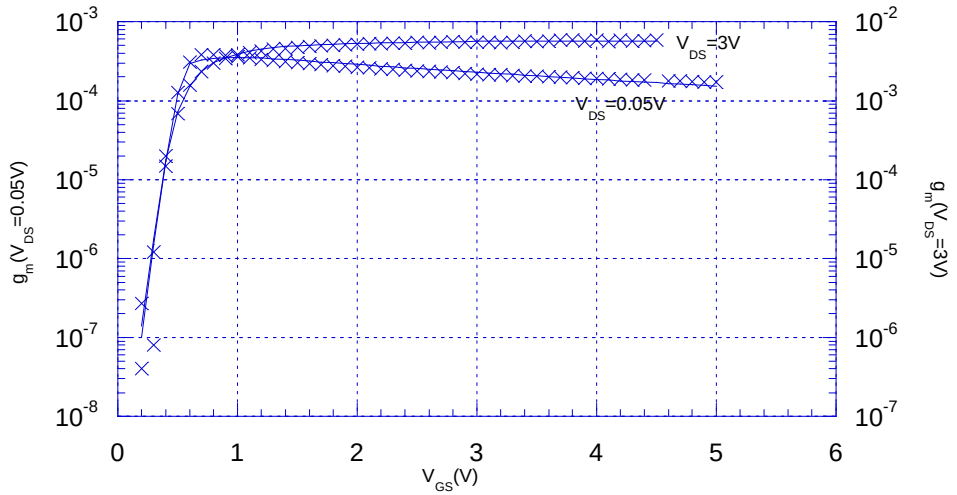

Figure 3.17 *Transconductance versus gate voltage for short device (1µm)*

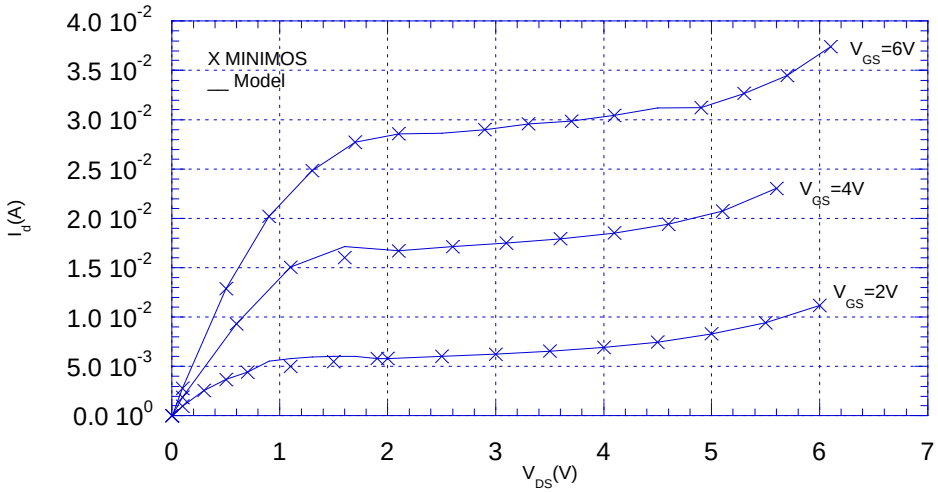

Figure 3.18 *Drain current versus drain voltage for short device (1µm)*

CHAPTER 4

Optimization Algorithm and Results

4.1 Introduction

An optimization problem begins with a set of independent variables and/or parameters, a set of dependent variables, and the existing or simulated functional relationship between the two sets. This relation can have various level of complexity and is inherently nonlinear in nature. In general, its evaluation consists of the execution of some underlying simulation tools that involve highly complex solution techniques which are computationally expensive. Furthermore, they are not suited for analytical manipulation and the use of numerical approximation is normally required. Typically, they have a continuous and well-behaved functional behavior. These characteristics influence the choice of the appropriate solution algorithm for any particular task.

It is clearly desirable to have a standard model formulation suitable for the description of the diverse tasks algorithms. In mathematical terms such an expression takes the form:

$$Y=f(X,P) \tag{4.1.1}$$

where

$$Y = [y_1, y_2, \dots , y_q] \tag{4.1.2}$$

$$X = [x_1, x_2, \dots , x_m] \tag{4.1.3}$$

$$P = [p_1, p_2, \dots , p_n] \tag{4.1.4}$$

are vectors of q model outputs, m independent variables and n model parameters respectively. f can also be formulated in terms of the individual output functions as:

$f = [f_1, f_2, \ldots, f_q]$ (4.1.5)

where each

$y_i = f_i(X,P)$ (4.1.6)

represent the model evaluation that relates the input and parameter vectors to the i-th response.

In the rest of this chapter the used algorithm is presented and discussed. It is a nonlinear least-squares optimization module which forms the nucleus of our work.

4.2 Nonlinear Least Squares Optimization

Given a certain CAD model and a set of observations (i.e. data) that relate the model independent variables (X) to its calculated responses (Y), the problem of optimization consists of finding the model parameter vector (P) that will result in the best possible fit between measurements and model predictions. In the present work, the weighted *sum of squares* (F) is used as a measure of the accuracy of fit:

$$F = \sum_{j=1}^{q} \sum_{i=1}^{m} w_{ji} r_{ji}^2 \quad (4.2.1)$$

where w_{ji} and r_{ji} are the weight and the residual for the j-th response at the i-th data point respectively. The residual is defined as the relative error at that data point:

$$r_{ji} = \frac{f_j(X_i, P) - y_{ji}^{\exp}}{y_{ji}^{\exp}} \quad (4.2.2)$$

where y_{ji}^{exp} is the measured j-th response at X_i. The weight is a user-defined positive value that increases or decreases the significance of a data point in the overall fit. This can be related to the user desire to achieve higher accuracy for a certain input or output variable range or to the prior knowledge about the expected accuracy of the measurements. It is noted that this definition of the objective is a variation on the *Chi-Square* fitting

criterion where the standard deviation of each measurement data point is used in the formulation.

By defining R, a vector of the n*q residuals, (4.2.1) can be written as:

$$F = R^T W R \qquad (4.2.3)$$

where **W** is a nq*nq diagonal matrix whose elements W_{ii} are the weights w_i. The solution of the nonlinear least squares problem reduces to minimizing (4.2.1). In general, the nonlinearity of CAD models dictates the use of gradient based iterative methods. The present implementation is based on the Levenberg-Marquardt (LM) algorithm [43-45] which has become the standard of nonlinear least squares routines [46]. The Levenberg-Marquardt method combines the inherent stability of steepest descent with the quadratic convergence rate of the Gauss-Newton method as described in the next section.

4.2.1 Algorithm Description

A Taylor series expansion of (4.2.1) around a nominal point $\mathbf{P_o}$ can be written as:

$$F(P_o + \Delta P) = F(P_o) + g^T \Delta P + \frac{1}{2} \Delta P^T H \Delta P + O(\|\Delta P\|^3) \qquad (4.2.4)$$

where

$$g = [\frac{\partial F}{\partial p_1}, \frac{\partial F}{\partial p_2}, ..., \frac{\partial F}{\partial p_m}] \qquad (4.2.5)$$

is the gradient of the objective function, and **H** is an m*m matrix of second derivatives called the Hessian matrix whose elements are given by:

$$H_{ij} = \frac{\partial^2 F}{\partial p_i \partial p_j} \qquad (4.2.6)$$

An intuitive iterative solution scheme consists of taking a step in the negative gradient direction:

$\Delta P = -g$ (4.2.7)

When the size of the step (α_k) is chosen appropriately, a monotonic decrease in the objective function is ensured. At each iteration, the size of the step can be determined via a line search along the negative gradient direction using a one-dimensional optimization technique (e.g. Brent's parabolic). The new values of the parameters are then calculated as:

$P_{k+1} = P_k + \alpha_k \Delta P_k$ (4.2.8)

This procedure is called steepest descent. It is a reliable and inherently stable method that will always lead to a minimum of F. Its disadvantage is that the step often has to be so small that it results in a very slow convergence especially as the minimum is approached.

An alternative solution technique is the Gauss-Newton method which is based on the premise that a quadratic approximation is an accurate representation of F at P_o. In this case, the $O(\|\Delta P\|^3)$ terms in (2.10) are dropped, and the necessary condition for the minimum of F, namely that the gradient must be zero, can be written as:

$g + 2*H \Delta P = 0$ (4.2.9)

which yields the following equation for ΔP:

$$\Delta P = -\frac{1}{2} H^{-1} g \quad (4.2.10)$$

In the case of the least-squares objective F, the elements of the gradient and the Hessian matrix can be expressed as:

$$g_j = \frac{\partial F}{\partial p_j} = 2\sum_{i=1}^{m} w_i r_i \frac{\partial r_i}{\partial p_j} \quad (4.2.11)$$

and

$$H_{jk} = \frac{\partial^2 F}{\partial p_j \partial p_k} = 2\sum_{i=1}^{n} w_i \left(\frac{\partial r_i}{\partial p_j}\frac{\partial r_i}{\partial p_k} + r_i \frac{\partial^2 r_i}{\partial p_j \partial p_k}\right) \quad (4.2.12)$$

For sufficiently small residuals, the second term in (4.2.12) can be neglected and the elements of the Hessian matrix are approximated as:

$$H_{jk} = \frac{\partial^2 F}{\partial p_j \partial p_k} \approx 2\sum_{i=1}^{n} w_i \left(\frac{\partial r_i}{\partial p_j}\frac{\partial r_i}{\partial p_k}\right) \qquad (4.2.13)$$

By introducing the n*m Jacobian matrix **J** whose elements are the partial derivative of the individual residual with respect to the parameters:

$$J_{ij} = \frac{\partial r_i}{\partial p_j} \qquad (4.2.14)$$

(4.2.11) and (4.2.13) can be written in vector form as:

$$g = 2J^T WR \qquad (4.2.15)$$

$$H \approx 2J^T WJ \qquad (4.2.16)$$

The above equations are the basis of the Gauss -Newton iteration scheme:

$$\Delta P = -\frac{1}{2}(J^T WJ)^{-1} J^T WR \qquad (4.2.17)$$

$$P_{k+1} = P_k - \frac{1}{2}(J_k^T WJ_k)^{-1} J_k^T WR_k \qquad (4.2.18)$$

Given an initial guess sufficiently close to the solution, the Gauss-Newton method has a quadratic convergence rate. However, a poor starting vector could cause the method to diverge due to the size of the neglected second term in (4.2.12). Furthermore, the method always fails when the Hessian matrix becomes singular or ill-conditioned. Several modifications have been proposed to the basic scheme to ensure convergence [47-48].

In the Levenberg-Marquardt method, the approximate Hessian matrix is replaced by:

$$J^T WJ + \lambda D \qquad (4.2.19)$$

and the iteration scheme becomes:

$$P_{k+1} = P_k - (J_k^T WJ_k + \lambda D)^{-1} J_k^T WR_k \qquad (4.2.20)$$

where λ is a conditioning factor and D is a diagonal matrix with entries equal to the diagonal elements of $J^T WJ$. The essence of the *Levenberg-Marquardt compromise* is that the step direction is intermediate between the steepest descent and the Gauss-Newton directions. As $\lambda \to 0$ the search direction approaches the Gauss-Newton direction. Alternatively when $\lambda \to \infty$, the method reduces to a steepest descent minimum search. A simple strategy to update the values of λ consists of decreasing its value when an iteration is successful in reducing the sum of squares fit criterion, and increasing it when the iteration fails:

$$\text{if } F_{k+1} < F_k \quad \rightarrow \quad \lambda_{k+1} = \lambda_k / factor$$
$$\text{else } \lambda_{k+1} = \lambda_k * factor \qquad (4.2.21)$$

where *factor* is a user defined parameter (default of 5).

4.2.2 Calculation of the Jacobian Matrix

The calculation of the elements of the jacobian matrix requires the values of the derivatives of the model function at the input data points. The used model functions are generally smooth but their analytical derivatives are unavailable. Numerical differentiation techniques are used to approximate the derivative using forward differences formula:

$$J_{ij} = \frac{r_i(P_k + h_j) - r_i(P_k)}{h_j} \qquad (4.2.22)$$

where h_j represents a small increment.

It was proven that the use of numerical approximation in the Levenberg-Marquradt algorithm does not jeopardize its convergence properties [45].

4.2.3 Parameters Constraints

To avoid deviations outside the expected range of the parameters during the initial stages of the solution, linear interval inequality constraints of the form:

$$L \leq P \leq U \qquad (4.2.23)$$

are enforced on the parameters. In the above equation **L** and **U** are vectors of lower and upper bounds on each of the model parameters. The constraints are incorporated into the Levenberg-Marquardt algorithm using a simple technique based on the concept of active constraints. A constraint becomes active if it is violated when the parameters are updated (i.e. if $p_i<l_i$ or if $p_i>u_i$). The parameters corresponding to the set of active constraints are not allowed to change by enforcing that $\Delta P_i=0$. This is accomplished by removing the appropriate equations from the linear system of (4.2.20).

4.2.4 Termination Criteria

The iterations are continued until convergence which is denoted by either a small relative change in the sum of squares error (F), or by a small change in each parameter value relative to the previous iteration values. Other termination criteria are indicative of error conditions that occur when the optimization problem is ill posed such as when:

- The number of iterations exceeds a maximum number ($N_{iter}>N_{max}$)
- The conditioning factor exceeds a preset maximum value ($\lambda>\lambda_{max}$). In this case, the algorithm is failing to move forward even though the method of steepest descent is used.
- The norm of the gradient is very small. This indicates the failure to find a search direction: $\|g\| < \varepsilon$.

As in other optimization problems, the convergence to a solution does not guarantee that the global minimum of F has been reached.

4.3 Results

To validate our system, measurement programs, model functions and optimization program we carry our measurements and characterization on sample transistor with the following parameters gate mask length=1.2 μm, gate mask width=100 μm, gate oxide thickness=28 nm, and bulk doping=5E16 cm^{-3}. We adopt the procedure explained in Section 3.4.2.1(G) to determine the impact ionization parameters, the low field mobility

parameters, threshold voltage, and series resistance are obtained by applying the developed program for the least squares error discussed in this chapter to the drain current vs. gate voltage at low drain voltage (10 mV), finally the high field mobility parameters are obtained from the drain current vs. gate voltage at high drain voltage (5V)

4.3.1 Obtained parameters

We present here the obtained parameters after optimization procedure, which will be used beside the given technological parameters mentioned above in our simulation.

Table 4.1 *Obtained parameters*

Parameter	Value	Unit
VTo	0.349	V
DEL	0.052	μm
Rt	24	Ohm
Muo	532	$cm^2/V.s$ ec
THETA	0.093	1/V
vmax	7e6	cm/sec
AI	6.693E-7	1/V
BI	4.911E5	V/cm

4.4 Comparison with simulation results

Comparison between the measured data, and the obtained results from our model simulations, is carried using the same set of the extracted parameters.

Figs. 4.1,4.2 show the comparison of the I_D-V_{GS} characteristics and the corresponding transconductances, on both linear and logarithmic scales, of the obtained measured data with those of our model at a small V_{DS} (V_{DS}=*0.01*

V). Continuity of the current model and its first derivative from subthreshold to strong inversion is clearly demonstrated.

Figs. 4.3,4.4 shows the same results but at a high V_{DS}. Effect of Longitudinal field on the mobility together with the series resistance effect are adequately modeled as shown in Figures.

Fig. 4.5 demonstrates the effect of V_{DS} on the threshold voltage (DIBL). The ability of the model to predict the dc characteristics in the vicinity of threshold and in the subthreshold region under different drain bias for short channel transistors is demonstrated by the results of this figure.

Fig. 4.6 shows the I_D-V_{DS} characteristics for four values of V_{GS} (V_{GS}=*1 V, 2 V, 3V,* and *4 V*). Continuity of the model from linear to saturation operation is clearly demonstrated. The modeling of saturation region characteristics is more clearly shown by the corresponding output drain conductance given in Fig. 4.7. From the results it is clear that the model is shown to fit the obtained data in all operating regions.

An additional test suggested by Tsividis and Suyama [12] is to compare measured and modeled g_m/I_D versus V_{GS}. They point out that some of the commonly used models show an anomalous spike as the drain current crosses the boundary between weak and strong inversion. We have performed this test and the result is shown in Fig. 4.8. The exponential relationship between I_D and V_{GS} results in a constant g_m/I_D in the subthreshold region. No anomalous spike is observed at the transition to strong inversion because in our model g_m is continuous across the boundary.

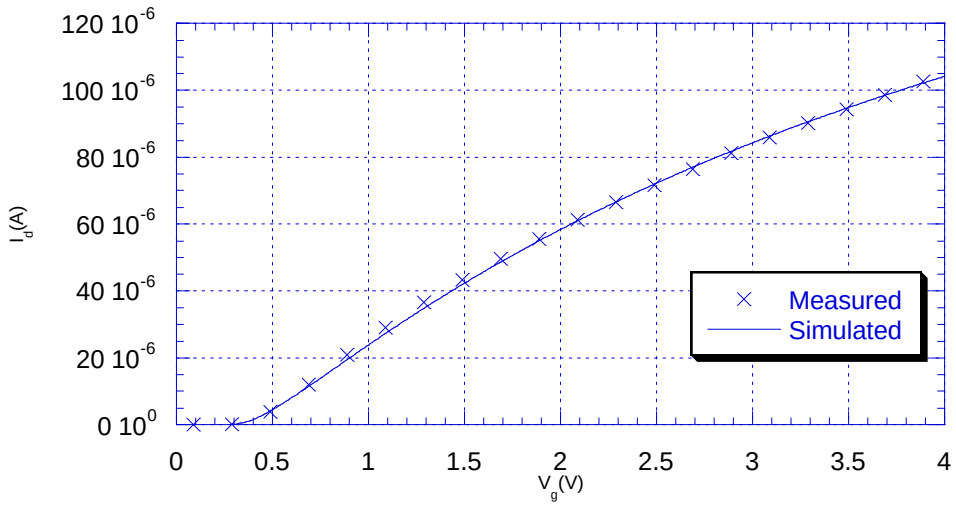

Figure 4.1.a *Drain current versus gate voltage for drain voltage=10mV [Linear Scale]*

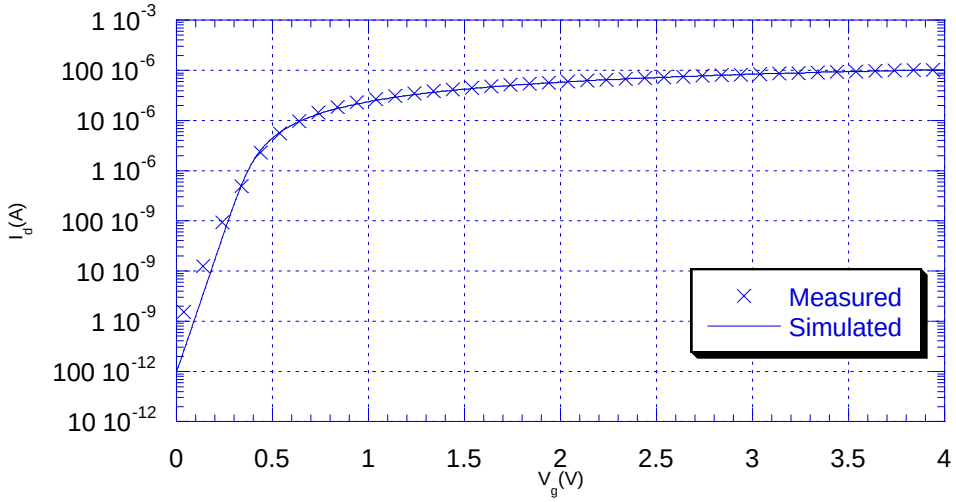

Figure 4.1.b *Drain current versus gate voltage for drain voltage=10mV [Log Scale]*

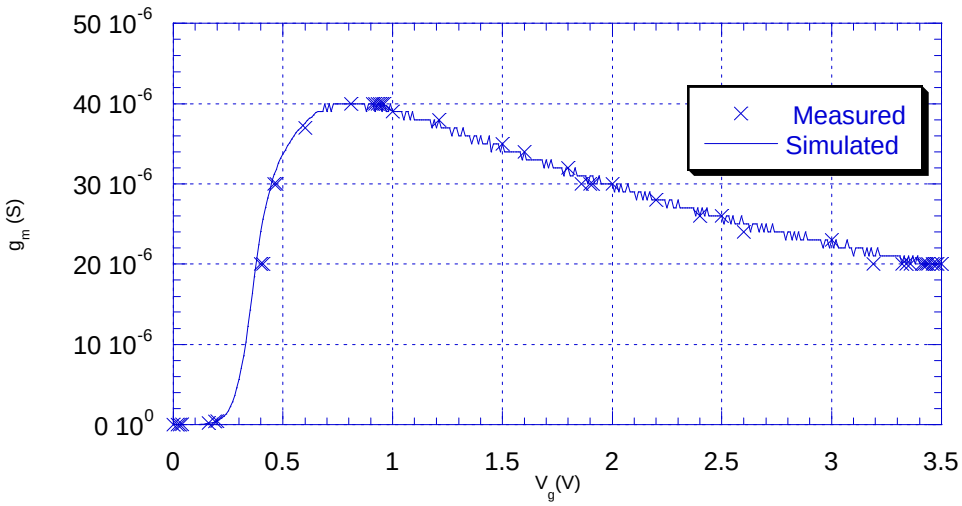

Figure 4.2 *Transconductance versus gate voltage for drain voltage=10mV*

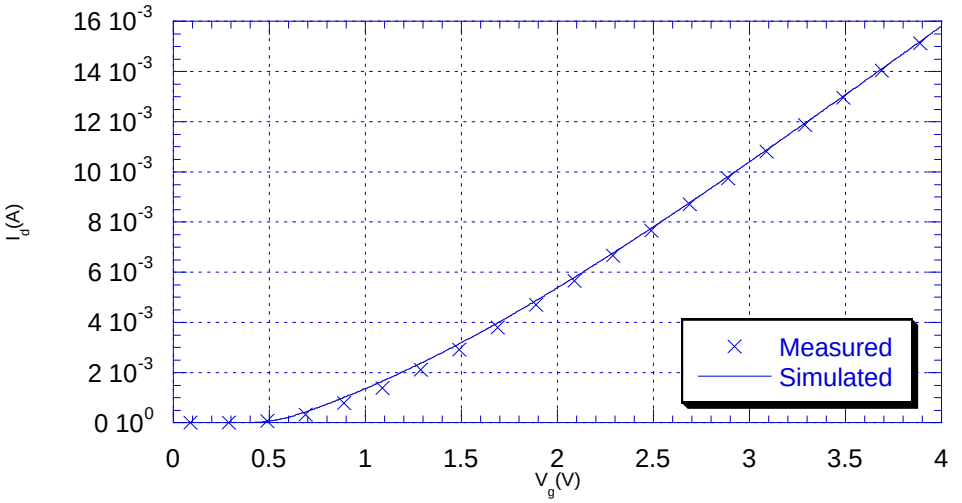

Figure 4.3.a *Drain current versus gate voltage for drain voltage=5V*

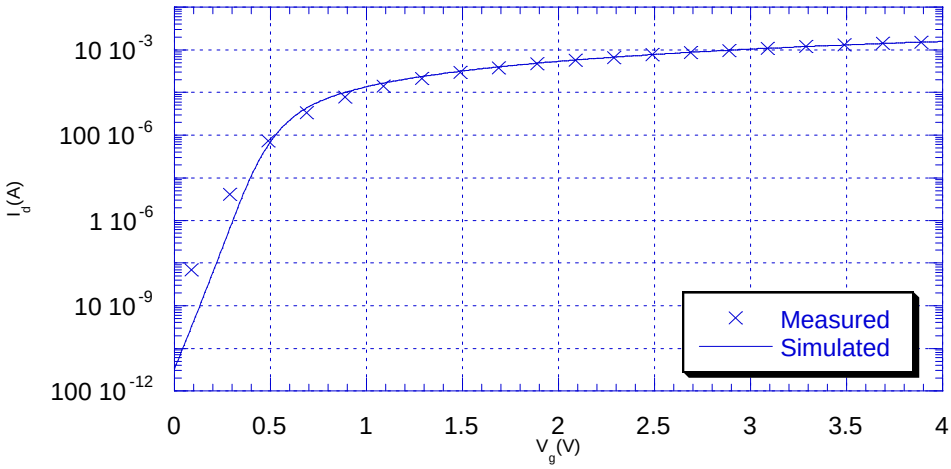

Figure 4.3.b *Drain current versus gate voltage for drain voltage=5V*

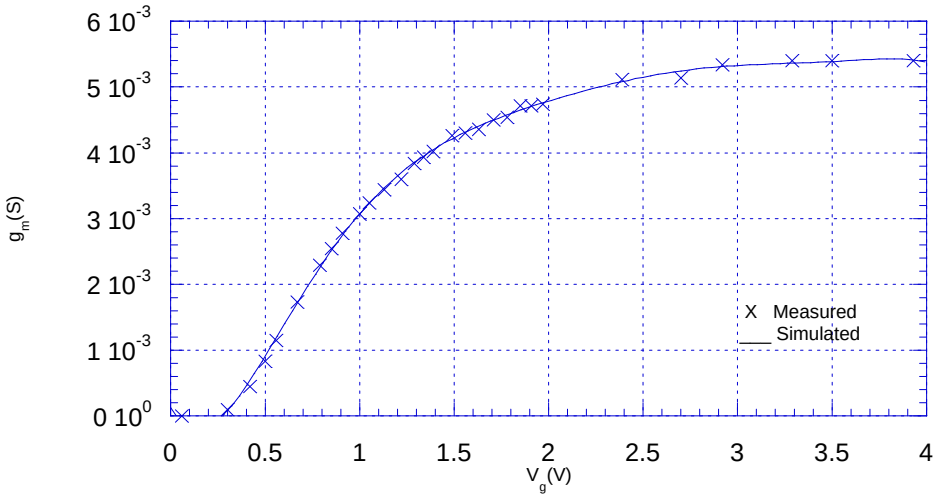

Figure 4.4 *Transconductance versus gate voltage for drain voltage=5V*

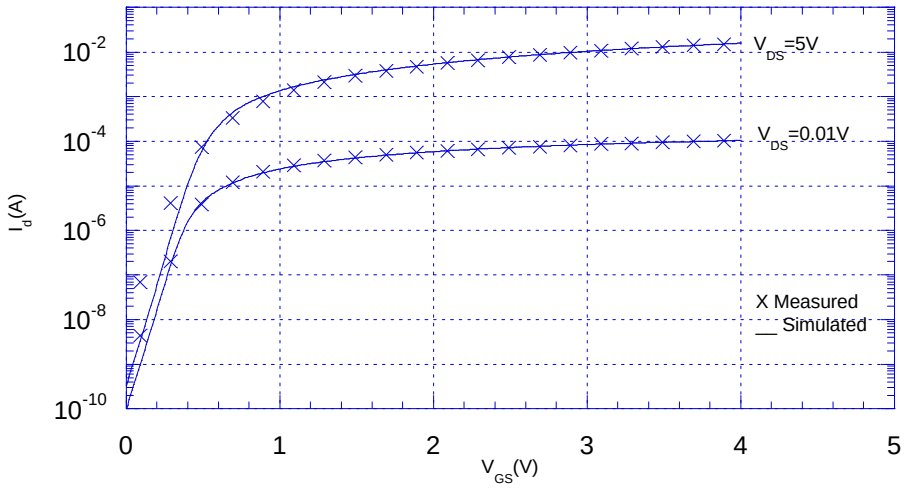

Figure 4.5 *Drain current versus gate voltage for different drain voltages*

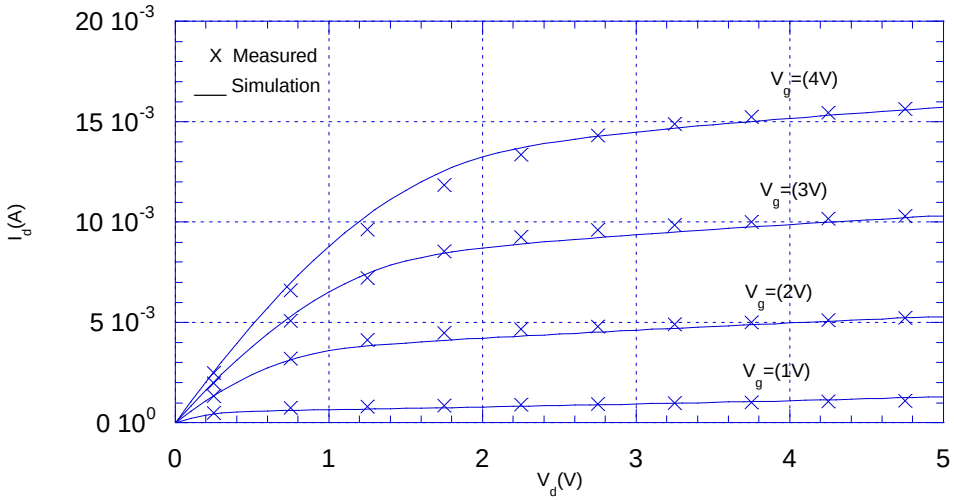

Figure 4.6 *Drain current versus drain voltage for different gate voltages*

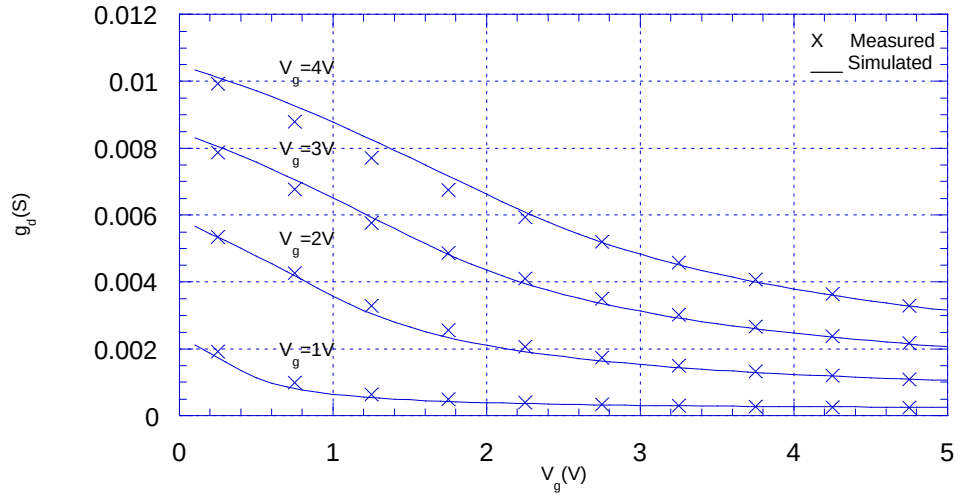

Figure 4.7 *Output conductance versus drain voltage for different gate voltages*

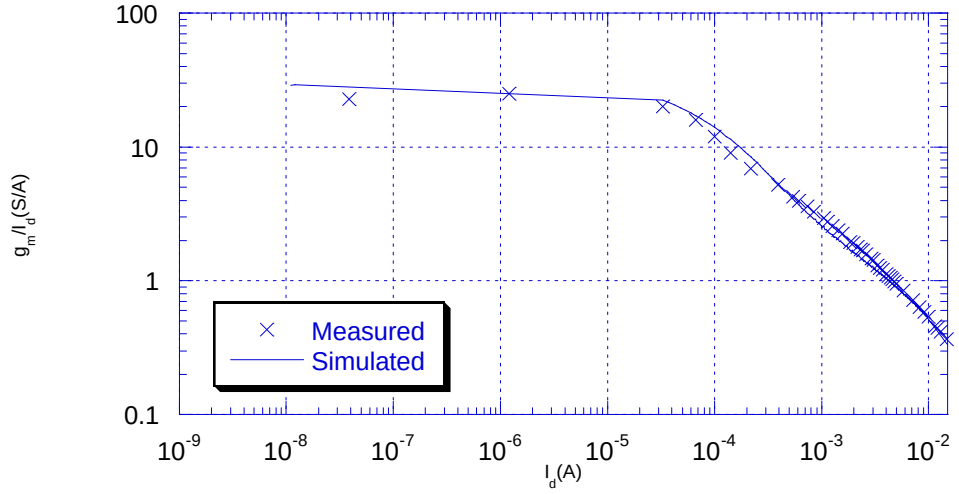

Figure 4.8 *g_m/I_d versus Drain current*

4.5 Other Models

Table 4.2 shows a comparison of the MOS Level (2) (SPICE) [49], BSIM [50], and aMOS [51] models with the proposed model. The table shows that the proposed model has a small number of parameters compared to the BSIM and aMOS models, while maintaining a good accuracy for the drain current and small signal parameters

4.6 Conclusion

The model presented in this thesis is a physical, scaleable and efficient model for VLSI analog/digital circuit simulation. It has built-in dependencies on geometry and process parameters. Small-size and non-uniform doping effects which are important in today's IC devices are built in the model. It also has a relatively small number of parameters which can be easily extracted and optimized. The continuity of the model reduces the number of iterations and CPU time during circuit simulation. The automated measurements programs presented in this work, make the measurements procedure more easier and accurate, since we adopted a good measurement technique as the first step to obtain good extracted parameters. Also the use of Levenberg-Marqudet algorithm which has become the standard of nonlinear least squares routines is used to develop parameters optimization program, which give us more accuracy to our extracted parameters. The developed program can be used in any other environment require least squares error method for optimization.

Table 4.2. *Comparison between SPICE Level (2) model, BSIM model, aMOS model, and this work.*

Model	***Developers***	***No. Of Para-meters***	***Conduc-tances***	***Small geometry effect***	***Applicability of parameter set***	***Moderate inversion***	g_m/I_D	D_{it}
SPICE Level (2)	Vladimirescu & Liu (1980)	21	Not Continuous	Charge Sharing	Limited	Discontinuity in slope	Spike	Simple model
BSIM	Sheu, Ko & Jeng (1985)	67	Not Continuous	Semi-empirical	Limited by abnormal sec. effects	Discontinuity in slope	Discontinuity in slope	Simple model
aMOS	Chartterje &Machala (1995)	56	Continuous	Semi-empirical	Limited by minimum dimensions	Continuous	Discontinuity in slope	Simple model
Our model	This+previous work[30]	31	Continuous	Quasi 2D analysis	Limited by minimum dimensions	Continuous	Continuous	Physical

References

[1] E. S. Yang, "Microelectronic Devices," McGraw-Hill, 1988.

[2] S. M. Sze, "Physics of Semiconductor Devices," Wiley Eastern Limited, 1981.

[3] G. Barbottin and A Vapaille (editors), "Instabilities in Silicon Devices, Silicon Passivation and Related Instabilities, Vol. 2," North-Holland, Amesterdam, 1989.

[4] E. H. Nicollian and J. R. Brews ,"MOS Physics and Technology," John Wiley & Sons, 1982.

[5] J. S. Brugler and P. G. Jespers, "Charge Pumping in MOS-devices, " IEEE Trans. Electron Devices, vol. ED-16, p. 297, 1969.

[6] G. Groeseneken, H. E. Maes, N. Beltran, and R. F. De keersmecker, "A Reliable Approach to Charge Pumping Measurements in MOS-Transistors, " IEEE Trans. Electron Devices, vol. ED-31, p. 41, 1984.

[7] R. J. Van Overstraeten *et al*., "Theory of the MOS Transistor in Weak Inversion - New Method to Determine the Number of Surface States," IEEE Trans. Electron Devices, vol. ED-22, No. 5, 1975.

[8] Y. P. Tsividis, "Operation and Modeling of the MOS Transistor McGraw-Hill, 1987.

[9] W. L. ENGL, H. K. Dirks, and B. Meinerzhagen, "Device Modeling, " Proceedings of the IEEE, vol. 71, No. 1, 1983.

[10] R. Vankemmel, "Device Simulations with PRISM Manual v. 4.0," IMEC, Kapeldreef 75, B-3001 Leuven Belgium, 1993.

[11] Stanley Wolf, "Silicon Processing For The VLSI ERA, Volume 3, The Submicron MOSFET, " Lattice Press, 1995.

[12] Y. P. Tsividis, and K. Suyama, "MOSFET Modeling for Analog Circuit CAD: Problems and Prospects," IEEE Journal of Solid-State circuits, vol. 29, NO. 3, Mar. 1994.

[13] R. M. Kielkowski, "Inside Spice: Overcoming the Obstacles of Circuit Simulation," McGraw-Hill, 1994.

[14] H. Pao and C. Sah, "Effects of diffusion current on characteristics of MOS transistors," Solid-State Electron, vol. 9, pp. 927-937, 1966.

[15] J. R. Brews, "Physics of the MOS Transistor," Academic Press, 1981.

[16] F. Van de Wiele, "A long-channel MOSFET model," Solid-State Electron, vol. 22, pp. 991-997, 1979.

[17] Y. A. El-Mansy and A. R. Boothroyd, "A New Approach to the theory and Modeling of insulated-Gate-Field-Effect Transistors," dc, IEE E Trans. Electron Devices, vol. ED-24, No. 3, 1977.

[18] C. Turchetti and G. Masetti, "A CAD-oriented analytical MOSFET model for high-accuracy applications," IEEE Trans. Computer-Aided Design, vol. CAD-3, pp. 117-122, 1984.

[19] A. R. Boothroyd, S. W. Tarasewicz and C. Slaby, "MISNAN - a physically based continuous MOS-FET model for CAD applications IEEE Trans. Computer-Aided Design, vol. 10, pp. 1512-1529, 1991.

[20] H-J. Park, P. K. Ko and C. Hu, "A Charge Sheet Capacitance Model of Short Channel MOSFET's for SPICE," IEEE Trans. Computer-Aided Design, vol. 10, No. 3, 1991.

[21] K. Lee, M. Shur, T. A. Fjeldly and T. Ytterdal, "Semiconductor Device Modeling for VLSI," Prentice-Hall, 1993.

[22] R. Howes *et al.*, "An SOS MOSFET Model Based on Calculation of the surface potential," dc, IEEE Trans. Computer-Aided Design, vol. CAD-13, No. 4, 1994.

[23] G. Merckel, J. Borel and N. Z. Cupcea, "An accurate large-signal MOS transistor model for use in computer-aided design," transient, IEEE Trans. Electron Devices, vol. ED-19, pp. 681-690, 1972.

[24] H. I. Hanafi, L. M. Camnitz and A. J. Dally, "An Accurate and Simple MOSFET Model for Computer-Aided Design," dc, IEEE J. Solid-State Circuits, vol. SC-17, No. 5, 1982.

[25] P. Yang and P. K. Chatterjee, "Spice Modeling for Small Geometry MOSFET Circuits," IEEE Trans. Computer-Aided Design, vol. CAD-1, No. 4, 1982.

[26] S. Liu and L. W. Nagel, "Small-Signal MOSFET Models for Analog Circuit Design," ac, IEEE J. Solid-State Circuits, vol. SC-17, No. 6, 1982.

[27] J. A. Power and W. A. Lane, "An enhanced Spice MOSFET model for analog applications," IEEE Trans. Computer-Aided Design, vol. 11, pp. 1418-1425, 1992.

[28] B. J. Sheu, D. I. Scharfetter, P. K. Ko and Jeng, "BSIM: Berkely short channel IGFET model for MOS transistors," IEEE J. Solid-State Circuits, vol. SC-22, pp. 558-565, 1987.

[29] S. M. Gowda and B. J. Sheu, "BSIM_plus: an advanced SPICE Model for submicron MOS VLSI Circuits," IEEE Trans. Computer-Aided Design, vol. 13, No 9, 1994.

[30] Mohamed Amin Ebrahim, "MOSFET Modeling for Micropower Analog Circuits, " M. Sc. Thesis, Cairo 1995.

[31] S Selberherr, A. Schutz and H. Potztl, "MINIMOS - A Two Dimensional MOS transistor analyzer," IEEE Trans. Electron Devices, vol. ED-27, 1980.

[32] G. W. Taylor, "Subthreshold conduction in MOSFETs," IEEE Trans. Electron Devices, vol. ED-25, pp. 337-349, 1978.

[33] L. D. Yau, "A Simple Theory to predict the threshold Voltage of Short-Channel IGFET's," Solid-State Electron, vol. 17, 1974.

[34] M. Shur, "Physics of Semiconductor Devices," Prentice-Hall, 1990.

[35] Z. Liu, C. Hu, J. Huang et al., "Threshold Voltage Model for Deep-Submicron MOSFET's," IEEE Trans. Electron Devices, vol. 40, No. 1, 1993.

[36] C. R. Viswanathan, B. C. Burkey et al., "Threshold Voltage in Short-Channel MOS Devices," IEEE Trans. Electron Devices, vol. 32, No. 5,1985.

[37] T. A. Fjeldly, M. Shur, "Threshold Voltage Modeling and the Subthreshold Regime of Operation of short-Channel MOSFET's," IEEE Trans. Electron Devices, vol. 40, No. 1, 1993.

[38] J. Mar and S-Y. Yu, "Substrate Current Modeling for circuit simulation," IEEE Trans. Computer-Aided Design, vol. 1, No 4, 1982.

[39] J. H. Huang, Z. H. Liu, M. C. Jeng, K. Hui, M. Chan, P. K. Ko and C. Hu, "BSIM3 Manual (version 2)," The Regents of the University of California, 1994.

[40] A. Hussein, H. Haddara, and M. El-Said, "A New Approach for HDL-A Modeling MOSFET Ion-Implanted Layers in CAD Applications, " ICM, 1996

[41] P. Antognetti and G. Massobtio (editors), "Semiconductor Device Modeling with SPICE," McGraw-Hill, 1988.

[42] LabView Basics, National Instruments®, 1993.

[43] D.W. Marquardt. "An algorithm for least squares estimation of nonlinear parameters," Journal of the Society of Industrial and Applied Mathematics (SIAM), 431-441, 1963.

[44] K. Levenberg. "A method for the solution of certain nonlinear problems in least squares," Quarterly of Applied Mathematics, 164-168, 1944.

[45] K. M. Brown and J.E. Dennis Jr. "Derivative free analogues of the Levenberg-Marquardt and Gauss algorithms for nonlinear least squares approximation," Numerical Methods, 289-297, 1972.

[46] J.G. Reich. "Curve Fitting and Modeling for Scientist and Engineers," McGraw-Hill, New York, USA, 1992.

[47] J. E. Dennis Jr. "Nonlinear least squares," 269-312. Academic Press, London and New York, 1977.

[48] Y. Bard. "Comparison of gradients methods for the solution of nonlinear parameter estimation problems," Journal of the Society of Industrial and Applied Mathematics (SIAM), 157-187, July 1970.

[49] A. Vladimirescu and S. Liu, "The Simulation of MOS Integrated Circuits Using SPICE2," Electronics Res. Lab., University of California, Berkeley, Memo ERL-M80/7, 1980.

[50] B. J. Sheu, D. L. Scharfetter, P. K. Ko, and M.-C. Jeng, "BSIM: Berkely short-channel IGFET model for MOS transistors," IEEE J. Solid-State Circuits, vol. 22, No. 4, 1987.

[51] A. Chatterjee, C. F. Machala, III, and P. Yang, "A Submicron DC MOSFET Model for Simulation of Analog Circuits," IEEE Trans. Computer-Aided Design, vol. CAD-14, No. 10, 1995.

Appendix A

Measurement program in G language

In this appendix we present the measurement program, which is written in the G language and run under LABView program. Fig. A.1 shows the control panel which represents the user interface to the program, while Fig. A.2 shows the block diagram which represents the program code in graphic format.

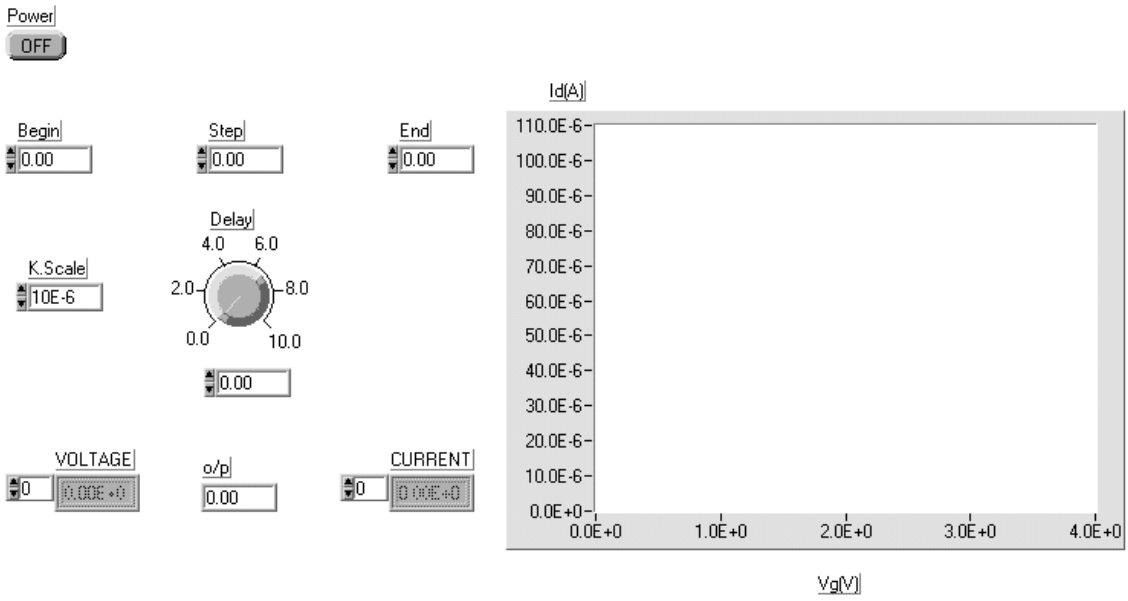

Figure A.1 *Measurement program control panel*

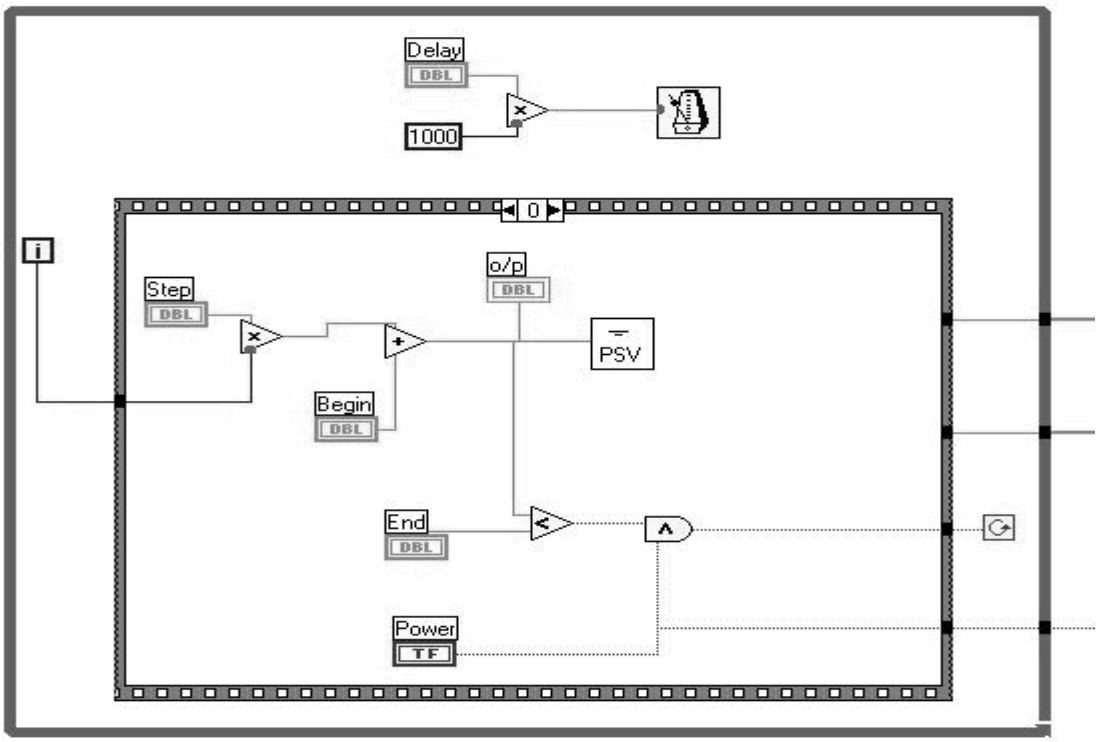
Delay
DBL
1000
0
i
Step
DBL
o/p
DBL
PSV
Begin
DBL
End
DBL
Power
TF

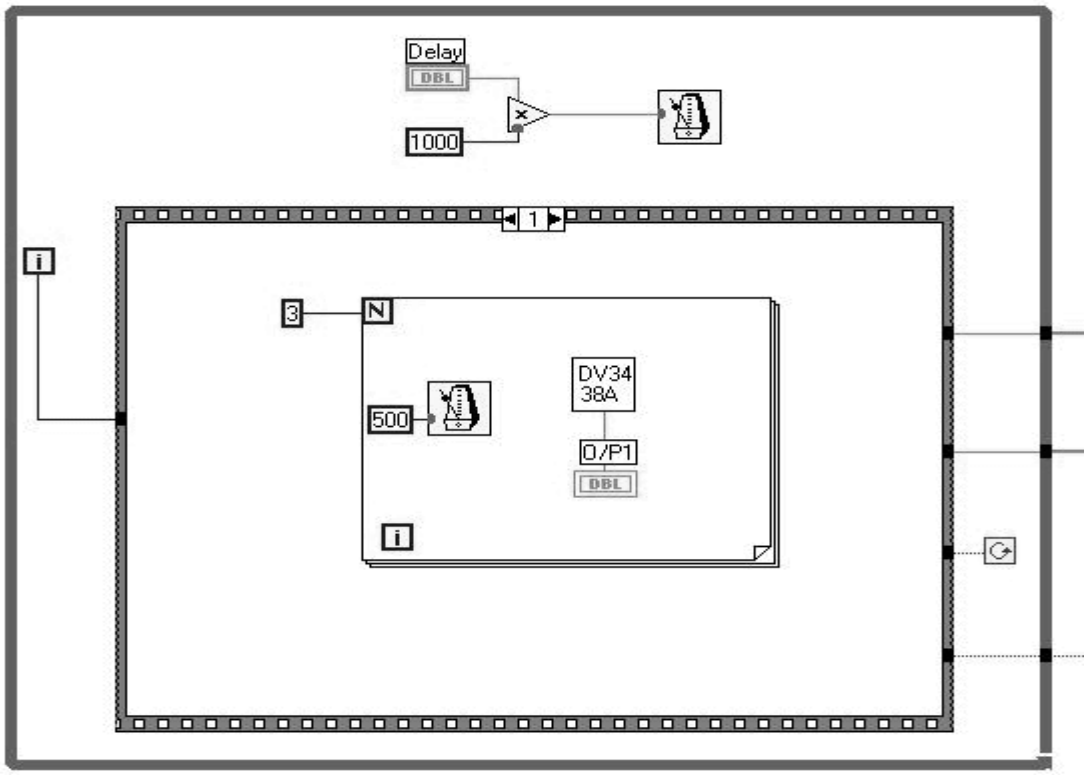
Delay
DBL
1000
1
i
3
N
500
DV34
38A
O/P1
DBL
i

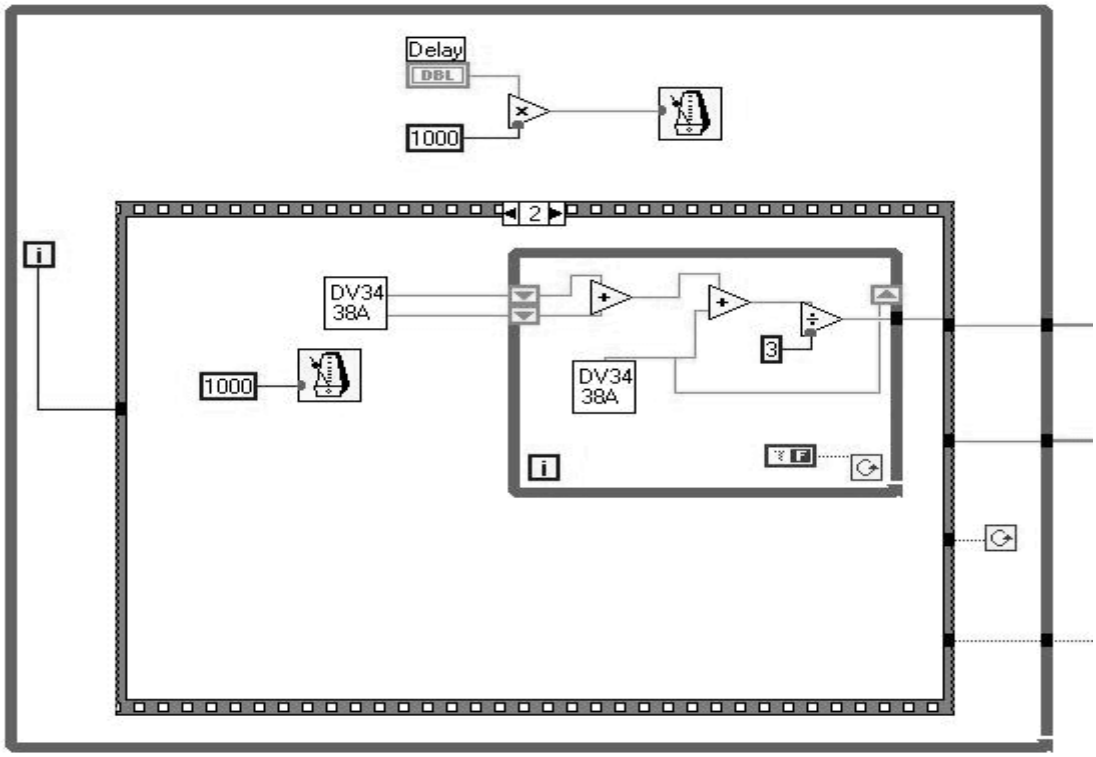
Delay
DBL
1000
2
i
DV34
38A
1000
DV34
38A
3
i

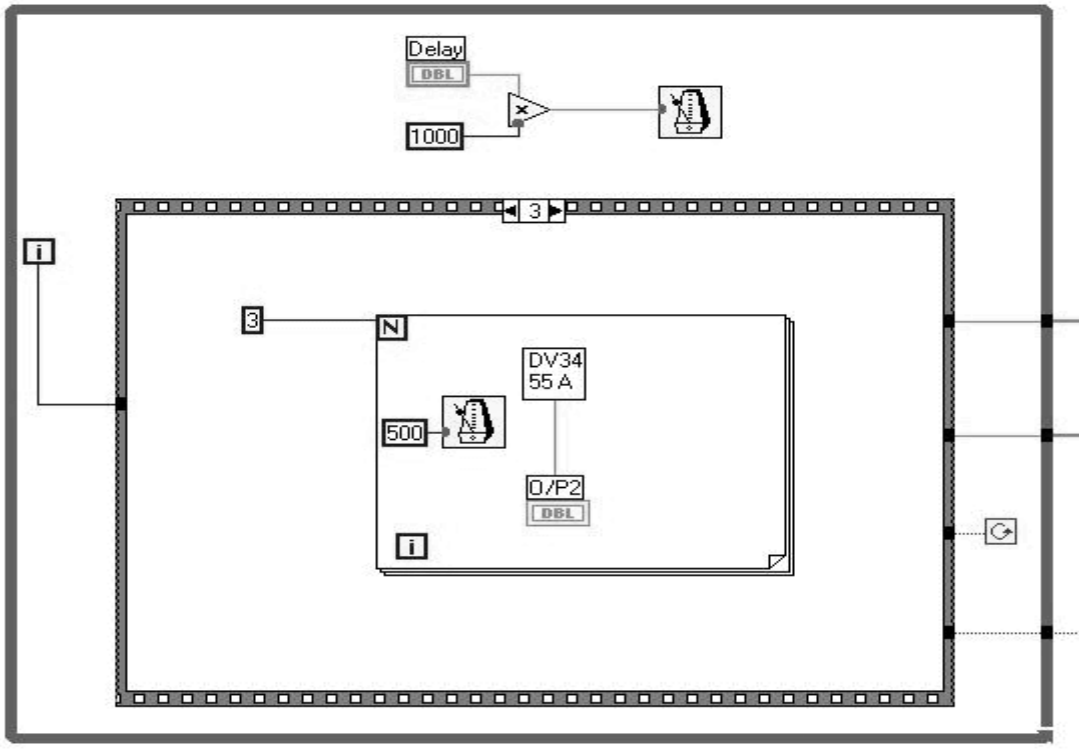
Delay
DBL
1000
3
i
3
N
DV34
55 A
500
0/P2
DBL
i

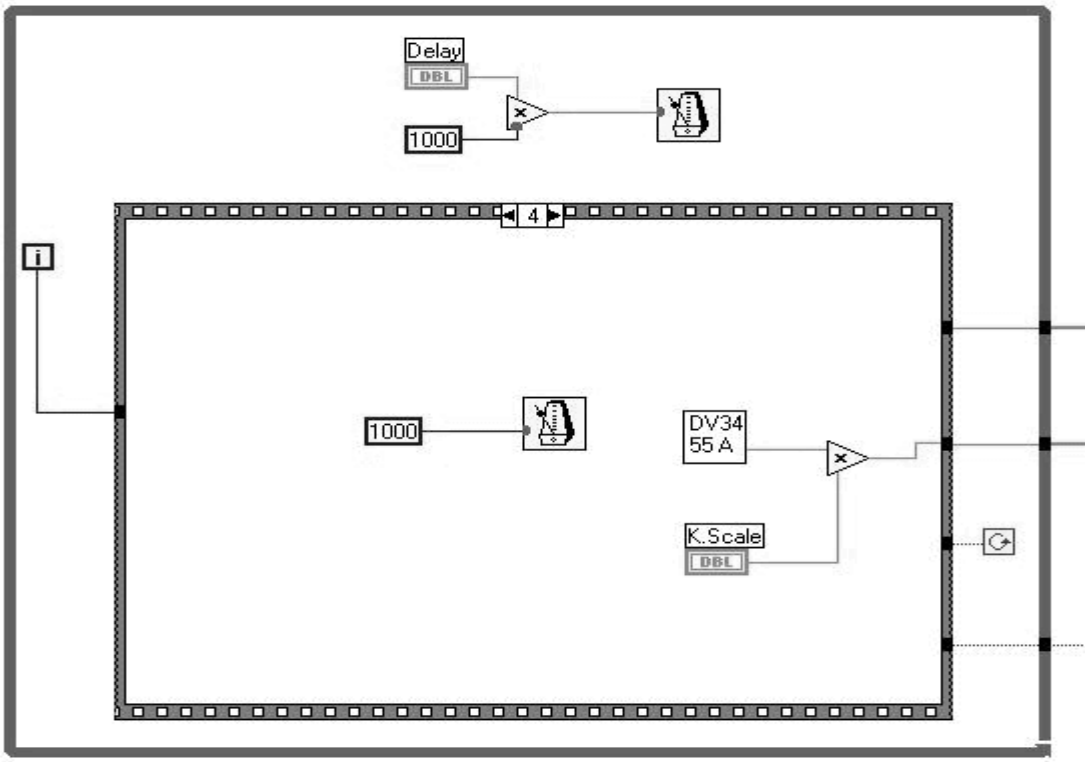
Delay
DBL
1000
4
i
1000
DV34
55 A
K.Scale
DBL

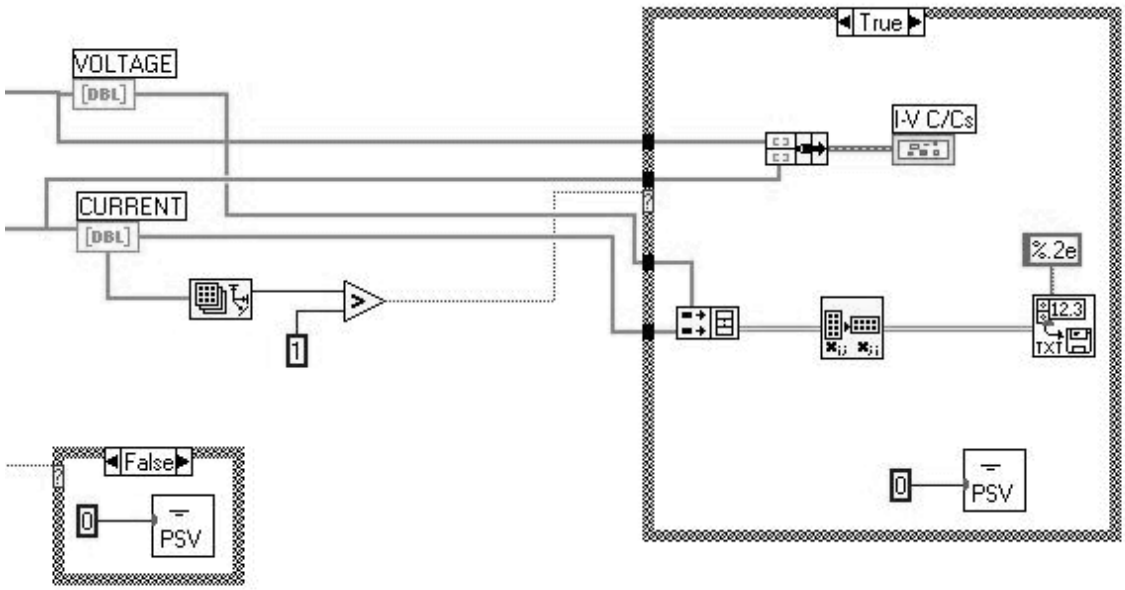
VOLTAGE
DBL
CURRENT
DBL
1
True
I-V C/Cs
%.2e
12.3
TXT
0
PSV
False
0
PSV

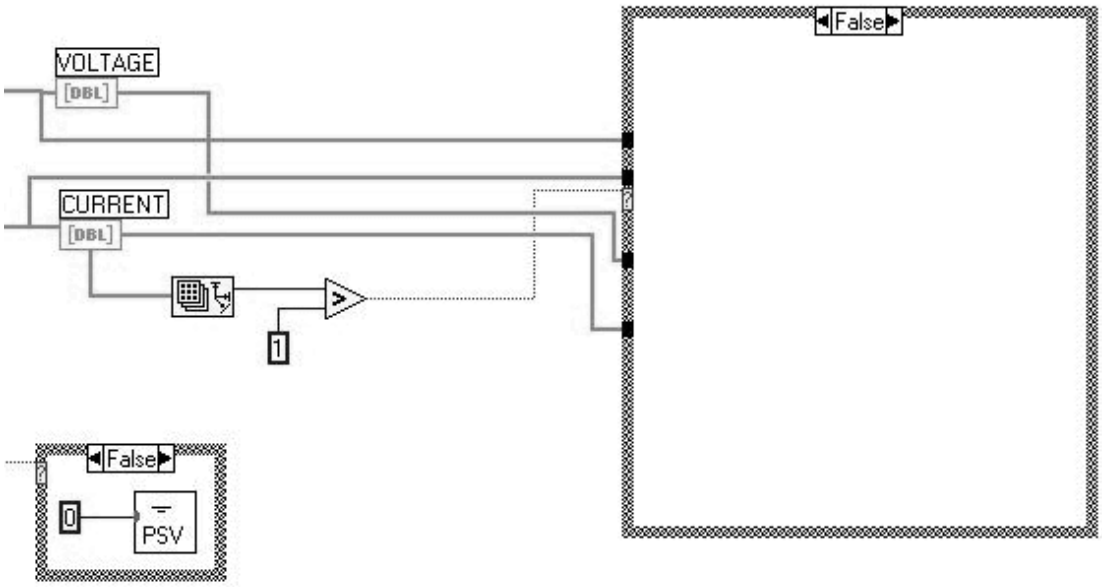

Figure A.2 *Measurement program block diagram*

Appendix B

Model Formulation in

HDL-A[1] Language

```
--
--  ICL Model for MOSFET
--
ENTITY NMOS IS

GENERIC (
        W,L,LDEL,DEW,yj,Tox,VTO,Gamma,PHI,VFB,Nsub,Nsd,Nox,
        Dit,TPG,PMS,MUo,Theta,vmax,beta,Rt,Ld,xsat,Neff,
        DSB,AI,BI,I_leak,Sleak,Dose,D,nimp,mimp :REAL );

PIN ( D,G,S,B: ELECTRICAL );
END ENTITY NMOS;

ARCHITECTURE a OF NMOS IS

-- (* Constants *)
   CONSTANT K,Eo,PHIt,q,ni,Eg,EGP :real;
   CONSTANT Ko,Ks,Cox,PHIf,Vbi :real;
   CONSTANT PHIms,Dit1,KP,EPSt :real;
--(* Constant model parameter *)
   CONSTANT VFB1,Gamma1:real;
   CONSTANT Leff,Weff,Rs :real;
   CONSTANT xep,EPS_MIN,lc :real;
   CONSTANT xdibl,K1,KW :real;

-- (* Variables *)

    STATE  VGB,VGB1,VGB2,VGBD,VSB:ANALOG ;
    STATE  VDB,VDB1,VDB2,VDS,VDS1,VDS2:ANALOG ;
-- (* EPS calculation numerically *)
```

[1] HDL-A is a Hardware Description Language developed by ANACAD Electrical Engineering Software.

```
    VARIABLE ii: integer;
    VARIABLE xd1,xd2:real;
    STATE EPSw1,EPSw2,EPSw3,EPSw4:ANALOG;
    STATE EPSst1,EPSst2,EPSst4:ANALOG;
    STATE EPS1,EPS2,EPS3,EPS4:ANALOG;
-- (* NOTE: EPS with
--    (1) -> at the source without Dit
--    (2) -> at the drain without Dit taking the effect of Dit on Vth
--    (3) -> at the source with Dit
--    (4) -> at the drain with Dit  *)
    VARIABLE X1,X2:real;
    VARIABLE d2Qsc_dEP,d2Qit_dEP:real;
    VARIABLE FF0,FF1,dFF1_dEP,d2FF1_dEP:real;

-- (* Charges *)
    STATE Qit_s1,Qit_d1:ANALOG;
    STATE Qvs1,Qvd1:ANALOG;

-- (* Currents *)
    VARIABLE ED,ED1,ED2,ED32,ED12,EPSs,EPSd:real;
    STATE ID,IDD,IDS,IDdiff,Iddrift :ANALOG;

-- (* Mobility model *)
    STATE FG,FL,FL0,j1:ANALOG;
    STATE MU,MU1,MU2:ANALOG;

-- (* Saturation *)
    STATE VTH1,VTH,VDSsat,Vss,Vsl,A,B1:ANALOG;
    STATE DL,IDdrift1,Isat,bb,bb1,FB:ANALOG;

-- (* Impact ionization current *)
    STATE Isub,Idam :ANALOG;

-- (* Threshold shift + DIBL *)
    STATE ddep,LAMDA,VGTH,V1,V2,k2:ANALOG;
    VARIABLE alaa1,alaa2,alaa3,alaa4,alaasnh1:real;
    STATE DIBL,DIBL1,XDIBL1,XDIBL2:ANALOG;
    STATE Vb_PHIs3,Vb_PHIs4:ANALOG;
    STATE PHIs3,PHIs4,L4,L5,L1,L2,L3:ANALOG;

-- (* Test variables *)
    STATE reg,j2,n1,n2,n3,n4:ANALOG;
```

BEGIN RELATION

PROCEDURAL FOR INIT =>

```
-- (*Parameters' default values*)
      W := 20.0e-4;          -- (*Width (cm) 20 um*)
      L := 20.0e-4;          -- (*Length (cm) 10 um*)
      LDEL := 0.0;           -- (*Total Length shortening (cm)*)
      DEW := 0.0;            -- (*Total Width shortening (cm)*)
      yj := 0.5e-4;          -- (*Junction depth (cm) 0.4 um*)
      Tox := 20.0e-7;        -- (*Oxide thickness (cm) 20 nm*)
      VTO := 0.0;            -- (*OPTIONAL, Threshold voltage at VSB  := 0
                             --  and for large L)
      Gamma := 0.0;          -- (*OPTIONAL, Body factor*)
      PHI := 0.0;            -- (*OPTIONAL, Surface potential at threshold*)
      VFB := 0.0;            -- (*OPTIONAL, Flat-band voltage*)
      Nsub := 1.0e+16;       -- (*Substrate doping (1/cm^3)*)
      Nsd := 1.0e+19;        -- (*Source/drain doping (1/cm^3)*)
      Nox := 0.0;            -- (*Oxide charge density (1/cm^2)*)
      Dit := 0.0;            -- (*Interface trap density (1/cm^2.V*)
                     -- (*+ve -> Donor like
                     -- -ve -> Acceptor like *)
      TPG := 0.0;            -- (*Gate type: 0  := Metal(Al),
                     --  -1  := NPOLY, +1  := PPOLY*)
      PMS := 0.0;            -- (*Work funcion difference (V)
                     --  0 use analytical model*)
      MUo := 650.0;          -- (*Low field mobility (cm^2/V.s)*)
      Theta := 0.05;         -- (*Gate effect on the mobility (1/V)*)
      vmax := 1.0e+7;        -- (*Electrons saturation velocity (cm/s)*)
      beta := 2.0;           -- (*Lateral mobility exponent (for electrons) *)
      Rt := 0.0;             -- (*Total series resistance (Ohm)*)
      Ld := 0.0;             -- (*DIBL charachteristic length (cm)*)
      xsat := 10.0;          -- (*Saturation velocity knee factor*)

-- (*Saturation *)
      Neff := 1.0;           -- (*Saturation slope factor*)
      DSB := 3.0;            -- (*DIBL dependence on the bulb voltage*)
      AI := 1.2;             -- (*Impact ionization multiplication coeff (V^-1)*)
      BI := 1.3e6;           -- (*Impact ionization c/c field (V/cm)*)
                     -- (* BI postpones the rise of the current,
                     -- AI controls the magnitude of the
                     -- impact ionization current *)
```

```
      I_leak := 1.0e-20;       -- (*Leakage current (amp)*)
      Sleak := 100.0;       -- (*Leakage current division factor.
                        -- Determines the knee of leakage current*)
      Dose :=0.0;    -- Dose in cm^-3
      D := 0.5e-4;    -- Non uniform doping effective width in cm
      nimp := 0.2;    -- Control doping shape
      mimp := 5.0;   -- Non uniform doping knee factor

-- (*Constants*)
      Eo := 8.854e-14;       -- (*Permittivity of free space (F/cm)*)
      K := 1.38066e-23;      -- (*Boltzmann's constant *)
      q := 1.6e-19;          -- (*Magnitude of electron charge (C)*)
      Ko := 3.9;             -- (*SiO2 relative permittivity*)
      Ks := 11.9;            -- (*Si relative permittivity*)

-- (*Temperature dependent constants*)
PHIt := K* Temperature/q;      -- (*Thermal voltage (V)*)
Eg := (1.16-7.02e-4*(Temperature ** 2.0)/(Temperature+1108.0)) /PHIt;
                        -- (*Si energy gap (eV)*)
                        -- (*Normalized to PHIt*)
      ni := (1.45E10)*((Temperature/300.0) ** 1.5)*exp((q*Eg*PHIt)
           /(2.0*K)*(1.0/300.0-1.0/Temperature));
                        -- (*Intrinsic density (1/cm^3)*)

-- (*constant model parameters*)
      lc := sqrt(Ks/Ko*Tox*yj);
      Rs := Rt/2.0;
      Leff := L-LDEL;        -- (*Effective channel length*)
      Weff := W-DEW;         -- (*Effective channel width*)
    IF (PHI = 0.0) THEN
       PHIf := ln(Nsub/ni);   -- (*Ei-Ef in the bulk (V)*)
                         -- (*Normalized to PHIt*)
    ELSE
       PHIf := PHI/(2.0*PHIt);
    END IF;
      EGP := EG/2.0-PHIf;
      EPS_MIN := 2.0;       -- (*Minimum EPSI allowed, ELSE current  :=
I_leak*)
      EPSt := 2.0*PHIf;      -- (*Strong inversion surface potential (V)*)
                        -- (*Normalized to PHIt*)
      Cox := Eo*Ko/Tox;     -- (*Oxide capacitance/area (F/cm^2)*)
    IF (Gamma = 0.0) THEN     -- (*Body factor (V^1/2)*)
```

```
                    -- (*Normalized to PHIt^1/2*)
      Gamma1 := sqrt(2.0*q*Ks*Eo*Nsub/PHIt)/Cox;
    ELSE
      Gamma1 := Gamma;
    END IF;

     KW := pi*Ks*Tox/(Ko*Weff);
                    -- (*Constants used in narrow channel effect*)

-- (* Threshold model *)
    IF (VTO = 0.0) THEN
    IF (VFB = 0.0) THEN

    IF (PMS = 0.0) THEN      -- (*Use analytical model for PMS *)
                    -- (*Normalized to PHIt*)
      IF (TPG = 1.0) THEN  --      (*PPOLY Gate*)
          PHIms := EG/2.0-PHIf;
      ELSE IF (TPG = -1.0) THEN -- (*NPOLY Gate*)
          PHIms := -EG/2.0-PHIf;
      ELSE                  -- (*METAL Gate*)
          PHIms := -0.05/PHIt-EG/2.0-PHIf;
        END IF;
      END IF;
    ELSE                -- (*Use the given PMS*)
       PHIms := PMS/PHIt;
    END IF;
      VFB1 := PHIms-(q*Nox)/Cox/PHIt;

    ELSE      -- (*VFB*)
      VFB1 := VFB/PHIt;
    END IF;     -- (*VFB*)
    ELSE      -- (*VTO*)
      VFB1 := VTO/PHIt-EPSt-Gamma1*sqrt(EPSt);
    END IF;     -- (*VTO*)

    IF (Dit = 0.0) THEN
      Dit1 := 0.0;
    ELSE IF (Dit > 0.0) THEN
      Dit1 := Dit;
      Vfb1 := Vfb1-(q*Dit1*(EG-EGP))/Cox;
    ELSE
      Dit1 := -Dit;
```

```
        Vfb1 := Vfb1+q*Dit1*EGP/Cox;
    END IF;
    END IF;
                    -- (*Flat band voltage (V)*)
                    -- (*Normalized to PHIt*)
     Vbi := ln(Nsub*Nsd/ni/ni);
                    -- (*Built-in junction voltage (V)*)
                    -- (*Normalized to PHIt*)
     KP := (Weff/Leff)*Cox*(PHIt ** 2.0);
                    -- (*Transconductance parameter (F.V^2/cm^2)*)
     xep := 10.0;        -- (*Knee factor for limiting EPSI in
                    -- Qit calculation *)

-- (* Threshold shift + DIBL *)
     K1 := (PHIt)*(2.0*Ks*Eo)/(q*Nsub);
                    -- (*Normalized to PHIt (V^-1)*)
     xdibl := 5.0;       -- (*Diffusion current CLM knee factor*)
     LAMDA := Ld;
```

PROCEDURAL FOR DC =>

```
-- (* All voltages are normalized to PHIt, and are referenced to
-- the bulk potential VB*)

-- (********************** Measure the pins' voltages ***********)
        VSB  := (S.v-B.v)/PHIt;
        VGB  := (G.v-B.v)/PHIt-VFB1-KW*(EPSt+VSB);
        VDB  := (D.v-B.v)/PHIt;
        VDS  := (D.v-S.v)/PHIt;

-- (*NOTE:  VDB1, VGB1, VDS1 are used in strong inversion, while
--   VDB2, VGB2, VDS2 are used in weak inversion *)

      IF (VDS = 0.0) THEN
            IDdiff := I_leak/Sleak;
            IDdrift := I_leak/Sleak;
      ELSE

      IF (VGB <= 0.0) THEN
           REPORT "VG-VB-Vfb is negative, the device is in
accumulation" SEVERITY WARNING;
            IDdiff := I_leak/Sleak;
            IDdrift := I_leak/Sleak;
```

```
      ELSE


-- (**** Threshold shift + DIBL using the threshold surface potential ****)

       EPSs := EPSt+real(VSB);

      IF (Ld = 0.0) THEN
            ddep := sqrt(K1*EPSs);
            LAMDA := 0.1 * ((yj*real(ddep)*Tox) ** (1.0/3.0));
      ELSE IF (B.v /=  0.0) THEN
            k2 := (real(LAMDA) ** (DSB))/EPSt;
            LAMDA := (real(k2)*(EPSs)) ** (1.0/DSB);
      END IF;
      END IF;

       alaa1 := exp(Leff/real(LAMDA));
       alaa2 := exp(-Leff/real(LAMDA));
       alaa3 := exp(Leff/(2.0*real(LAMDA)));
       alaa4 := exp(-Leff/(2.0*real(LAMDA)));
       alaasnh1 := (alaa3-alaa4) ** 2.0;

       V1 := Vbi+VSB-EPSs;
       V2 := V1+VDS;

      DIBL := (2.0*real(V1)+real(V2)*(1.0-alaa2)+2.0*sqrt((real(V1) **
      2.0)+real(V1*V1)*(alaa1-1.0)))/alaasnh1;    -- (*DIBL with VDS*)

       VGB2 := VGB+DIBL;
                    -- (*VGB to be used in the diffusion component*)

-- (*Local bias dependent constants*)
       FB := 1.0+GAMMA1/(2.0*sqrt(1.0/PHIt+VSB+EPSt));
                    -- (*Saturation voltage division factor
                    -- as in Tsividis*)

       VTH1 := (EPSt+VSB+Gamma1*sqrt(EPSt+VSB)-DIBL)*2.5;
       VGTH := real(VGB2/VTH1) ** 5.0;
       XDIBL1 := 1.0-VGTH/(1.0+VGTH);       -- (*Used in VGB1*)

       VTH1 := (EPSt+6.0+VSB+Gamma1*sqrt(EPSt+6.0+VSB)-DIBL);
       VGTH := real(VGB2/VTH1) ** 15.0;
```

```
        XDIBL2 := 1.0-VGTH/(1.0+VGTH);       -- (*Used in VDB2*)

        VGB1 := VGB+DIBL*xdibl1*1.2;
                    -- (*VGB to be used in the drift component*)


-- (********** Initial Guess for the surface potentials ****************)

-- (* Weak inversion estimated maximum surface potential  *)

      IF ((Gamma1/2.0) ** 2.0 + VGB2-1.0  < 0.0) THEN
           REPORT "Weak inversion Surface potential is negative"
SEVERITY WARNING;
            IDdiff := I_leak/Sleak;
            IDdrift := I_leak/Sleak;
      ELSE

--     (* Estimated EPSW without Dit *)
       EPSw1  := VGB1+(Gamma1 ** 2.0)/2.0-Gamma1*
                 sqrt((Gamma1/2.0) ** 2.0 + VGB1-1.0);
                 --      (*used in EPS1 and EPS2*)
       EPSw2  := VGB2+(Gamma1 ** 2.0)/2.0-Gamma1*
                 sqrt((Gamma1/2.0) ** 2.0 + VGB2-1.0);
                 --      (*used in EPS3 and EPS4*)

--     (* Estimated EPSW with Dit *)
      IF (Dit1 /=  0.0) THEN

            X1 := 1.0+q*Dit1/Cox;

            X2 := real(VGB2)-q*Dit1*(-real(VSB)+ln(1.0+exp(-
            (real(EPSw2)+EGP-real(VSB)))))/Cox;
            EPSw3 := (X1*X2+(Gamma1 ** 2.0) / 2.0 - Gamma1*
            sqrt((Gamma1/2.0) ** (2.0) + X1*X2 - X1 ** (2.0)))
            / (X1 ** 2.0);

            X2 := real(VGB2)-q*Dit1*(-real(VDB2)+ln(1.0+exp(-
            (real(EPSw2)+EGP-real(VDB2)))))/Cox;
            EPSw4 := (X1*X2+(Gamma1 ** 2.0) / 2.0 - Gamma1*
            sqrt((Gamma1/2.0) ** (2.0) + X1*X2 - X1 ** (2.0)))
            / (X1 ** 2.0);
```

```
        ELSE
                EPSw3 := EPSw2;
                EPSw4 := EPSw2;
        END IF;
                EPSw2 := EPSw1;

-- (*EPS Check*)

        if ( (EPSw1 <=  EPS_MIN) OR (EPSw2 <=  EPS_MIN) OR
        (EPSw3 <=  EPS_MIN) OR (EPSw4 <=  EPS_MIN)) THEN
              REPORT "EPSW is negative" SEVERITY WARNING;
                IDdiff := I_leak/Sleak;
                IDdrift := I_leak/Sleak;

        ELSE

-- (* Strong inversion estimated surface potential    *)

        IF (abs(VGB1-EPSt-VSB) < 1.5) THEN
                EPSst1 := EPSt+VSB+2.0;
        ELSE
                EPSst1 := EPSt+VSB+2.0*ln(abs(VGB1-EPSt-VSB)/Gamma1);
        END IF;

-- (Continuous estimated surface potential (first approximation, empirical))

          xd1 := 9.0+9.0*real(VSB)*PHIt;
          xd2 := 9.0+9.0*real(VDB)*PHIt;

--      (* xd  := 9 in the above calculations the error in epsi is less than 0.08%
--        in the range of Nsub  := 1e15-1e18 and Dit1  := 0-3e11 *)

          EPS1 := real(EPSw1)/(1.0+(real(EPSw1)/real(EPSst1)) **
          xd1)**(1.0/xd1);
          EPS3 := real(EPSw3)/(1.0+(real(EPSw3)/real(EPSst1)) **
          xd1)**(1.0/xd1);

-- (*To compute EPS2 and EPS4 we must take into account the saturation
-- effect by calculating VDSsat *)

-- (*Normal field effect on the mobility *)
          EPSs := real(EPS1);
```

```
        EPSd := real(EPS1);
        ED2  := (EPSd+EPSs)/(2.0);

        FG := 1.0+Theta*PHIt*(VGB1-ED2);

        MU1 := MUo/FG;

-- (* calculation of pre-VDS1 saturation for EPS2 and EPS4 calculation*)

        Vss := vmax*Leff/(MU1*PHIt);
        VTH := EPS1+Gamma1*sqrt(EPS1-1.0);
        bb := w/Leff*MU1*Cox;
        Vsl := (VGB1-VTH)/FB;
        bb1 :=
sqrt(1.0+2.0*real(bb)*real(Vsl)*PHIt*Rs+(real(Vsl)/real(Vss))
         ** 2.0);

        Isat := (bb1-(1.0+bb*Vsl*PHIt*Rs))/(bb*
                (1.0/((real(bb)*real(Vss)*PHIt) ** 2.0)-(Rs ** 2.0)));

        VDSsat := 0.01+(Vsl*PHIt+(Rs-1.0/(bb*Vss*PHIt))*Isat)/PHIt;

        VDS1 := (real(VDS)/(1.0+(real(VDS)/real(VDSsat))**
        xsat)**(1.0/xsat));
        VDB1 := VDS1+VSB;     -- (*VDB taking saturation into effect*)

        VDS2 := VDS1*(1.0-Xdibl2)+VDS*Xdibl2;
        VDB2 := VDS2+VSB;     -- (*VDB taking saturation into effect*)


-- (* EPS2*)

      IF (abs(VGB1-EPSt-VDB1) < 1.5) THEN
            EPSst2  := EPSt+VDB1+2.0;
      ELSE
            EPSst2  := EPSt+VDB1+2.0*ln(abs(VGB1-EPSt-
VDB1)/Gamma1);
      END IF;

        EPS2  := real(EPSw2)/(1.0+(real(EPSw2)/real(EPSst2)) ** xd2) **
        (1.0/xd2);
```

```
-- (* EPS4 *)

--      (* For EPS4 the drain saturation voltage is equal to VDS in weak
--       inversion and VDS1at in strong inversion*)

       IF (abs(VGB2-EPSt-VDB2) < 1.5) THEN
             EPSst2  := EPSt+VDB2+2.0;
       ELSE
              EPSst2  := EPSt+VDB2+2.0*ln(abs(VGB2-EPSt-
              VDB2)/Gamma1);
       END IF;

        EPS4  := real(EPSw4)/(1.0+(real(EPSw4)/real(EPSst2)) ** xd2) **
        (1.0/xd2);


-- (*EPS Check*)

       if ((EPS1 <=  EPS_MIN) or (EPS2 <=  EPS_MIN) or
          (EPS3 <=  EPS_MIN) or (EPS4 <=  EPS_MIN)) THEN
             REPORT "EPSes is negative" SEVERITY WARNING;
              IDdiff  := I_leak/Sleak;
              IDdrift  := I_leak/Sleak;
       ELSE


--(* Continuous estimated surface potential (second approximation,
-- second order Newton-Raphson)  *)

         Qvs1 := real(EPS3)/((1.0+(real(EPS3)/(EG-EGP+real(VSB))) ** xep)
** (1.0/xep));
         Qvd1 := real(EPS4)/((1.0+(real(EPS4)/(EG-EGP+real(VDB2))) **
xep) ** (1.0/xep));

       FOR ii IN 1 TO 2  LOOP          -- (*Using 2 iterations*)

-- (* Compute EPS3 and EPS4 used in the calculation of the diffusion
component*)

-- (*Normal field effect on the mobility *)
         EPSs  := real(EPS1);
```

```
        EPSd  := real(EPS2);
        ED  := EPSd-EPSs;
        ED2  := (EPSd+EPSs)/(2.0);
        ED32  := (EPSd) ** (1.5) -
              (EPSs) ** (1.5);

      IF (ED = 0.0) THEN
              FG := 1.0+Theta*PHIt*(VGB1-ED2);
      ELSE
              FG  := 1.0+Theta*PHIt*(VGB1-
ED2+(1.0/1.5)*Gamma1*ED32/ED);
      END IF;

        MU1 := MUo/FG;

-- (* calculation of VDS1 saturation for EPS4 calculation*)

        Vss := vmax*Leff/(MU1*PHIt);
        VTH := real(EPS1)+Gamma1*sqrt(real(EPS1)-1.0);
        bb := w/Leff*MU1*Cox;

        Vsl := (VGB1-VTH)/FB;
        bb1 :=
sqrt(1.0+2.0*real(bb)*real(Vsl)*PHIt*Rs+(real(Vsl)/real(Vss)) ** 2.0);

        Isat := (real(bb1)-(1.0+real(bb)*real(Vsl)*PHIt*Rs))/
            (real(bb)*(1.0/((real(bb)*real(Vss)*PHIt) ** 2.0)-(Rs ** 2.0)));

        VDSsat := 0.01+(Vsl*PHIt+(Rt/2.0-1.0/(bb*Vss*PHIt))*Isat)/PHIt;

        VDS1 := (real(VDS)/(1.0+(real(VDS)/real(VDSsat)) ** xsat) **
        (1.0/xsat));
        VDB1 := VDS1+VSB;     -- (*VDB1 taking saturation into effect*)

        VDS2 := VDS1*(1.0-Xdibl2)+VDS*Xdibl2;
        VDB2 := VDS2+VSB;       -- (*VDB2 taking saturation into effect*)

      IF (Dit1 /=  0.0) THEN

-- (**********EPS3**)

        X1 := exp(-(EGP+real(Qvs1)-real(VSB)));
```

```
        d2Qit_dEP := -q*Dit1*(X1/(1.0+X1))*(1.0-X1/(1.0+X1));

        X2 := exp(real(EPS3)-2.0*PHIf-real(VSB));
        FF0 := sqrt(real(EPS3)-1.0+X2);
        d2Qsc_dEP := -Gamma1*Cox/(2.0*FF0)*(X2-((1.0+X2)
                ** (2.0)) /(2.0*FF0 ** 2.0));
        FF1  := real(EPS3)-real(VGB2)+(Gamma1*Cox*FF0+q*Dit1*
              (real(Qvs1)-real(VSB)+ln((1.0+X1))))/Cox;
        dFF1_dEP  := 1.0+(q*Dit1*(1.0-X1/(1.0+X1))
              +Gamma1*Cox/(2.0*FF0)*(1.0+X2))/Cox;
        d2FF1_dEP  := -(d2Qsc_dEP+d2Qit_dEP)/Cox;

        EPS3  := EPS3-(FF1/dFF1_dEP)/(1.0-(FF1*d2FF1_dEP)/
              (2.0*(dFF1_dEP) ** 2.0));

-- (**********EPS4**)

        X1 := exp(-(EGP+real(Qvd1)-real(VDB2)));
        d2Qit_dEP := -q*Dit1*(X1/(1.0+X1))*(1.0-X1/(1.0+X1));

        X2 := exp(real(EPS4)-2.0*PHIf-real(VDB2));
        FF0 := sqrt(((real(EPS4)-1.0)+X2));
        d2Qsc_dEP := -Gamma1*Cox/(2.0*FF0)*(X2-((1.0+X2)
                ** (2.0)) /(2.0*FF0 ** 2.0));

        FF1 := real(EPS4)-real(VGB2)+(Gamma1*Cox*FF0+q*Dit1*
              (real(Qvd1)-real(VDB2)+ln((1.0+X1))))/Cox;
        dFF1_dEP := 1.0+(q*Dit1*(1.0-X1/(1.0+X1))
              +Gamma1*Cox/(2.0*FF0)*(1.0+X2))/Cox;
        d2FF1_dEP := -(d2Qsc_dEP+d2Qit_dEP)/Cox;

        EPS4 := EPS4-(FF1/dFF1_dEP)/(1.0-(FF1*d2FF1_dEP)/
              (2.0*(dFF1_dEP) ** 2.0));


-- (**********Qit**)
        Qvs1  := real(EPS3)/((1.0+(real(EPS3)/(EG-EGP+real(VSB))) **
        xep) ** (1.0/xep));
        Qvd1  := real(EPS4)/((1.0+(real(EPS4)/(EG-EGP+real(VDB2))) **
        xep) ** (1.0/xep));

        Qit_s1  := -q*Dit1*(Qvs1-VSB+ln(1.0+(exp(-EGP+VSB-Qvs1))));
```

```
        Qit_d1  := -q*Dit1*(Qvd1-VDB2+ln(1.0+(exp(-EGP+VDB2-
        Qvd1))));

      ELSE                      -- (*Dit  := 0.0*)

-- (**********EPS3**)

        X2 := exp(real(EPS3)-2.0*PHIf-real(VSB));
        FF0 := sqrt(((real(EPS3)-1.0)+X2));
        d2Qsc_dEP := -Gamma1*Cox/(2.0*FF0)*(X2-((1.0+X2)
                  ** (2.0)) /(2.0*FF0 ** 2.0));

        FF1 := real(EPS3)-real(VGB2)+(Gamma1*Cox*FF0)/Cox;
        dFF1_dEP := 1.0+(Gamma1*Cox/(2.0*FF0)*(1.0+X2))/Cox;
        d2FF1_dEP :=  -(d2Qsc_dEP)/Cox;

        EPS3 := EPS3-(FF1/dFF1_dEP)/(1.0-(FF1*d2FF1_dEP)/
              (2.0*(dFF1_dEP) ** 2.0));

-- (**********EPS4**)

        X2 := exp(real(EPS4)-2.0*PHIf-real(VDB2));
        FF0 := sqrt(((real(EPS4)-1.0)+X2));
        d2Qsc_dEP := -Gamma1*Cox/(2.0*FF0)*(X2-((1.0+X2)
                  ** (2.0)) /(2.0*FF0 ** 2.0));

        FF1 := real(EPS4)-real(VGB2)+(Gamma1*Cox*FF0)/Cox;
        dFF1_dEP := 1.0+(Gamma1*Cox/(2.0*FF0)*(1.0+X2))/Cox;
        d2FF1_dEP :=  -(d2Qsc_dEP)/Cox;

        EPS4 := EPS4-(FF1/dFF1_dEP)/(1.0-(FF1*d2FF1_dEP)/
              (2.0*(dFF1_dEP) ** 2.0));


        Qit_s1 :=  0.0;
        Qit_d1 :=  0.0;

      END IF;

-- (*The effect of Qit on the threshold for the drift component*)

        VGBD := VGB1+Qit_s1/Cox;
```

```
-- Compute EPS1 and EPS2 used in the calculation of the drift component

-- (**************EPS2**)

        X2 := exp(real(EPS2)-2.0*PHIf-real(VDB1));
        FF0 := sqrt(((real(EPS2)-1.0)+X2));
        d2Qsc_dEP := -Gamma1*Cox/(2.0*FF0)*(X2-((1.0+X2)
                  ** (2.0)) /(2.0*FF0 ** 2.0));

        FF1 := real(EPS2)-real(VGBD)+(Gamma1*Cox*FF0)/Cox;
        dFF1_dEP := 1.0+(Gamma1*Cox/(2.0*FF0)*(1.0+X2))/Cox;
        d2FF1_dEP :=  -(d2Qsc_dEP)/Cox;

        EPS2 := EPS2-(FF1/dFF1_dEP)/(1.0-(FF1*d2FF1_dEP)/
              (2.0*(dFF1_dEP) ** 2.0));

-- (**************EPS1**)

        X2 := exp(real(EPS1)-2.0*PHIf-real(VSB));
        FF0 := sqrt(((real(EPS1)-1.0)+X2));
        d2Qsc_dEP := -Gamma1*Cox/(2.0*FF0)*((X2)-(1.0+X2)
                  ** (2.0) / (2.0*FF0 ** 2.0));

        FF1 := real(EPS1)-real(VGBD)+(Gamma1*Cox*FF0)/Cox;
        dFF1_dEP := 1.0+(Gamma1*Cox/(2.0*FF0)*(1.0+X2))/Cox;
        d2FF1_dEP :=  -(d2Qsc_dEP)/Cox;

        EPS1 := EPS1-(FF1/dFF1_dEP)/(1.0-(FF1*d2FF1_dEP)/
              (2.0*(dFF1_dEP) ** 2.0));

      END LOOP;                  -- (*End of iteration loop*)


-- (*EPS Check*)

      IF ((EPS1 <=  EPS_MIN) or (EPS2 <=  EPS_MIN) or
        (EPS3 <=  EPS_MIN) or (EPS4 <=  EPS_MIN)) THEN
          REPORT "EPS is negative" SEVERITY WARNING;
           IDdiff := I_leak/Sleak;
           IDdrift := I_leak/Sleak;
```

```
      ELSE


-- (************************ Mobility ******************)

-- (* Lateral Mobility model *)
        EPSs := real(EPS1);
        EPSd := real(EPS2);
        ED := EPSd-EPSs;
        ED2 := (EPSd+EPSs)/(2.0);
        ED32 := (EPSd-(1.0)) ** (1.5) -
            (EPSs-(1.0)) ** (1.5);

        FL0 := (PHIt*MU1/(vmax))*(abs(ED))/Leff;
        FL  := (1.0+real(FL0) ** beta) ** (1.0/beta);

        MU2  := MU1/FL;

-- (*Series resistance effect*)
      IF (ED = 0.0) THEN
            j1 := 1.0+W/Leff*MU2*Cox*Rt*PHIt*(VGBD-ED2
                -2.0*Gamma1*sqrt(EPSs));
      ELSE
            j1 := 1.0+W/Leff*MU2*Cox*Rt*PHIt*(VGBD-ED2
                +(1.0/1.5)*Gamma1*ED32/ED-2.0*Gamma1*sqrt(EPSs));
      END IF;

        MU  := MU2/j1;


-- (***************************** Current Components ************)

-- (* Drift current *)
        EPSs := real(EPS1);
        EPSd := real(EPS2);
        ED := EPSd-EPSs;
        ED2 := EPSd ** (2.0) - EPSs ** (2.0);
        ED32 := (EPSd-1.0) ** (1.5) -
            (EPSs-1.0) ** (1.5);
        IDdrift1 := KP*MU*(VGBD*ED-0.5*ED2-
(1.0/1.5)*Gamma1*ED32);
```

```
-- (* Channel length modulation *)

-- (* Saturation CLM*)
        A := q*Neff*Nsub*(Leff ** 2.0) / (Eo*Ks*PHIt);
        B1 := 2.0*(ln(yj/1.0e-6)-1.0)/(q*Neff*Nsub*vmax*W*yj);
        DL := (sqrt((real(Vss) ** 2.0) +
        2.0*real(A)*(1.0+real(B1)*real(IDdrift1))*(real(VDS)-real(VDS1)))
        -real(Vss))/(real(A)*(1.0+real(B1)*real(IDdrift1)));


-- (* Subthreshold *)

        PHIs3 := EPS3-VSB;
        PHIs4 := EPS4-VDB;

        n4 := 1.0;
        Vb_PHIs3 := n4*ln(1.0+exp((Vbi-PHIs3)/n4));
        Vb_PHIs4  := n4*ln(1.0+exp((Vbi-PHIs4)/n4));

        L4 := sqrt(K1*(Vb_PHIs3));
        L5 := sqrt(K1*(Vb_PHIs4));

--      (* Preventing the DIBL from diverging *)
        L4  := real(L4)/((1.0+(real(L4)/(Leff-0.2*Leff)) ** xdibl)
            ** (1.0/xdibl));
        L5  := real(L5)/((1.0+(real(L5)/(Leff-real(L4)-0.1*Leff)) ** xdibl)
            ** (1.0/xdibl));
        L2  := Leff-2.0*L4;

        L3  := Leff*(1.0-DL);
        L1  := L2*xdibl2+L3*(1.0-xdibl2);

        IDdrift  := IDdrift1*Leff/L1;

-- (* Diffusion current *)
        EPSs := real(EPS3);
        EPSd  := real(EPS4);
        ED1  := EPSd-EPSs;
        ED12  := sqrt((EPSd-(1.0))) -
              sqrt((EPSs-(1.0)));
        IDdiff  := KP*(Leff/L1)*MU*(ED1+Gamma1*ED12-(Qit_d1-
```

```
        Qit_s1)/Cox);

      IF (IDdrift<I_leak/Sleak) THEN
            IDdrift  := I_leak/Sleak;
      END IF;
      IF (IDdiff<I_leak/Sleak) THEN
            IDdiff  := I_leak/Sleak;
      END IF;

      END IF;       -- (* IF VDS   :=  0  *)
      END IF;       -- (* IF VGB2 < 0.0  *)
      END IF;       -- (* IF EPSW < 0.0 *)
      END IF;       -- (* IF EPSw1 < 0.0 *)
      END IF;       -- (* IF EPSES < 0.0 *)
      END IF;       -- (* IF EPS < 0.0 *)
-- (* total current *)
        ID  := (IDdrift+IDdiff);

-- (* Impact ionization current *)

      IF (VDS-VDS1 > 0.0) THEN
            Isub  := AI*(VDS-VDS1)*PHIt*ID*exp(-BI*lc/((VDS-
VDS1)*PHIt));
            IDam  := AI*(VDS-VDS1)*PHIt*ID/Leff*exp(-BI*lc/((VDS-
VDS1)*PHIt));
      ELSE
            Isub  := 0.0;
            IDam  := 0.0;
      END IF;

-- (* Drain and source currents *)
        IDD  := ID+(1.0-2.0/Sleak)*I_leak+Isub+IDam;
        IDS  := -ID+(1.0-2.0/Sleak)*I_leak-IDam;

-- (* Application of currents *)
        D.i %= IDD;
        S.i %= IDS;
        B.i %= -Isub;

END RELATION;

END ARCHITECTURE a;
```